Studying Biomolecular Interactions using Atomic Force Microscopy

Carolin Madwar

A Thesis

in

The Department

of

Chemistry and Biochemistry

Presented in Partial Fulfillment of the Requirements

for the Degree of Master Science (Chemistry) at

Concordia University

Montréal, Québec, Canada

December 2009

Your file Votre référence
ISBN: 978-0-494-67235-8
Our file Notre référence
ISBN: 978-0-494-67235-8

ABSTRACT

Studying Biomolecular Interactions using Atomic Force Microscopy

Carolin Madwar

Many biological systems involve mechanical interactions and specific molecular recognition events that are essential for their function. Single molecule force spectroscopy (SMFS) is a powerful and versatile atomic force microscopy (AFM)-based technique, which allows probing such interactions at the single molecule level, with piconewton sensitivity, thereby illuminating their dynamics as well as their structural and mechanical properties. A fundamental requirement in these studies is the immobilization of biomolecules between the AFM probe and the sample surface, preferably by a long flexible molecular spacer, such as poly(ethylene glycol) (PEG). The goal of this project is to investigate the binding interactions in four distinct biomolecular systems at the single molecule level, using SMFS. A new amination strategy was used to attach a novel bifunctional PEG spacer containing amine- and thiol-reactive termini. Biomolecules under investigation were tethered to AFM tips by formation of covalent linkages to this versatile spacer. Various tests, including surface plasmon resonance and a UV-based enzyme assay, were carried out to evaluate and confirm AFM tip functionalization. SMFS of biotin/streptavidin yielded an average unbinding force of 59 pN at 4000 pN/s loading rate. SMFS of concanavalin A/mannose yielded an average unbinding force of 50 pN at loading rate of 6000 pN/s. SMFS of a *de novo* heterodimeric E/K coiled/coil yielded an average unbinding force of 41 pN at 7000 pN/s loading rate with a k_{off} rate calculated to be 15.8 s^{-1}. SMFS of these biomolecular systems were not only successful and informative, but also provide exciting directions towards future applications.

Acknowledgements

First of all, I would like to express my sincere gratitude to my research supervisor, Prof. Louis Cuccia for his dedication, sacrifice, support, and guidance. But for his endurance and understanding, I could not have finished my master's degree. He was willing to give me insights to address various problems and to listen to my hardships. Especially, he taught me how enthusiastic and diligent every professional should be. I am grateful for the continuous guidance of my committee members, Prof. J. Powlowski and Prof. C. Skinner. I am also grateful to the endless help and patience of our collaborators: Prof. P. Davies and S. Gauthier (Queen's University), Prof. G. De Crescenzo, B. Liberelle and C. Boucher (Université de Montréal). I am also indebted to Dr. Shan Zou for always being available to generously share her knowledge and expertise in the field of SMFS. I also thank Dr. Rolf Schmidt for developing data analysis programs, passing on his expertise in instrumental techniques, and most importantly, for his helpful discussions and friendship. I would like to thank numerous individuals who helped me at various stages of this project: Prof. J. Turnbull, Prof. J. Kornblatt, Prof. J. Kornblatt, Prof. Pawelek, Prof. P. Joyce, Dr. P. Hanic, Dr. P. Ulycznyj, Prof. T. Hugel and T. Prizer. I also thank Liyan Xing, James Mousseau, Marta Kocun, Monica Cheung, Maria Paola Aviles and everyone else in the Cuccia group and in the Department for nurturing a friendly working atmosphere. I especially thank Monica and Marta for their true friendship and for always being by my side. Finally my love and this thesis are dedicated to my parents and my sister: I owe my whole life to my beloved family. For everything, I thank God who has been always with me, before time even began.

Dedicated with love to my Father

Table of Contents

List of figures

List of tables

List of equations

List of abbreviations

AFM	atomic force microscope (or microscopy)
APTES	(3-aminopropyl)triethoxysilane
APTMS	(3-aminopropyl)trimethoxysilane
A.U.	absorbance units
Biotin-PEG3400-NHS	biotin-poly(ethylene glycol)-*N*-hydroxy succinimate, MW 3400
Biotin-PEG3400-SH	biotin-poly(ethylene glycol)-SH, MW 3400
Bp	base pairs
CFS	chemical force spectroscopy
CH_3O-PEG5000-NHS	methoxy-poly(ethylene glycol)-*N*-hydroxy succinimate, MW 5000
CH_3O-PEG750-NHS	methoxy-poly(ethylene glycol)-*N*-hydroxy succinimate, MW 750
CLI	command line interface
ConA	concanavalin A
DCC	dicyclohexyl carbodiimide
DCU	dicyclohexyl urea
DMSO	dimethyl sulfoxide
DMF	dimethyl formamide
DMG	*N*,*N*-dimethyl glycine
DNA	deoxyribonucleic acid

dsDNA	double-stranded DNA
2,2'-DTDP	2,2'-dithiodipyridine
EAP	ExtrAvidin®-peroxidase
EDC	ethyl-*N*'-(3-dimethylaminopropyl)carbodiimide hydrochloride
EDTA	ethylene diamine *N,N,N',N'*-tetraacetic acid
f	unbinding force
f_0	cantilever resonant frequency
e-FJC	extended freely jointed chain model
e-FJC$_{PEG}$	extended freely jointed chain model for poly(ethylene glycol)
EGF	epidermal growth factor
EGFr	epidermal growth factor receptor
ΔG	Gibbs free energy difference
ΔG_0	Gibbs energy difference at zero applied force
ΔL	length difference between the helical and planar PEG conformations
Gdn•HCl	guanidinium hydrochloride
GUI	graphical user interface
h_N	histogram bin width
HIV	human immunodeficiency virus
k_B	Boltzmann's constant

k_C	cantilever spring constant
L_C	contour length
LC-SPDP	succinimidyl 6-(3-[2-pyridyldithio]-propionamido)hexanoate
$L_{helical}$	length of poly(ethylene glycol) segment in the helical conformation
l_K	Kuhn length
L_{planar}	length of poly(ethylene glycol) segment in the planar conformation
N	number of data points in a histogram
$N_{helical}$	number of poly(ethylene glycol) segments in the helical conformation
NH_2-PEG3500-COOH	amino-poly(ethylene glycol)-carboxyl, MW 3500
NH_2-PEG3500-COOH•HCl	amino-poly(ethylene glycol)-carboxyl, HCl salt, MW 3500
NHS	*N*-hydroxylsuccinimide
NHS-PEG6000-NHS	*N*-hydroxy succinimate -poly(ethylene glycol)-*N*-hydroxy succinimate, MW 6000
NHS-PEG3500-PDP	*N*-hydroxy succinimate- poly(ethylene glycol)- 3-(2-pyridyldithio)-propionate, MW 3500
NMR	nuclear magnetic resonance
N_{planar}	number of poly(ethylene glycol) segments in the planar conformation
OPD	*o*-phenylenediamine•2HCl
p	persistence length
PBS	phosphate-buffered saline

PBT	phosphate-buffered saline with 0.5% Tween®-20
PCR	polymerase chain reaction
PDMS	poly(dimethyl siloxane)
PDP-OH	3-(2-pyridyldithio)-propionic acid
PDS	2-pyridyldisulphide
PEG	poly(ethylene glycol)
PFPA	perfluorophenylazide
PFPA-disulfide	perfluorophenylazide-disulfide
PFPA-mannose:	α-D-mannose- perfluorophenylazide
RNA	ribonucleic acid
R.U.	arbitrary resonance units
S	photodiode sensitivty
SAM	self-assembled monolayer
SATP	*N*-succinimdyl 3-(acetylthio)propionate
SMSF	single molecule force spectroscopy
SPDP	*o*-succinimidyl-3-(2-pyridyl)-dithiopropionate
SPR	surface plasmon resonance
ssDNA	single-stranded DNA
TEA	*N,N,N*-triethylamine
THF	tetrahydrofuran

TLC	thin layer chromatography
TSTU	*N,N,N',N'*-tetramethyl-*O*-(*N*-succinimidyl)-uronium tetrafluroborate
ttg	*trans-trans-gauche* conformation of PEG segment
ttt	*trans-trans-trans* conformation of PEG segment
UV	ultra violet
V	photodiode voltage
WLC	worm-like chain model
x	extension
Z	amplitude of cantilever oscillation

Chapter 1. General Introduction

1.1. Single Molecule Techniques

Many biological reactions are too complex to be fully understood through the use of conventional ensemble techniques. At the most fundamental level, all biological reactions take place *via* the action of single enzymes, DNA molecules, or RNA molecules. Studying one biomolecule at a time, or performing single molecule studies, can provide us with amazingly clear and often unforeseen views of these molecules in action.[1,2]

The use of single molecule techniques to study biological processes and address biomolecular interactions is a relatively new venture, which started less than 25 years ago, and has been growing tremendously since then. The two main categories are: (*i*) fluorescence imaging and spectroscopy, and (*ii*) force-based manipulation and detection. The work presented herein is based on the use of Single Molecule Force Spectroscopy (SMFS), an Atomic Force Microscopy (AFM)-based force technique, in order to address, detect and measure biomolecular interactions.[2]

Investigating the mechanisms that govern biological interactions and understanding the strength of biomolecular linkages are challenging tasks in both molecular as well as structural biology. Such biomolecular interactions are mainly governed by multiple weak non-covalent bonds that take place within defined regions of the interacting bio-partners.[3-5] In recent years, a number of techniques were developed to explore such interactions, including the surface force apparatus,[6] pipette suction,[7] magnetic beads,[8] flow chamber apparatus,[9] optical traps and tweezers[10,11] and AFM-based techniques.[12,13]

The techniques using optical and magnetic tweezers have proven to be unique tools for force microscopy due to their sensitivity. However, in addition to their small force range (no more than 200 pN), from a biological perspective these techniques are limited by the need to artificially attach a micron-sized handle with which to apply a significant force without altering the behaviour of the system under investigation. In addition, visible and ultraviolet radiation carry sufficient energy to disrupt nearly all types of bonds if directly absorbed and is therefore a limitation to many forms of optical imaging.[14] On the other hand, beside the ability to access higher forces (up to 100000 pN), AFM-based SMFS has many advantages.[12,15] Sample requirements are relatively simple and measurements can be performed under both ambient and liquid environments, thereby providing an excellent opportunity to probe biomolecular interactions at the single molecule level, as will be explored in the following chapters.

The AFM is mainly used in two different modes, one as an imaging tool and the other as a force probe. The latter is the technique known as SMFS. In either mode, AFM is an ideal and powerful tool for probing and directly measuring interactions within a wide range of molecular systems. With nanometer spatial resolution and piconewton force sensitivity, the AFM not only produces nanometer to micron scale images of surface topography, adhesion, friction and many others, but also detects and directly measures intra- and intermolecular forces precisely at the single molecule level. [13,16,17] These features make the AFM a unique instrument for elucidating new aspects in material and macromolecule studies and render its force mode as an essential characterization tool for fields ranging from biology to materials science. This field is amazingly dynamic, and technical developments enabling novel experiments and significant improvements of new

as well as existing approaches, provide biochemists, chemists as well as physicists a source of continuing excitement and inspiration.

1.2. Single Molecule Force Spectroscopy

This chapter provides a brief overview of the main principles behind AFM, focusing on the technique of SMFS. It also describes examples of its applications for probing the mechanical properties of various biomacromolecules.

A typical AFM instrument consists of: (*i*) a tip-cantilever assembly, which acts as the probe that interacts with the sample surface, (*ii*) a piezoelectric scanner, which provides three dimensional positioning with high resolution, and (*iii*) a position-sensitive photodiode detector, which measures the probe displacement and translates it into a readable output (Figure 1).[18]

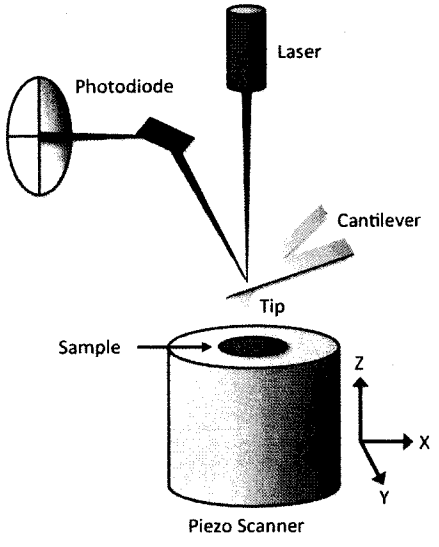

Figure 1. Schematic diagram of the AFM microscope

The AFM tip-cantilever assemblies are typically made of silicon or silicon nitride and can have either single- or V-shaped beams, as shown in Figure 2. The cantilevers differ in their dimensions, spring constants, as well as their resonance frequencies, which is often critical for their chosen applications.[19]

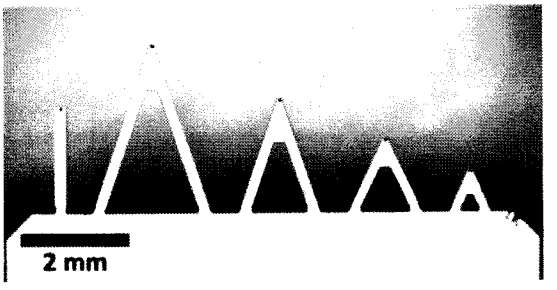

Figure 2. Optical microscope image (reflection mode) of AFM cantilevers and tips: one substrate has different cantilevers, with nominal spring constants of 0.02, 0.01, 0.03, 0.10, 0.50 N/m (from left to right). Note the presence of the pyramidal tips at the end of each cantilever

The tip, with a radius of curvature in the nanometer range[19], can scan the sample in different ways. For imaging, the AFM tip scans the sample surface in a raster fashion, and may do so in: (*i*) contact, (*ii*) tapping (also known as intermittent-contact) or (*iii*) non-contact mode (Figure 3 a, b, c, respectively). In contact mode, the tip is scanned over the sample surface while monitoring the cantilever's motion with a photodiode detector. At each point, a constant deflection is maintained between the cantilever and the sample by vertically moving the scanner *via* a feedback mechanism. The distance the scanner moves is then used to form the topographic image of the surface. Operating in this mode allows for molecular resolution images with high scan speeds, however the forces that the tip exerts when touching the surface could damage features especially for soft biological samples. Tapping mode™, on the other hand, operates by scanning the tip of an oscillating cantilever across the sample surface, while maintaining constant oscillation

amplitude. In this case the tip lightly taps on the surface during scanning, contacting the surface only at the bottom of its swing. The advantage of this mode is the high lateral resolution obtained on most surfaces as well as the fact that there is less force exerted on the sample. In the non-contact mode, the tip does not contact the sample surface at all and is therefore the least intrusive of the three modes. In this case, the oscillating cantilever interacts with the surface only through long range forces, such as van der Waals interactions, thus decreasing the amplitude of oscillation.[20,21]

Figure 3. Different modes of AFM: (a) Contact mode, (b) Tapping mode™, and (c) Non-contact mode

In either of these modes, the AFM operates in the three dimensions: x, y, and z, and the probe displacement is converted by the position-sensitive photodiode detector into a topographic image, with molecular and sometimes atomic resolution.[13] However, when operating only in the z-direction, the cantilever's deflection can be can be converted to force values, and the AFM can be used to measure interaction forces with piconewton sensitivity. Depending on the cantilever's stiffness, manifested as its spring constant (k_C, 0.1 – 100 N/m range),[22] and the AFM instrumental deflection sensitivity (*ca.* 0.1 Å), minimal forces in the femto- to nanonewton range can be measured. This means that the AFM can theoretically measure molecular interactions as weak as van der Waals interactions ($< 10^{-12}$ N) and also as strong as covalent bonds (10^{-7} N).[23] Practically, the sensitivity of AFM is affected by the cantilever's thermal vibrations as well as its optical and electronic noise. These limit the minimal forces measured in fluids to about 10 pN at

room temperature.[22] The piconewton range accessible using AFM-based SMFS is in fact difficult to fathom; for example, the force required to lift a weight of 1 gram is nearly 10 billion piconewtons (*i.e.* $(1 \times 10^{-3}\ \text{kg}) \times (9.8\ \text{m/s}^2) = 9.8 \times 10^{-3}\ \text{N}$; *ca.* 10×10^9 pN).

In the AFM force mode commonly known as SMFS, force-distance curves (*i.e.* force curves) are generated when monitoring the cantilever's deflection as a function of the tip-surface separation (Figure 4). A typical experiment starts with the cantilever far from the surface where there is no deflection since there are no forces acting on the tip. The approach curve (Figure 4, red) is developed by moving the cantilever towards the sample surface until contact is established and then further extending the cantilever towards the surface allowing interactions to take place. The retract curve (Figure 4, blue) is then obtained when the cantilever is withdrawn from the surface until tip contact with the surface is lost. During this approach-retract cycle, the deflection of the cantilever in the z-direction changes as exemplified in the force curve.[12]

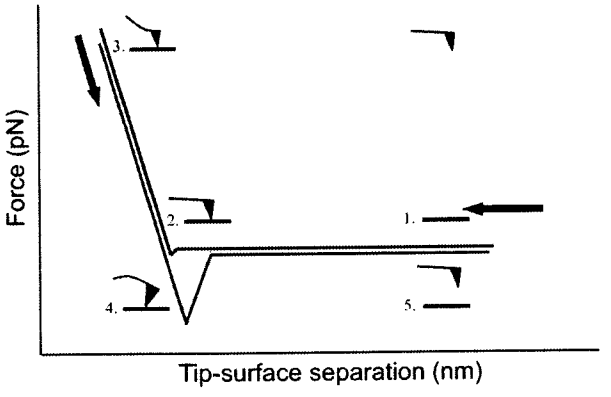

Figure 4. Features of a typical force-distance curve

Initially there are no forces acting on the tip and therefore the cantilever remains undisturbed (Figure 4, part 1). However, upon contact (Figure 4, part 2) and further

extension into the surface (Figure 4, part 3), interactions between functional groups on the tip and the sample surface can develop (Figure 4, part 4) before the tips is retracted and detached from the surface (Figure 4, part 5). The interaction forces are represented by peak(s) on the retract curve and can be calculated by converting the cantilever deflection (*i.e.* peak height) to force using the cantilever's spring constant.[17] Due to the presence of capillary interactions between the tip and the sample surface under ambient conditions, a large adhesion force (nanonewton range) represented by a large interaction peak at the start of the force curve results. Since most (bio)molecular interactions of interest are in the piconewton range, adhesion forces are usually eliminated by performing AFM-force based experiments in fluid environment.[24]

In addition to imaging, AFM can measure forces between as well as within molecules. Figure 5 shows some of the various applications of AFM-SMSF to single macromolecule manipulations. These include the detection and mechanical characterization of DNA, proteins, polysaccharides, synthetic polymers, as well as supramolecular interactions. In addition, the interactions between two molecular partners or simply between two chemical groups can also be measured. When studying polymers using SMFS, one can obtain parameters such as Kuhn length, persistence length as well as segment elasticity. When studying the interaction between molecular partners, the force required to break this interaction, commonly known as the rupture force, can be obtained under varying conditions.

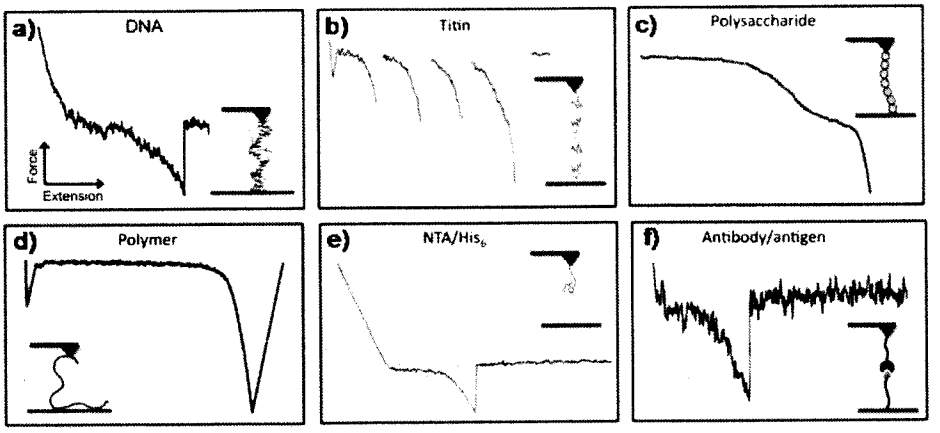

Figure 5. Examples of SMFS applications: (a) Force-induced melting of complementary DNA strands (5'-G-G-C-T-C-C-C-T-T-C-T-A-C-C-A-C-T-G-A-C-A-T-C-G-C-A-A-C-G-G-3' and complementary strand), displaying stretching followed by unbinding,[25] (b) Force-induced unfolding of titin, displaying a saw-tooth pattern characteristic for multi-domain proteins,[26] (c) force-induced conformational transitions in polysaccharides (dextran, α-(1,6)-D-glycopyranose), showing a characteristic chair-to-boat transition of pyranose ring,[27] (d) Force-induced stretching of synthetic polymers (PEG) in water, displaying entropic and enthalpic elasticity,[28] (e) Force-induced rupture of a supramolecular interaction (His_6–Ni^{2+}–NTA), showing the complex unbinding force peak,[29] (f) Force-induced rupture of an antigen-antibody interaction (anti-sendai antibodies to sendai-epitopes), showing the complex unbinding force peaks[30]

1.3. Chemical Force Spectroscopy

The AFM-based force technique has opened new horizons for measuring the strength of biomolecular interactions because of its ability to sense forces that develop between the end of its probe and the sample surface with an extremely high degree of sensitivity as well as specificity.[31] The concept of chemically modifying AFM tips in order to develop probes that contain certain chemical functionalities and thereby becoming sensitive to specific molecular interactions was first introduced in 1994. In this approach, which was termed *Chemical Force Spectroscopy* (CFS), C. Lieber and coworkers functionalized AFM probes with methyl as well as carboxyl groups and used them for mapping the spatial arrangement of surfaces by specifically interacting with similar groups on the surface.[32] A few years later, a major advance in CFS was achieved by developing AFM probes functionalized with carbon nanotubes.[33] Nanotube functionalized probes were

indeed a breakthrough in the field of CFS; their chemical sensitivity towards surface composition, along with their flexibility, high aspect ratio and small effective radius allowed chemically-sensitive imaging of patterned surfaces. All together, this led to the development of chemical imaging contrast in CFS experiments, a field that would make AFM-force spectroscopy a versatile surface analysis tool.[34] More importantly in the context of this work, nanotube functionalized probes have also been used in measuring specific ligand-receptor interactions, particularly when biotin was covalently bound to nanotube tips and streptavidin immobilized on biotin surfaces (Figure 6).[33]

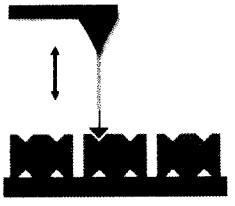

Figure 6. Schematic representation of a nanotube functionalized AFM tip, where the terminal end of the nanotube was coupled to biotin in order to become sensitive towards streptavidin surfaces[33]

Since then, the concept of chemically modifying (*i.e.* functionalizing) AFM tips by the covalent attachment of molecules (including biological macromolecules) has proven to be an excellent tool in probing and measuring forces between a tip and a sample. Measuring the strength of biomolecular interactions between bio-partners is possible if they are immobilized between the AFM probe and the sample surface. In a simplified description, approaching the tip to the sample allows the interaction(s) to take place and then retracting the tip away from the sample breaks the interaction(s). The height of the peak on the retract curve represents the magnitude of the rupture force required to break the molecular interaction between the bio-partners. Following this methodology, CFS has been used to probe a wide variety of both biological and chemical interactions, such as

antibody-antigen[3,35] lectin-carbohydrate pairs[36,37,38] complementary DNA strands,[39] supramolecular polymer chains,[40] gold and self-assembled monolayers.[41]

This chapter gives a basic introduction to AFM-tip functionalization strategies, including different chemical methods to add functional groups to the AFM tip as well as methods developed to attach molecular spacers when required (either on the tip or the sample surface). Most of the examples presented here focus on the application of amine-terminated functional groups on the AFM tip surface. There are many well-developed surface functionalization methodologies that can be applied towards AFM tip functionalization and the reader is directed to a comprehensive review article by Ebner *et al.*[42] In all cases, tip functionalization chemistry requires meticulous care to obtain favourable and reproducible results.

1.3.1. AFM Probe Cleaning

As mentioned earlier, AFM tips are usually made of silicon nitride (Si_3N_4), which oxidizes to form a layer of silicon dioxide (SiO_2) under ambient conditions. Most cleaning procedures involve the use of oxidative conditions to produce a continuous uniform silanol layer on the surface (Si–OH).[42] A number of chemical reactions may then be used convert the hydroxyl groups to other functionalities in order to subsequently attach molecules of interest. The presence of a uniform contamination-free silanol layer is essential for successful coupling reactions, therefore it is of critical importance to clean the surface of AFM tips prior to their functionalization. Commercial AFM tips are often contaminated with derivatives of poly(dimethylsiloxane) present in the Gel-Pak® adhesive in tip storage containers.[43] An effective way to remove polysiloxanes involves

the careful use of piranha solution (H_2SO_4/H_2O_2, 70:30 (v/v)). However, one must also consider that such harsh chemical treatment can damage the tip and also the gold reflective surface of the cantilever thereby decreasing the deflection sensitivity. The use of oxygen plasma or UV-generated ozone is an attractive method for cleaning AFM tips by removing organic and other oxidizable surface contaminants that might be present.[42] After cleaning, the tips should be stored in such a way as to avoid contamination from volatile organics or polymer-based containers (*i.e.* in glass petri dishes under vacuum). It is highly recommended for the tips to be used immediately after cleaning to minimize undesirable contamination.

1.3.2. AFM Tip Pre-Functionalization

After tip cleaning, processes of silanization, esterification or metal deposition are carried out in order to attach functional organic groups to the tip's silanol surface layer (*i.e.* 'pre-functionalization'). As mentioned earlier, an additional layer of molecular spacers (*e.g.* poly (ethylene glycol)) can be subsequently added (*i.e.* 'functionlaization').

Silanization of AFM tips involves the use of organosilane reagents which attach to the silanol surface groups by Si–O–Si bonds. Organosilanes used for tip pre-functionalization typically have the chemical formula, $RSi(OR')_3$, where, R' is an alkyl chain and R contains a reactive group that will be used for subsequent functionalization. Aminosilanes where the R group is an aminoalkyl chain are mostly used, however in other cases organosilanes that contain thiol, vinyl and alkoxyl groups may also be used, depending on the chemical nature of the next species to be attached.[31] The most common method used for tip functionalization is aminosilanization, which is usually carried out

using either (3-aminopropyl) triethoxysilane (APTES) or (3-aminopropyl) trimethoxysilane (APTMS) (Figure 7).

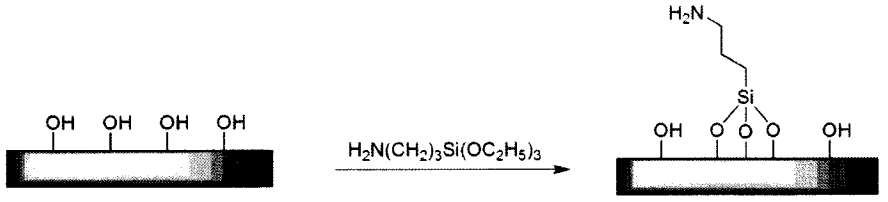

Figure 7. Pre-functionalization of AFM tips using 3-aminopropyltriethoxysilane (APTES)

Other aminosilanes were found to be much less efficient and are used very rarely.[42] The ethoxy/methoxy groups must be hydrolyzed for the reaction to take place, and in the case of APTES or APTMS, the amino group serves as the base needed to catalyze the hydrolysis step. However, the disadvantage of this 'autocatalytic' hydrolysis is that such aminosilanes are very likely to polymerize into networks when dissolved in the reaction solvent or even during storage, unless water is completely excluded.[42] Therefore aminosilanes are usually stored under argon and preferably used fresh after distillation. The aminosilanization reaction is carried out in the vapour phase in order to promote the formation of uniform aminosilane layer. In addition, the process must be carried out under nitrogen, again in order to avoid the polymerization of the organosilane reagents on the AFM tip surface. Finally, the aminosinalized tips should be used directly or shortly after preparation in order to avoid surface hydrolysis, as well as contamination. This process is somewhat time consuming but is well-established, characterized and has been proven to be useful for a variety of applications.[42]

Another process by which surface silanol groups of AFM tips are pre-functionalized is esterification. In this reaction, alcohols are used to add a new organic functional group to

the AFM tip surface. Esterfication is a simple condensation reaction that can be easily applied to silica surfaces.[44] However, activation of the silanol groups on the surface is required prior to their reaction with alcohols. This is usually achieved by treating the cleaned AFM tip surface with tertrachlorosilane ($SiCl_4$) and diethylamine (Et_2NH). The resulting $Si(NEt_2)_4$ is thought to aminate/activate the silanol surface groups thereby making their reaction with alcohol much faster.[23] The esterification reaction developed for functionalizing AFM tips with amino groups similarly involves the use of ethanolamine hydrochloride in order to activate the silanol functionality (Figure 8).

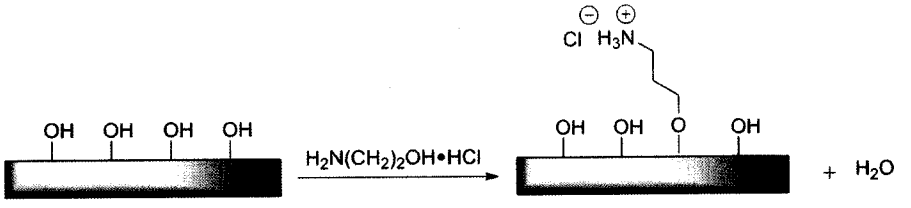

Figure 8. Pre-functionalization of AFM tips using ethanolamine hydrochloride

The same principles developed for using ethanolamine hydrochloride may be applied with other types of alcohols in pre-functionalizing the AFM tips. Of course, each system will require specific reaction conditions (temperature, incubation time, reagent concentrations, *etc.*) in order to obtain optimal pre-functionalization. For example, when using ethanolamine hydrochloride, the reaction usually involves the use of molecular sieves in order to remove the water generated during the reaction and takes place in a non-volatile solvent dimethyl sulfoxide (DMSO) since the process requires about 15 hours.[35] This reaction appears to be simpler compared to the use of aminosilanes, however applications have shown a number of distinct disadvantages for the esterification method with ethanolamine. The experimental results in different studies

detected rupture lengths 10-20 nm longer than expected. This was attributed to the fact that short polymers are being formed on the tip in the presence of ethanolamine and DMSO, with the possible involvement of oxygen.[42] This unsupported conclusion connects to the other disadvantage of the reaction, which is its unknown and somewhat vague chemical mechanism. Studies have shown the reaction to require very high temperature when using other types of alcohols and initiated doubts about the mechanism described above.[45] Despite the disadvantages, the esterfication method is used for force applications and is found to be convenient for measuring unbinding forces.[42]

Another method for functionalizing AFM tips does not involve chemically modifying the surface groups, but rather coating the surface with metal. A consequence of metal deposition in comparison to other AFM tip functionalization methods is that it not only changes the chemical reactivity of the surface but also its mechanical, thermal, optical and resistive properties.[46] Vapor deposition is the most common method used for coating AFM tips with a variety of metals, including aluminium, gold, nickel, chromium and platinum. The vapor deposition process involves heating the metal (source material) until it evaporates and condenses on the desired surface. All the different evaporation methods follow this principle and mostly differ in the heating method used. When metal deposition is achieved by thermal (resistive) evaporation, the source material is incorporated within a high melting point container, which once heated by electrical current causes the metal to evaporate. The required low pressure environment inside the chamber allows the metal atoms to evaporate freely until they condense uniformly on the tip surface. This process is performed under high vacuum conditions in order to prevent the metal vapor from reacting with any residual gas molecules or contaminants that may

be present within the chamber.[46] Although the presence of a metal layer on the AFM chip surface may decrease the cantilever flexibility, which is undesirable in certain situations, it has been useful for a variety of applications. In particular, the thermal evaporation of gold has been applied in many studies for AFM tip pre-functionalization to subsequently add an additional functionality of interest using thiol chemistry.[39,47,48] An example of aminating AFM tips using amino-self assembled monolayers (SAMs) is given in Figure 9.[49]

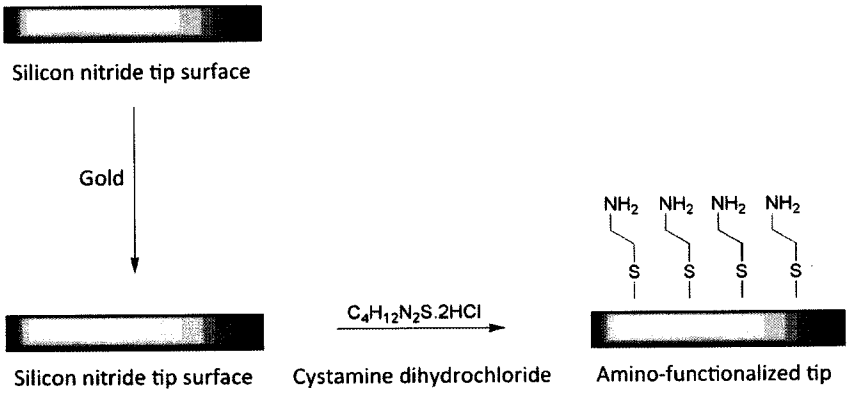

Figure 9. Pre-functionalization of AFM tips using gold coating: cystamine dihydrochloride is used to form amino-SAMs by the formation of gold-sulfur bonds[49]

In general, the pre-functionalization of AFM tips with any of the described methods (silanization, esterfication or metal coating) is only a required initial step that is typically followed by a final functionalization procedure. These may include the addition of self-assembled monolayers,[39,50] polymers,[51-53] or even biological molecules.[36,54,55] In the following section, the attachment of molecular spacers to AFM tips will be discussed, in particular poly(ethylene glycol) (PEG) and their use as spacers in force applications.

1.3.3. AFM Tip Functionalization

Polymers, such as PEG, may be used in AFM tip functionalization to serve as molecular spacers between the AFM tip and the substrate surface (Figure 10).

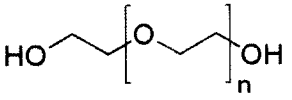

Figure 10. Structure of poly(ethylene glycol)

In general, the spacers used are functionalized (*i.e.* terminated with a reactive functional group) at both ends. One end of the spacer conjugates to the AFM tip surface and the other end either contains the functional group of interest or another reactive functional group that can be further conjugated to a biomolecule, for example. This linking distance allows the interacting functionalities to freely re-orient and properly interact with their complementary entities between the AFM tip and the substrate surface. The majority of SMFS applications have shown PEG linkers that are 6 – 10 nm in length (which contain 18 – 30 monomer units) to be sufficient for this purpose. The presence of spacers on the AFM tip also allows a higher degree of control on the number of biomolecules that can be attached to the probe. In most cases, a high ratio of mono- to bifunctionalized spacers is used to minimize the number of biomolecules present at the tip surface. As shown in Figure 11, the advantages of using long flexible molecular spacers are mainly to increase the chance of detecting single molecule events as well as to prevent the detection of non-specific adhesion interactions (such as van der Waals, electrostatic and hydrophobic forces) that may develop between the two surfaces when in close contact.[56]

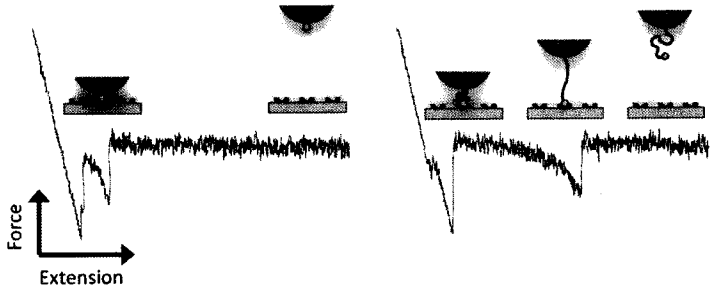

Figure 11. Advantages of using molecular spacers in AFM tip functionalization: (a) In the absence of a spacer, non-specific interactions occur at the same tip-surface separation as specific interactions, making it difficult to distinguish the interactions of interest, (b) In the presence of a spacer, the specific interactions occur at a distance from the surface, separate from the non-specific interactions, facilitating the analysis of interactions of interest

Spacer attachment to AFM tips requires the use of functionalization methods as previously described. The attachment is achieved through chemical reaction between functionalized polymers and pre-functionalized AFM tips (*i.e.* through silanization, esterfication or metal coating). In some studies, PEG molecules containing thiol-reactive functional groups (*e.g.* maleimide, pyridyl disulfide and vinylsulfone) were attached to thiol- SAMs on gold-coated AFM tips by a thioether bond (Figure 12).[57,58] Although the gold-thiol interaction is very strong (20 – 35 kcal/mol),[46] coating AFM tips (and cantilevers) with a metal layer causes an increase in their stiffness as mentioned earlier, therefore this method is used more for attachment of PEG molecules to gold-coated substrates rather than AFM tips.[42]

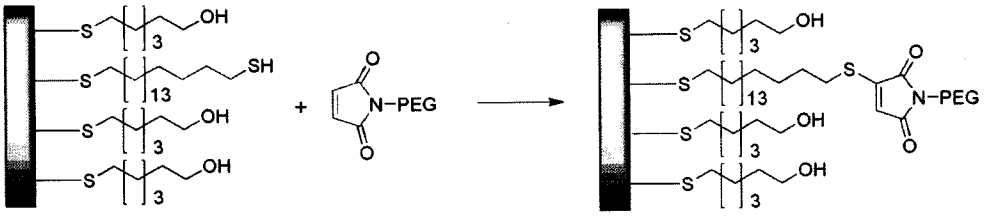

Figure 12. Attachment of PEG spacers to thiol-functionalized AFM tips: gold coating AFM tips, followed by the formation of thiol-SAMs with 5% dithiol and 95% mercaptohexanol allows for the attachment of maleimidie-PEG by a thioether bond.[57,58]

PEG molecules functionalized with amine-reactive functional groups may be attached to aminated AFM tips. As described earlier, the addition of amine functionality to the AFM tip surface may be achieved through silanization (*i.e.* using APTES),[36,59] esterfication (*i.e.* using ethanolamine),[60] or gold coating (*i.e.* followed by formation of amino-SAMs).[48] PEG molecules functionalized with the highly reactive ester *N*-hydroxysuccinimide (NHS) are typically attached to aminated AFM tips *via* a stable amide linkage (Figure 13). In fact, this is arguably the most common method for attaching PEG molecules to AFM tips.[42]

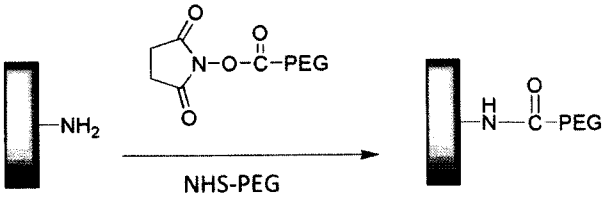

Figure 13. Attachment of PEG spacers to amino-functionalized AFM tips: reaction of NHS with amino groups on the AFM tip surface allow for the attachment of NHS-PEG by amide bond formation

The syntheses of homo- and heterobifunctional PEG molecules, containing the NHS functionality at one end and another reactive group at the other end have been extensively

described in the literature for AFM tip functionalization.[34,61] Examples of bifunctional PEGs are shown in Figure 14.

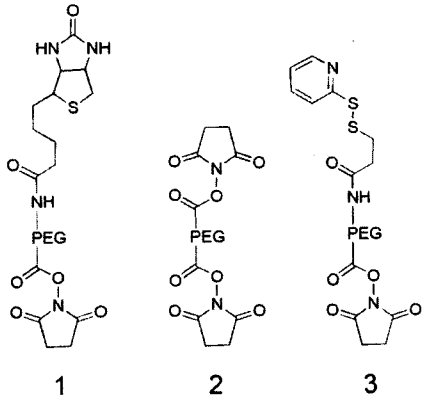

Figure 14. Examples of homo- and heterobifunctional PEG spacers used in this study: (1) NHS-PEG-biotin, (2) NHS-PEG-NHS, (3) NHS-PEG-PDP

The general chemistry of tethering biomolecules to AFM tips *via* these three bifunctional PEG spacers is shown in Figure 15.

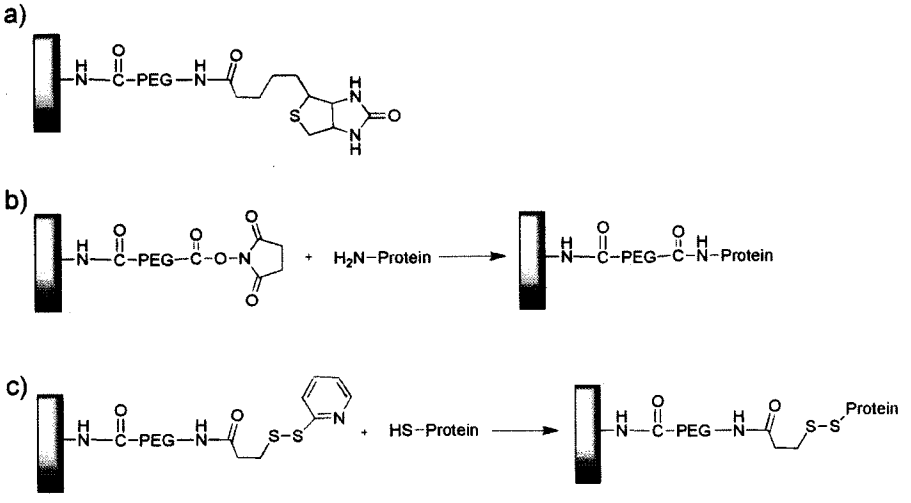

Figure 15. Tethering biomolecules to AFM tips *via* bifunctional PEG spacers: (a) tethering biotin to AFM tips using NHS-PEG-biotin, (b) tethering proteins to AFM tips using NHS-PEG-NHS, which forms amide bonds with amino groups, and (c) tethering proteins to AFM tips using NHS-PEG-PDP, which forms disulfide bonds with thiol groups. In all cases the PEG spacers are attached to aminated AFM tips by amide linkages to their NHS end

As mentioned earlier, the PEG spacer attached to the AFM tip could directly carry the functionality of interest. PEG molecules functionalized with biotin (Biotin-PEG-NHS) have been attached to aminated AFM tips in order to study their interaction with avidin surfaces (Figure 15, a).[61,62] Similarly, fluorescein was attached to AFM tips using fluorescein-PEG-NHS in order to address the interaction with several mutant forms of fluorescein-antibodies.[63,64] The reactions involved in attaching other biomolecules to the PEG spacer depend on the type of their exposed and available functional groups. In the case of proteins, surface amino acids such as cysteine and lysine are widely used for their attachment to functionalized PEG on AFM tips. Lysine residues, which are abundant in proteins, contain an amine functionality and can therefore be coupled to aminated AFM tips *via* the homobifunctional spacer NHS-PEG-NHS (Figure 15, b).[48,54] One drawback for this reaction is the fact that NHS esters are very likely to hydrolyze under aqueous conditions[65] especially at high pH.[66] The incubation time for the reaction of the remaining NHS group with the protein in buffer is therefore extremely critical and may dramatically affect the coupling efficiency. In some studies, the hydrolyzed carboxyl groups were reactivated using NHS/EDC (1-ethyl-3-[3-dimethylaminopropyl]carbodiimide hydrochloride) in order to overcome this instability problem.[67,68] Another consideration for the use of homobifunctional linkers, including NHS-PEG-NHS, is the fact that they may loop and bind twice to the aminated AFM tip. Although this might affect the efficiency of coupling to the amino group of the protein, it might also be useful for lowering the protein density on the surface thereby promoting single molecule events.[42] Using short bifunctional spacers is a possible way to avoid such situations, since they can only link very closely spaced amino groups on the surface (Figure 16).[69,70]

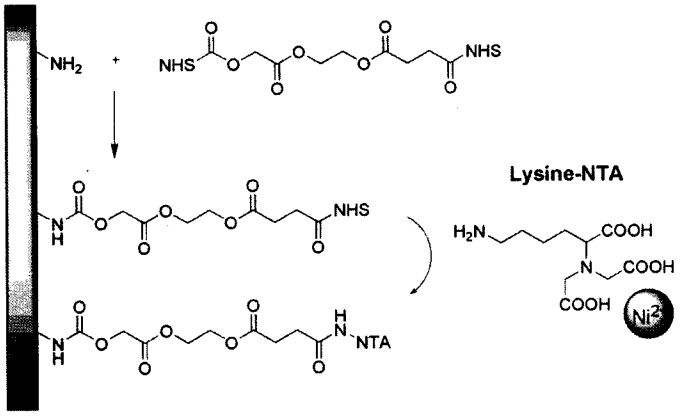

Figure 16. Use of short homobifunctional linkers to tether biomolecules to AFM tips: attachment of linker to aminated AFM tips by an amide linkage to one NHS end, followed by tethering of lysine-NTA by an amide linkage to the other NHS end. The short length of the linker prevents it from looping and binding twice to the tip[69]

Proteins may also be attached to functionalized PEG spacers through reactions of their exposed cysteine residues. Thiol-reactive groups such as maleimides, vinyl sulfones and pyridyldithiopropionate (Figure 17) can react with surface-exposed cysteines and have been shown to effectively couple to proteins.[71,72]

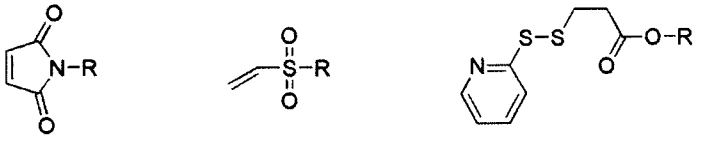

1 2 3

Figure 17. Examples of thiol-reactive groups: (1) maleimide, (2) vinyl sulfone, and (3) pyridyldithiopropionate

Most often, the coupling of thiol-containing biomolecules including proteins to aminated AFM tips has been achieved using the 3-(2-pyridyldithio)propionyl group (PDP) of the bifunctional PDP-PEG-NHS (Figure 15, c).[60,73,74] The coupling efficiency, especially for antibodies, was found to be much higher when using PDP-PEG-NHS compared to other bifunctionalized PEG spacers (*e.g.* aldehyde-PEG-NHS).[73] A disadvantage of the PDP

group to link proteins to AFM tips is the requirement of a free thiol group (*i.e.* an exposed cysteine residue). However, thiol residues can be introduced in proteins using reagents such as *N*-succinimdyl-3-(acetylthio)propionate (SATP) or pyridyldithiopropionic acid hydrazine.[73,75,76]

In summary, a multitude of PEG spacers with different functional groups and polymer lengths have been used in AFM tip functionalization with biomolecules. The examples presented in this chapter represent a small percentage of the work that has been done in this research field and were chosen based on their relevance to this thesis.

1.4. Experimental Considerations

The main objective of this chapter is to point out some experimental considerations required for performing force spectroscopy measurements. These include the choice of AFM cantilevers, spring constant calibration and the use of mathematical models to analyze and interpret the resulting SMFS data.

1.4.1. AFM Cantilever Choice

When conducting SMFS experiments, the choice of AFM cantilevers depends on the type of biological molecules being studied and the magnitude of forces applied as well as measured. Two important properties of AFM cantilevers that influence this choice are: (*i*) the cantilever's spring constant, k_C (pN/nm) and (*ii*) its resonant frequency, f_0 (Hz).[77] When measuring small forces on soft biological samples such as those involved in the folding of proteins, soft cantilevers having low spring constants (k_C < 10 pN/nm) are the most suitable. AFM tips with spring constant as low as 3 pN/nm are commercially

available.[78] Their main drawbacks are their high cost and the fact that they are extremely delicate (*e.g.* they can break even upon immersion in solution). Additionally, in force measurements it is important to take into account the cantilever's thermal noise due to Brownian motion, as it is the major source of experimental noise. Shorter cantilevers give a better signal to noise ratio, in the low-frequency bandwidth (0 – 1000 Hz) at which most force measurements are collected.[22] Cantilevers as short as 60 μm are commercially available and are practical for force applications requiring low-noise measurements. [22,78] For practical reasons, most force measurement studies make use of cantilevers with a spring constant, k_C, of 10 – 20 pN/nm and even some as high as 100 – 160 pN/nm. In our hands, a cantilever with a spring constant of 10 pN/nm has peak-to-peak noise as low as 5 pN with a signal-to-noise ratio of *ca.* 3. Therefore, forces as small as 15 pN, which is at the low end of the interaction forces reported for most biomolecular systems (20 – 240 pN) can be measured.[16] The use of cantilevers with extremely low spring constants is typically not required.[79]

1.4.2. Spring Constant Calibration

Another issue concerning cantilever spring constants is the absolute need for their calibration for each force experiment. Almost all AFM-based SMFS studies have shown the measured spring constant values to be quite different from the nominal values supplied by the manufacturers and the variation is sometimes as high as 50%.[22] A number of different methods have been developed to calibrate the spring constant of AFM cantilevers,[17] and the 'thermal noise' method is the most commonly used. Table 1 summarizes some of these methods and their main source of measurement uncertainty.[80]

Table 1. Different methods for calculating the AFM cantilever spring constant

Method	Equation	Uncertainty (%)	Main source of error
Simple Beam [a]	$k = \frac{Ewt^3}{4L^3}$	16	Cantilever thickness
Parallel Beam Approximation [b]	$k = \frac{Ewt^3}{2L^3}\cos\theta\left[1+\frac{4w^3}{b^3}(3\cos\theta-2)\right]^{-1}$	26	Elastic modulus of Si_3N_4
Frequency Scaling [c]	$k \approx \frac{2\pi^3 w\left(f_0 L\sqrt{\rho}\right)^3}{\sqrt{E}}$	9	Si density
Reference Cantilever [d]	$k = k_{ref}\left(\frac{S_{ref}}{S_{hard}}-1\right)$ & $k = k_{off}\left(\frac{L}{L-\Delta L}\right)^3$	9	Deflection sensitivity
Added Mass [e]	$k = \frac{(2\pi)^2 M_1}{\left(1/f_1^2 - 1/f_0^2\right)}$ & $M_{eff} = M_{meas}\left(\frac{L-\Delta L}{L}\right)^3$	15 – 30	Particle diameter
Sader [f]	$k = 7.5246\rho_f w^2 L Q f_0^2 \Gamma_i(\mathrm{Re})$ & $\mathrm{Re} = \frac{2\pi\rho_f f_0 w^2}{4\eta_f}$	4	Cantilever width
Thermal Noise [g]	$k = 0.817\frac{k_B T}{Z^2}\left[\frac{1-\left(\frac{3D}{2L}\right)\tan\phi}{1-\left(\frac{2D}{L}\right)\tan\phi}\cos\phi\right]^2$	8	Deflection sensitivity

[a] E is the elastic modulus of the cantilever, w is width, t is thickness and L is length.

[b] b is the width at the base of the "V" in V-shaped cantilevers, θ is half the angle between the two legs, w is the width of the legs measured parallel to the front edge of the substrate and L is the length of the cantilever measured straight out to the apex from the substrate.

[c] f_0 is the resonant frequency of the cantilever, ρ is density of the cantilever, w is width, L is length and E is elastic modulus.

[d] k_{ref} is the spring constant of a reference cantilever, S_{ref} is the deflection sensitivity measured on the reference cantilever and S_{hard} is the deflection sensitivity measured on a hard surface. k_{off} is the spring constant measured offset from the end of the cantilever, L is length and ΔL is the distance that the tip is offset from the end of the reference cantilever.

[e] M_1 is an additional mass applied to the end of the cantilever, f_0 is the resonance frequency of the original cantilever and f_1 is that after the addition of one mass. M_{eff} is the effective mass of a particle added to the tip of the cantilever, M_{meas} is the measured mass of the particle, L is the length of the cantilever and ΔL is the distance that the particle is offset from the tip of the cantilever.

[f] ρ_f is the density of the fluid in which the measurement is taken, η_f is the viscosity of that fluid, Q is the quality factor of the cantilever oscillation, and Γ_i is the imaginary component of the hydrodynamic function, which is a function of the Reynolds number, Re. f_0 is the resonant frequency of the cantilever, w is width and L is length.

[g] k_B is the Boltzmann's constant, T is the temperature, Z is the degree of cantilever bending determined using the power spectral density analysis, D is the height of the tip, L is length.

As seen in Table 1, each method makes use of specific parameters that require certain estimates and assumptions and carry with them corresponding errors and uncertainties. The thermal noise method, described below, was used for AFM cantilever spring constant calibration in this research, however, it should be noted that there is no standard method for calibration. The thermal noise method is based on the energy equipartition theorem, which, when the cantilever system is modeled as a simple harmonic oscillator, states that the average potential of the cantilever, $\frac{1}{2}k_C Z^2$, due to its thermal (*i.e.* Brownian) motion is equal its thermal energy, $\frac{1}{2}k_B T$. Therefore the cantilever's spring constant calibration requires the determination of Z^2 (Z is the amplitude of the cantilever's random oscillation at thermal equilibrium; Equation 1).[22]

$$\frac{1}{2}k_C Z^2 = \frac{1}{2}k_B T \Rightarrow k_C = \frac{k_B T}{Z^2} \qquad \text{Equation 1.}$$

In commercial AFM instruments, Z is determined by performing what is known as a 'power spectral density' analysis of the cantilever's oscillation at thermal equilibrium (Figure 18).

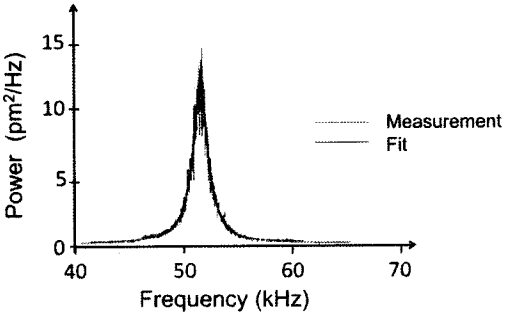

Figure 18. Power spectral density analysis of an AFM cantilever's thermal noise

In practice, the power density spectral analysis first determines the sensitivity, S, of the photodiode voltage, V (volts), which is generated by the laser beam tracing the cantilever's movement, and then relates it to the degree of cantilever bending, Z(nm), since $S = V/Z$. In the power spectral density analysis, V is not evaluated in the time domain, but rather the frequency domain through a Fourier transformation of the time signal (*i.e.* $V(t)$). The advantage of such frequency-type analyses is the possibility of eliminating most of the external noise sources from the measurement. These could either appear at specific frequencies, which can be distinguished from the cantilever's resonance frequency, or are mostly broadband noise (such as white noise) which can be baseline corrected.[22]

Note that the equation reported in Table 1 is not simply $k_C = k_B T / Z^2$, and the correction comes mainly from two later realizations. First, the assumption that the cantilever's oscillatory mode can be described as a simple harmonic oscillator is not necessarily correct since cantilevers do not behave as ideal springs. Second, the cantilever's displacement, which is measured using a reflected laser spot on the position-sensitive photodiode detector is different from the actual displacement, which depends on the bending of the cantilever and the angular changes in the cantilever's position. These factors alone contribute a degree of uncertainty of *ca.* 10% when calibrating the spring constant using the thermal noise method.[22] In addition, calibration uncertainty can also arise from using different solutions and experimental conditions and in these cases, the change in spring constant may or may not be negligible which reinforces the need for calibration in each experiment. It is generally accepted that the variation in spring constant determination using the thermal noise method can be as high as 20%.[22,79]

The rest of this chapter provides a brief overview of polymer mechanical properties (in particular those for PEG), in light of basic models for entropic and enthalpic elasticity. This discussion is relevant to the methods of analyzing, interpreting as well as discriminating the resulting data in force measurements.

1.4.3. Fitting Equations

Applying an external force to a polymer molecule causes each of its monomeric components to align in the force direction, thereby decreasing the overall configurational entropy. The polymer, in response, develops tension in an effort to restore its random configuration. Such a response classifies polymers as 'entropic springs'. The elastic

behaviour of polymers may then be described using mathematical models, as exemplified in Figure 19. As implied from its name, one model describes the polymer as a freely jointed chain (FJC) consisting of orientationally independent, rigid, inextensible Kuhn segments (l_K) (Figure 19, b).[81] On the other hand, the worm-like chain model (WLC) describes the polymer as an elastic rod, whose stiffness is characterized by the persistence length (p), which is the shortest distance over which the polymer keeps its original orientation (Figure 19, a).[82,83]

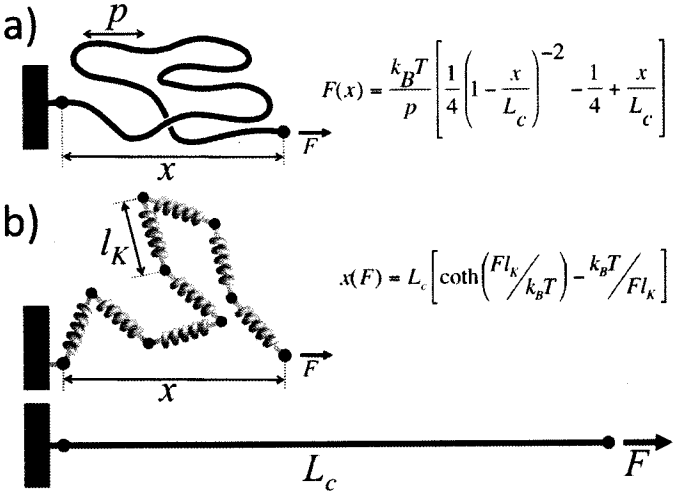

Figure 19. The worm-like chain (a) and freely-jointed chain (b) models of polymer elasticity

These models can be further extended to account for the intrinsic enthaplic elasticity of the polymer's monomeric components.[84] For example, the stretching of PEG under an applied force can be described using the FJC model; however this model becomes inadequate under certain circumstances. An extended freely jointed chain model (e-FJC) was developed to describe the stretching of PEG due to monomer entropic elasticity as well as to account for its conformational transitions.[28] In aqueous solution, the PEG strand can exist in one of two conformations, either *trans-trans-gauche* (*ttg*) or *trans-*

trans-trans (*ttt*) with a specific difference in Gibbs free energy (ΔG) and a length difference (ΔL) (Figure 20). The all-*trans* extended conformational segment is less favourable in the absence of strain, however under an applied external stretching force the equilibrium shifts away from the shorter helical *ttg* conformational segment and towards the extended *ttt* planar state. Hydrogen-bonding with water plays an essential role in the above-described conformational transition.[28]

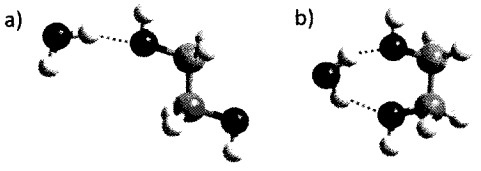

Figure 20. Force induced PEG conformational changes in aqueous solution: (a) extended ethylene glycol monomer (*trans*) and (b) helical ethylene glycol monomer (*gauche*). Hydrogen bonding with water molecules (indicated by dashed lines) plays an important role in the stabilization of PEG conformational transition between the two states in aqueous solution under applied force

The general form for the e-FJC model of polymer stretching is given in Equation 2.

$$x(F) = L_c\left[\coth\left(Fl_k/k_BT\right) - k_BT/Fl_K\right] + N_S\frac{F}{K_S} \qquad \text{Equation 2.}$$

In Equation 2, N_S is the number of segments and K_S is the segment elasticity. Due to the conformational transitions described above, this equation does not fully describe PEG stretching in aqueous solution. To resolve this issue, one must calculate the total contour length (L_C) of the stretched PEG from the lengths of both of its segments, helical (*ttg*) and planar (*ttt*):

$$L_c = N_{planar}L_{planar} + N_{helical}L_{helical} \qquad \text{Equation 3.}$$

Where L refers to the segment length of each conformation and N refers to the number of segments existing in that particular conformation. The values of $L_{helical}$ and L_{planar} for PEG in aqueous solution are 2.80 Å and 3.58 Å, respectively.[28] If $N_{helical}$ and N_{planar} were also fixed values independent of the applied force then the contour length describes the distance between the two polymer ends attached between the AFM tip and the surface thus determining the overall extension length of the force curve. However, the ratio of the total number of monomers is dependent on the force and described as:

$$\frac{N_{helical}}{N_{planar}} = e^{\Delta G(F)/k_B T} \qquad \text{Equation 4.}$$

where:

$$\Delta G(F) = \Delta G_0 - F\left(L_{planar} - L_{helical}\right) \qquad \text{Equation 5.}$$

In this equation, $\Delta G(F)$, the difference in free energy between the two conformations, is the force-dependent parameter and ΔG_0, the energy difference at zero applied force, is fixed at 7.45 kJ/mol.[28] Combining the previous equations (Equations 2, 4 and 5), the extension-force relation describing PEG in aqueous solution (e-FJC$_{PEG}$) is then given by:

$$x(F) = N\left(\frac{L_{planar}}{e^{+\Delta G/k_B T}+1} + \frac{L_{helical}}{e^{-\Delta G/k_B T}+1}\right)\left[\coth\left(\frac{Fl_K}{k_B T}\right) - \frac{k_B T}{Fl_k}\right] + N\frac{F}{K_s} \qquad \text{Equation 6.}$$

Stretching models are used in force measurement data analysis when PEG is used as the spacing linker. For example, when PEG is used as the linker tethering biomolecules between an AFM tip and a sample surface, the e-FJC model is used to fit the resulting

force curves. The fitting parameters thus obtained (*i.e.* Kuhn length, contour length and segment elasticity) are used to evaluate the force curves. If these values correspond well with the literature values for PEG (L_K *ca.* 7 Å, L_C depends on the length of PEG used and K_S *ca.* 150 N/m)[28] then the force curves indeed represent PEG stretching and this particular event can be used for subsequent data analysis. When the force measurements are carried out in order to address the unbinding of molecular bio-partners, the events of interest are rupture forces which are extracted from the selected force curves (after fitting).

1.4.4. Histograms

To have confidence in single-molecule studies, one must collect hundreds, if not thousands, of events. In the case of SMFS for studying the unbinding of molecular bio-partners, one must use a systematic method to evaluate the collected rupture forces. Calculating the mean force is an approximation that most probably is incorrect since the mean of a distribution is a function of all data, with equal probability. However, within one force experiment, there may be measurements that do not represent the ideal interaction between single molecules and including these values in calculating a mean can sometimes lead to incorrect conclusions. In order to avoid such error, with each rupture force value being a sample within a continuous distribution, a histogram is created placing each of the force values in a class, or *bin* of fixed size. The question becomes what bin size to choose. Various methods have been proposed for bin size selection and application of a theoretical study of synthetic data showed Scott's rule,[85]

described by Equation 7, to be very accurate and useful for both Gaussian as well as non-Gaussian distributions.[86]

$$h_N = 3.49\sigma N^{-1/3} \qquad \text{Equation 7.}$$

In this equation, σ is the estimate of the standard deviation among the collected data, N is the number data points used to construct the histogram and h_N is the calculated bin width.

1.4.5. Binding Kinetic Parameters

Over the past decade, the field of SMFS has advanced not only in theory, but also in experimental practice and data analyses. Developments have shown the possibility of measuring kinetic parameters for biomolecular interactions, including dissociation rates and change of energy over transition states.[87-89] When studying biomolecular interactions using SMFS, force is applied to binding partners by tethering one member of the interacting pair to the AFM tip and the other to a surface, and then extending and detaching the pair. According to the theory, introduced by Bell[90] and expanded upon by Evans and Ritchie,[87] measuring the rupture force of the biomolecular interaction at variable probe loading velocities allows defining their kinetic parameters, specifically the dissociation rate k_{off} and the distance between the binding complex and the transition state x_β. The equation that links these parameters together is given by:

$$f^* = \frac{k_B T}{x_\beta} \ln\left(\frac{x_\beta}{k_{off} k_B T}\right) + \frac{k_B T}{x_\beta} \ln r_l \qquad \text{Equation 8.}$$

In this equation, r_l is the loading rate which is the product of the probe velocity (nm/s) and the spring constant (pN/nm) and f^* is the most probable rupture force estimated from the histogram of a set of measurements performed at a specific probe velocity. Plotting f^* versus the logarithm of the loading rate $\ln r_l$ displays a linear relationship from which the k_{off} can be estimated from the intercept of the vertical axis (*i.e.* when $\ln(r_f) = 0$) where x_β can be estimated from the slope.[91,92] The dissociation rate k_{off} is related to the lifetime τ_0 of the complex ($\tau_0 = k_{off}^{-1}$), and provides information on the specificity of the interaction. It is important to keep in mind that a linear relationship between the logarithm of the loading rate and the unbinding force is characteristic only for a single-energy barrier interactions in the thermally activated regime. In addition, the velocity at which the force can be varied is limited by the mechanics of the SMFS instrument, usually between 10 and 5000 nm/sec, before thermal drift or hydrodynamics become significant.[86]

A procedure for the determination of the association rate k_{on} was also described in the literature, which allows for calculating the association constant ($K_a = k_{on}/k_{off}$) providing information on the affinity of the interacting bio-partners.[1]

SMFS measurements probe single biomolecular interactions, which means that thermal fluctuations can significantly affect the strength of rupture forces. Noy and co-workers studied the effect of temperature dependence on tip-sample interaction strength and developed a quantitative interpretation, as described in Equation 9.[93]

$$f = \frac{\Delta H}{x_\beta} - \frac{\Delta S}{x_\beta} T - \frac{k_B T}{x_\beta} \ln\left[\frac{k_B T}{r_f \tau_D x_\beta}\right] \qquad \text{Equation 9.}$$

Where τ_D represents the inverse of the diffusion-limited frequency and x_β is the distance to the transition state. The first two terms in Equation 9 represent the enthalpic and entropic energy contributions to the interaction strength, respectively, and the third represents the thermal motion contribution. This means that the first two terms represent a true energy-barrier contribution whereas the third term represents what can be considered as 'thermal weakening' of the binding strength between two interacting species where thermal fluctuations help the system cross over the activation barrier thus breaking at a lower rupture force. This explains why at higher temperature and/or higher loading rates unbinding forces appear to be lower.[86]

In summary, chemically modifying probes and surfaces opens the door for SMFS measurements to reveal new exciting information regarding the strength and the kinetics of biomolecular interactions. In addition, this approach allows one to address the influence of different environmental factors on the strength of these interactions. In general, considerations in both experimentation and data analysis must be taken into account in order to accurately apply the theory.

1.5. Summary and Goals

The main goal of the present study is to address a variety of biomolecular interactions using the outlined principles of SMFS. In particular, the technique was used to investigate the binding in four types of biomolecular interactions: (*i*) the DNA double

helix, (*ii*) the biotin/streptavidin interaction, (*iii*) the concanavalin A/mannose interaction and (*iv*) the two coils in a synthetic E/K-coiled-coil system.

Biomolecular interactions are governed by a complex collection of intermolecular and interfacial forces forming specific non-covalent contacts. The four systems chosen for this investigation represent distinct types of biomolecular interactions, which are controlled by the chemical and physical structures of the biomolecules and are highly influenced by their environment. In order to investigate their binding interactions by SMFS, the immobilization of these biomolecules between the AFM tip and a surface is required. The surface chemistry by which the different biomolecules are covalently coupled to AFM tips is described in Chapter 2. The fundamental requirement for using molecular spacers when functionalizing AFM tips with biomolecules is achieved by using a family of bifunctional PEG spacers. The synthesis, characterization and chemistry for attaching these versatile PEG molecules are also described in Chapter 2. Specific recognition and binding between the biomolecules in each of the above mentioned systems is measured by carrying out force measurements as described in the previous sections. Each of the following chapters will include a brief introduction for the particular biomolecular system under investigation as well as a detailed description of the experimental set up that was used, followed by a discussion of the data analysis and results (Chapter 3 – Single molecule force spectroscopy of DNA, Chapter 4 – Single molecule force spectroscopy of biotin/streptavidin, Chapter 5 – Single molecule force spectroscopy of concanavalin A/mannose & Chapter 6 – Single molecule force spectroscopy of the E/K coiled-coil).

Chapter 2. Experimental

2.1. Materials

2-Thiopyridone, 3-mercaptopropionic acid, triethanolamine, *N,N*-dimethylglycine, pyridine, dicyclohexylurea, triethylamine, triethanolamine, dimethyl formamide, pyridine, *N,N,N',N'*-tetramethyl-*O*-(*N*-succinimidyl)-uronium tetrafluroborate, Tween®-20, streptavidin, *d*-biotin, and concanavalin A (*Canavalia ensiformis*, Jack Bean, Type VI), were all purchased from Sigma-Aldrich Chemicals (Canada Ltd.) and used as received. Lambda DNA/*Eco* 91I (*Bst* EII) Marker 15 was purchased from Fermentas (Canada). *O*-phenylenediamine•2HCl, used for UV-assays, was purchased from Fluka (Canada). Ultra pure silica gel (particle size: 40 – 60 μm; pore diameter: 60 Å), used for column chromatography, was obtained from Silicycle (Canada). Silica gel plates (0.25 mm) were purchased from Sigma-Aldrich Chemicals (Canada Ltd.) VECTABOND™ reagent, used for surface amination, was purchased from Vector Laboratories (Canada), and aliquots (50 μL) were stored at –20 °C until used. NHS-PEG3500-Biotin and NH_2-PEG3500-COOH•HCl polymers were purchased from JenKem Technology (USA). CH_3O-PEG750-NHS, CH_3O-PEG5000-NHS and NHS-PEG6000-NHS polymers were purchased from Rapp polymere GmbH (Germany). HS-PEG3400-Biotin was purchased from Nanocs Inc. (USA). Hellmanex, used for cleaning glass surfaces, was purchased from Sigma-Aldrich (Canada Ltd.). Chromium pellets (57 x 3.2 mm) were purchased from Ted Pella Inc. (USA) and gold (1 g bullion, 999.9 purity) was from Istanbul Gold Refinery (Turkey). Substrates used to prepare functionalized surfaces include glass

microscope slides (Bio Nuclear Diagnostics Inc., Canada), muscovite mica sheets (Ted Pella Inc., USA) and silicon wafers (Wafer World Inc., West Palm Beach, FL). Additional materials required to conduct ConA force experiments (PEG20000, perfluorophenylazide-disulfide and perfluorophenylazide-mannose) were generously supplied by Dr. Olof Ramström (KTH Royal Institute of Technology, Sweden). [94]

K-coil surfaces[95], cysteine-tagged E-coil peptide (5 heptad repeats)[96], epidermal growth factor (EGF), epidermal growth factor receptor (EGFr),[97] carboxymethylated dextran (CM4) sensor chips and the amine coupling kit (NHS, EDC, and ethanolamine) used for the SPR assay were generously provided by Prof. G. De Crescenzo (École Polytechnique de Montréal, Canada). Cysteine-tagged K-coil peptide (5 heptad repeats)[98] was generously provided by Prof. P. Davies (Queens University, Canada).

Other common chemicals used in this work were either purchased from Sigma-Aldrich Chemicals (Canada Ltd.) or Fisher Scientific (Canada).

2.2. Instruments and Techniques

A UV-ozone oven (UVO-Cleaner, Model No. 342, Jelight Company Inc, USA) was used for cleaning AFM tips. AFM imaging was carried out using a Digital Instruments' Nanoscope IIIa (Santa Barbara, CA, USA) operating with NanoScope version 6.13r software. Single molecule force experiments were carried out using an Asylum Research MFP-1D (USA) operating with IgorPro version 4.0.9.0 software, or a Digital Instrument's AFM equipped with the PicoForce control module. Silicon nitride NP-20 probes were used for AFM imaging and silicon nitride triangular Microlever Probes MLCT-AUNM were used for single molecule force experiments; both were purchased

from Veeco Probes (Santa Barbara, CA, USA). Analysis of the SMFS results was carried out using *Hooke* software,[99] IGOR Pro version 5.0.4.8 software and Microsoft Excel 2007. Histograms were prepared using OriginPro 8 software. Gold-coating was carried out using a Polaron E 6300 Bench Top Thermal Evaporator equipped with a Cressington crystal balance thickness monitor (USA). Surface plasmon resonance (SPR) experiments were carried out at Prof. G. De Crescenzo's laboratory (École Polytechnique de Montréal, Canada) using a Biacore 3000 instrument (GE Healthcare, Baie d'Urfe, QC). Thickness measurements of silicon surfaces were carried out in the De Crescenzo lab using an automatic M2000 ellipsometer (J.A. Woollam Co. Inc., Lincoln, NE). Contact angle measurements on the same surfaces were carried out using a FTA200 Dynamic Contact Angle Analyzer (First Ten Angstrom Inc., Portsmouth, VA). For all synthesized materials, the recorded R_f values were determined by a standard TLC procedure eluting with the specified solvents. 300 MHz ^{1}H-NMR spectra were recorded at room temperature on a Inova Varian 300 spectrometer (Cary, NC, USA). The residual proton signals of the deuterated solvent were used as internal standards ($CDCl_3$: δ (^{1}H) = 7.27 ppm). The following notation is used for the ^{1}H-NMR splitting patterns: singlet (s), doublet (d), triplet (t), mutiplet (m) and broad signal (bs). ^{1}H coupling constants are given in Hz and the values are for three-bond coupling protons. UV irradiation was achieved using a Rayonet photochemical reactor equipped with 300 nm lamps (Southern New England Ultraviolet Company, Middletown, Connecticut, USA). UV quantitative assays were carried out using a Varian Cary 1 UV-Vis Spectrophotometer (Cary, NC, USA).

2.3. Buffers and Aqueous Reagents

All buffers were prepared using Milli-Q water and were sterilized through a 0.2 μM filter (Millipore) prior to use.

Table 2. List of buffers

Buffer	Components	pH*
A	100 mM NaH_2PO_4	6.0
B	600 mM NaH_2PO_4	6.0
C	100 mM H_3PO_4	2.0
D	50 mM NaCl, 1 mM EDTA	7.5
E	100 mM $Na_2B_4O_7$	8.5
F	100 mM $(PO_4)^{-3}$**	7.0
G	100 mM CH_3COONa, 1 M NaCl	4.5
H	50 mM NaH_2PO_4, 100 mM NaCl, 1mM EDTA	7.5
I	25 mM $(PO_4)^{-3}$**	8.0
J	25 mM $(PO_4)^{-3}$**	5.0
K	10 mM Tris, 150 mM NaCl, 1mM EDTA	8.0
L	50 mM $C_5H_7O_5COOH$	5.5
M	50 mM DMG, 100 mM NaCl, 1.0 mM $CaCl_2$ and 1.0 mM $MnCl_2$	6.0
HBS	20 mM HEPES, 150 mM NaCl	7.4
PBS	5 mM NaH_2PO_4, 150 mM NaCl	7.4
PBT	0.5% Tween®-20 in PBS	7.4

* pH was adjusted using either NaOH (aq.) or HCl (aq.)

** Prepared by adding the appropriate amounts of NaH_2PO_4 and Na_2HPO_4

2.4. Synthesis

2,2'-dithiodipyridine, 3-(2-pyridyldithio)-propionic acid, *o*-succinimidyl-3-(2-pyridyl)-dithiopropionate, as well as *N*-hydroxysuccinimate-poly(ethyleneglycol)-3-(2-pyridyldithio)-propionate[73] were synthesized according to literature procedures as described below.

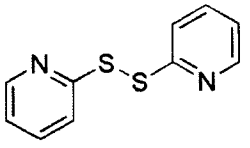

2-thiopyridone (2,2'-DTDP)

2,2'-DTDP: 2-thiopyridone (22.4 g, 200 mmol) was dissolved in water (600 mL) and cooled to 15 °C. The cooling bath was removed and a mixture of water (155 mL) and 30% H_2O_2 (155 mL) was gradually added and stirring was continued for a period of 30 minutes. At 0, 15 and 30 minutes, 200 µL aliquots of the reaction mixture were diluted with 20 mL of Buffer A and the insoluble product was filtered. The reaction was followed by monitoring the absorbance at 343 nm reflecting the presence of 2-thiopyridone (ξ_{343} = 8080 $M^{-1}cm^{-1}$). The reaction was stopped when the absorbance no longer changed (Abs = 0.19 A.U.). Subsequently, the solution was cooled to –4°C and the precipitated product was collected by filtration and then washed with ice-cold water (50 mL). Drying under vacuum overnight yielded 2,2'-DTDP (19.2 g, 87 mmol, 87%); R_f = 0.86 (silica; $CHCl_3$/MeOH/H_2O (70:30:4).

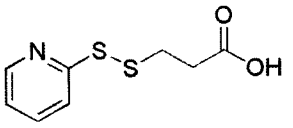

3-(2-pyridyldithio)-propionic acid (PDP-OH)

PDP-OH: In a 500 mL 3-neck flask, 2,2'-DTDP (15 g, 68 mmol) was dissolved in ethanol (100 mL). Subsequently, 37% HCl (20 mL) and water (100 mL) were slowly added with stirring. The flask and the attached addition funnel were flushed with argon. Ethanol (20 mL) and 3-mercaptopropionic acid (4.74 mL, 55 mmol) were mixed in the addition funnel under argon and this solution was added slowly to the 2,2'-DTDP solution with vigorous stirring. After 15, 30 and 40 minutes, 10 μL aliquots were withdrawn and mixed with Buffer B (10 mL) and filtered from insoluble material. The reaction was followed by monitoring the absorbance at 343 nm, which reflected the presence of 2-thiopyridone (ξ_{343} = 8080 $M^{-1}cm^{-1}$). The reaction was stopped after 40 minutes when the absorbance no longer changed (Abs = 1.1 A.U.). The volume was reduced under vacuum to 25 mL keeping the rotatory evaporator bath temperature below 20 °C. Afterwards, chloroform (50 mL) was added to this solution and the pH was gradually raised to 7.5 with 15% Na_2CO_3 (*ca.* 100 mL). The mixture was then transferred into a separatory funnel, the organic layer was collected and the aqueous layer was further extracted with chloroform (6 x 20 mL). The combined organic phase was taken to dryness and unreacted 2,2'-DTDP (*ca.* 5 g) was recovered. The pH of the aqueous phase was lowered to 2.5 using concentrated HCl at which point the product, PDP-OH, begins to precipitate. The PDP-OH was subsequently extracted with chloroform (6 x 50 mL), the

organic phase was dried over sodium sulfate (*ca.* 5 g) and filtered. The filtrate was taken to dryness, yielding crude PDP-OH (5.8 g, 27.1 mmol) which contained 3,3'-dithiopropionic acid as a by-product (detected by ^{1}H NMR).

The crude PDP-OH (1.4 g, 6.54 mmol) was purified by flash chromatography on silica (100 g, 44 mm column diameter, *ca.* 30 mL/min) using dichloromethane/methanol (95:5) as eluent (*ca.* 1.5 L was used for both column packing and elution). Pooled fractions (*ca.* 50 mL) yielded pure PDP-OH (1.2 g, 5.61 mmol, 86%); R_f = 0.35 (silica; CH_2Cl_2:MeOH (95:5)); ^{1}H-NMR (300 MHz, $CDCl_3$): δ = 2.80 (t, J = 7 Hz, 2H: C***H*****$_2$**-COOH), 3.07 (t, J = 7 Hz, 2H: S-S-C***H*****$_2$**), 7.13-7.22 (m, 1H: ***H5*** of the pyridyl group), 7.64-7.72 (m, 2H: ***H3*** and ***H4*** of the pyridyl group), 8.50-8.51 (m, 1H: ***H6*** of the pyridyl group), 11.8 (br s, 1H: COO***H***).

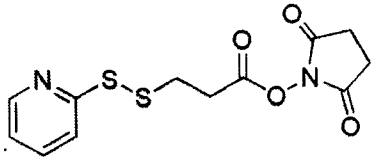

***o*-succinimidyl 3-(2-pyridyl)-dithiopropionate (SPDP)**

SPDP: PDP-OH (1.0 g, 4.7 mmol) and NHS (0.80 g, 7.0 mmol) were dissolved in dry THF (15 mL) at room temperature. The solution was cooled to 0 °C and DCC (1.44 g, 7.0 mmol) was added. Precipitation of a white product (dicyclohexyl urea) was observed. The mixture was stirred for 1 hour at 0 °C and overnight at room temperature. The precipitate was then removed by filtration and the filtrate was taken to dryness under vacuum. The solid residue was recrystallized from isopropanol; the SPDP crystals were kept on ice for 4 hours and then at –20 °C for 3 days. White crystals (1.06 g, 3.4 mmol)

were collected by filtration, washed with cold isopropanol and dried. SPDP (0.5 g, 1.61 mmol) was then applied on a silica column (100 g, 44 mm column diameter, *ca.* 30 mL/min) using dichloromethane/methanol (95:5) as eluent (*ca.* 1.5 L was used for both column packing and elution). Pooled fractions (*ca.* 50 mL) yielded pure SPDP (0.41 g, 1.32 mmol, 82%); R_f = 0.6 (silica; CH_2Cl_2:MeOH (95:5)); ^{1}H-NMR (300 MHz, $CDCl_3$): δ = 2.81 (s, 4H: NHS residue), 3.02-3.14 (m, 4H: S-S-C***H*****$_2$**-C***H*****$_2$**-COOH), 7.05-7.13 (m, 1H: ***H5*** of the pyridyl group), 7.60-7.75 (m, 2H: ***H3*** and ***H4*** of the pyridyl group), 8.47 (d, J = 4.7 Hz, 1H: ***H6*** of the pyridyl group).

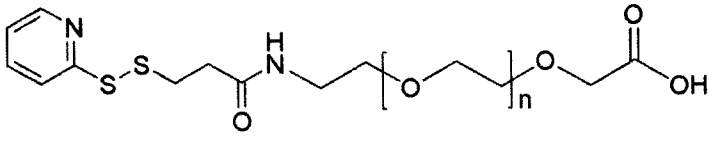

3-(2-pyridyldithio)-propionate - poly(ethylene glycol)- caroboxylic acid (PDP-PEG3500-COOH)

PDP-PEG3500-COOH: NH_2-PEG3500-COOH•HCl (0.50 g, 140 μmol) was dissolved in 6 M NaCl (20 mL), and the pH of the resulting solution was adjusted to 7.5 with 1.25 M NaOH (90 μL). The solution was then extracted with chloroform (5 x 15 mL) and the combined organic layer was dried over sodium sulfate (*ca.* 2 g) and filtered. The filtrate was taken to dryness yielding NH_2-PEG3500-COOH (0.46 g, 130 μmol). To a solution of NH_2-PEG3500-COOH (0.40 g, 110 μmol) in chloroform (4.5 mL), SPDP (0.06 g, 180 μmol) was added under argon. The reaction was initiated by adding excess TEA (60 μL) and monitored by TLC. After 4 hours, the solvent was removed and the solid residue was

redissolved in water (200 mL, pH pre-adjusted to 2.0 using dilute phosphoric acid). The solution was transferred into 50 mL Falcon tubes and centrifuged (10 minutes, 4000 RPM, 1800 g_{max}) in order to remove insoluble material. The supernatant was filtered through a 0.45 μm filter and the pH of the filtrate was increased to 7.7 using triethanolamine. This solution was washed with ethyl acetate (3 x 120 mL) and the resulting aqueous layer was stirred under argon for 3 hours at room temperature in order to hydrolyze unreacted SPDP. The aqueous solution was extracted with chloroform (5 x 100 mL) and the collected organic phase was subsequently washed with Buffer C (3 x 120 mL), dried over sodium sulfate (*ca.* 2 g), and taken to dryness. The resulting solid residue was dried under vacuum overnight yielding PDP-PEG3500-COOH (0.16 g, 43.3 μmol, 31%); R_f = 0.8 (silica; $CHCl_3$/MeOH/H_2O (70:30:4)); ^{1}H-NMR (300 MHz, $CDCl_3$): δ = 2.60 (t, J = 7.1 Hz, 2H: NH-CO-C***H***$_2$-CH_2-S-S), 3.10 (t, J = 7.2 Hz, 2H: NH-CO-CH_2-C***H***$_2$-S-S), 3.64 (PEG), 7.05-7.15 (m, 1H: ***H5*** of the pyridyl group), 7.57-7.66 (m, 2H: ***H3*** and ***H4*** of the pyridyl group), 8.45-8.51 (m, 1H: ***H6*** of the pyridyl group).

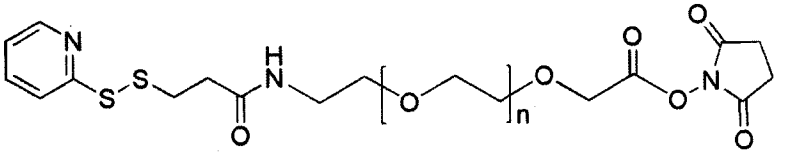

3-(2-pyridyldithio)-propionate - poly(ethylene glycol)- *N*-hydroxy succinimate

PDP-PEG3500-NHS

PDP-PEG3500-NHS: PDP-PEG3500-NHS (0.15 g, 40.6 μmol) was dissolved in DMF (1 mL) under argon and then pyridine (1 mL) was added while stirring. TSTU (0.19 g,

64.5 μmoles) was dissolved in DMF (1 mL) and then added dropwise to the PDP-PEG3500-NHS solution. The reaction mixture was allowed to stir for 2 hours. After this time, most of the pyridine was removed by rotary evaporation without heating. In order to remove the DMF, the solution was frozen in liquid nitrogen and left under vacuum overnight. The obtained white solid was dissolved in a mixture of chloroform (50 mL) and methanol (10 mL), and insoluble material was filtered out. More chloroform (30 mL) was added and then Buffer D (2 x 50 mL) was used to extract the solution. The combined organic layers were washed with water (3 x 20 mL), dried over sodium sulfate (*ca.* 1 g) and filtered. The filtrate was taken to dryness under vacuum yielding pure PDP-PEG3500-NHS (0.14 g, 35. 6 μmol, 87% yield); R_f = 0.7 (silica; $CHCl_3$/MeOH/H_2O (70:30:4)); ^{1}H-NMR (300 MHz, $CDCl_3$): δ = 2.56 (t, J = 7.1 Hz, 2H: NH-CO-C***H*****$_2$**-CH_2-S-S), 2.82 (s, 4H, CO-C***H*****$_2$**-C***H*****$_2$**-CO in NHS residue), 3.04 (t, J = 7.2 Hz, 2H: NH-CO-CH_2-C***H*****$_2$**-S-S), 3.64 (PEG), 7.03-7.13 (m, 1H: ***H5*** of the pyridyl group), 7.61-7.65 (m, 2H: ***H3*** and ***H4*** of the pyridyl group), 8.45-8.46 (m, 1H: ***H6*** of the pyridyl group).

2.5. Surface Plasmon Resonance Assays

SPR assays were conducted at 25 °C, and all immobilization steps were performed at a flow rate of 5 μL/min, using PBT as running buffer. Cysteine-tagged K-coil peptides were immobilized on CM4 sensorchips according to the following procedure. First, the carboxylic groups on the sensorchip surface were activated by injecting a 50 μL mixture of NHS (0.05 M) and EDC (0.2 M) in Buffer E. Afterwards, the NHS esters were converted into amine groups by reacting them with 50 μL ethylenediamine (1 M). The

remaining unreacted NHS ester groups were blocked by injecting 50 μL ethanolamine (1 M). The amine groups available on the sensorchip surface were then reacted with the NHS of the PEG spacer by injecting PDP-PEG3500-NHS (3 x of 1000 nM) in HBS. The PDP groups were then available to react with the cysteine-tagged K-coil peptides (5000 nM) in Buffer F. Finally, 150 μL of freshly prepared cysteine solution (50 mM) in Buffer G was injected in order to block any unreacted PDP sites.

Injecting E-coil tagged EGF protein (100 nM) allowed for immobilization onto these sensorchips through the E/K coiled-coil interaction. EGFr (5 nM) was then injected to amplify the SPR signal. Regeneration of the sensorchip surface and removal of the immobilized proteins was achieved by injecting 50 μL of Gdn•HCl (5 M; 100 μL/min). Finally EGFr was injected once again as a control.

2.6. Tip Functionalization

New silicon nitride cantilevers were cleaned in an ozone oven for 30 minutes prior to functionalization. Cantilevers were aminated by immersion in a solution containing 50 μL VECTABOND™ reagent in acetone (2.5 mL). The amination was allowed to take place for 10 minutes after which time the tips were removed and dipped immediately in chloroform (hereafter referred to as being rinsed). Residual solvent was removed from the tips by allowing the substrate to carefully come into contact with a clean piece of filter paper (hereafter referred to as being dried). Subsequent functionalization was carried out as explained below. All functionalized tips were passivated by using a methoxy-terminated polymer (CH_3O-PEG750-NHS). All functionalized tips were stored

in buffer solution at 4 °C for no more than 3 to 4 days and best results were obtained when functionalized tips were used within several hours of their preparation.

2.6.1. Biotin-Functionalized AFM tips

For functionalization with biotin, the aminated tips were incubated in a chloroform solution containing biotin-PEG3400-NHS (1 mg/mL), CH_3O-PEG750-NHS (250 mg/mL) and TEA (0.5% vol.%) for 1 hour. Subsequently, the tips were rinsed extensively with chloroform (3 x 10 minutes) to remove any unbound polymer. The tips were carefully dried and rinsed with PBS (10 minutes). Functionalization with biotin was also achieved when the aminated tips were incubated in a chloroform solution containing PDP-PEG3500-NHS (1 mg/mL), CH_3O-PEG750-NHS (250 mg/mL) and TEA (0.5% vol. %) for 1 hour. Then, the tips were rinsed extensively with chloroform (3 x 10 minutes) and then with Buffer H (10 minutes). The tips were then incubated in a solution of the same buffer containing biotin-PEG3400-SH (1 mg/mL) for 1 hour. Finally, the tips were washed extensively with Buffer H (3 x 10 minutes), dried and then rinsed with PBS (10 minutes).

2.6.2. E-coil-Functionalized AFM tips

For functionalization with E-coil, the aminated tips were incubated in a chloroform solution containing PDP-PEG3500-NHS (1 mg/mL), CH_3O-PEG750-NHS (250 mg/mL) and TEA (0.5% vol. %) for 1 hour. After which the tips were rinsed extensively with chloroform (3 x 10 minutes), dried and then rinsed with Buffer H (10 minutes). Afterwards the tips were incubated in a solution of the same buffer containing E-coil (*ca.* 10 μM) for 1 hour. Again, the tips were washed extensively with Buffer H (3 x 10

minutes), dried and then rinsed immediately with PBS followed by Milli-Q water (10 minutes each).

2.6.3. ConA-Functionalized AFM Tips

For functionalization with ConA, the aminated tips were incubated in a chloroform solution containing NHS-PEG6000-NHS (1 mg/mL), CH_3O-PEG750-NHS (250 mg/mL) and TEA (0.5% vol.%) for 1 hour. Subsequently, the tips were rinsed extensively with chloroform (3 x 10 minutes), dried and then rinsed immediately with Buffer I (10 minutes). Afterwards the tips were incubated in a solution of the same buffer containing ConA (2 mg/mL) for 1 hour. Again the tips were washed briefly with Buffer I (10 minutes), and then with Buffer J (3 x 10 minutes), in order to remove excess ConA.

2.6.4. Control AFM tips

For control experiments, the aminated AFM tips were incubated in a chloroform solution containing CH_3O-PEG5000-NHS (1 mg/mL) and TEA (0.5% vol.%) for 1 hour. After which, the tips were rinsed in chloroform (3 x 10 minutes) and dried.

2.7. Functionalized Surfaces

2.7.1. DNA-Functionalized Surfaces

A stock solution of lambda DNA/*Eco*91I (*Bst*EII) digest (length distribution 117 – 8454 basepairs) was first diluted using Buffer K to a final concentration of 100 μg/mL. A drop of this solution was spotted on a clean gold-coated glass slide and allowed to incubate for 24 hours in a closed container. The gold surface was then rinsed with a stream of the same buffer (5 minutes) and immediately used for force measurements.

2.7.2. Streptavidin-Functionalized Surfaces

A streptavidin stock solution (1 mg/mL) was prepared in PBS and aliquots (10 μL) were stored at -20 °C. Prior to use, the stock solution was diluted by adding Milli-Q water (90 μL) to reach a final concentration of 0.1 mg/mL. A drop of this solution was then added to a freshly cleaved mica surface for 15 minutes. The mica substrate was then rinsed with a stream of 10% PBS (3 x 10 minutes) and used immediately for force measurements.

2.7.3. K-coil-Functionalized Surfaces

K-coil surfaces were prepared by Dr. Benoit Liberelle in Prof. G. De Crescenzo's group. Silicon surfaces were first aminosilanized using APTES and then cysteine-tagged K-coil peptides were immobilized onto the APTES-coated surfaces using a LC-SPDP spacer. [95,100] The K-coil surfaces were stored at room temperature in a petri dish and cleaned before and after their use by immersion in Milli-Q water (5 x 5 minutes) and then drying with a stream of nitrogen.

2.7.4. Mannose-Functionalized surfaces

A clean gold-coated glass surface was immersed into a CH_2Cl_2 solution of PFPA-disulfide (14 mM) at room temperature in the dark overnight. Afterwards, the surface was rinsed with CH_2Cl_2 (10 minutes) in order to remove excess PFPA-disulfide, and dried with a stream of nitrogen. The PFPA-coated gold surface was immersed into a chloroform solution containing PEG20000 (90 mg/mL) for a period of 30 minutes, after which it was removed and dried with a stream of nitrogen. The surface was then subjected to UV irradiation at 300 nm for 7 minutes. The resulting surface was then sonicated in Milli-Q water (3 x 10 minutes) in order to remove unbound polymer, and

then dried with a stream of nitrogen. The PEG-coated glass surfaces were either used immediately for subsequent functionalization or stored in a closed glass container. For functionalization with mannose, the surface was immersed in a methanol solution containing PFPA-mannose (10 mM) for 5 minutes in the dark, and then removed and dried with a stream of nitrogen. The surface was then subjected to UV irradiation at 300 nm for 7 minutes. Afterwards, the surface was rinsed extensively with a stream of methanol (3 x 10 minutes) in order to remove non-covalently bound mannose, and then dried with a stream of nitrogen. The mannose-coated surface was either used directly for force measurements or stored in a closed glass container for no longer than one week.

2.8. Gold Coating

Prior to gold coating, glass microscope slide were cleaned thoroughly, as described in Section 2.14.1. Using thermal evaporation, the clean glass slides were then pre-coated with 5 nm of chromium followed by 30 nm of gold (for the DNA substrates) or 75 nm of gold (for the ConA substrates). The slides were used immediately for functionalization or stored in a covered container. In the latter case, these slides were cleaned according to the procedure described in Section 2.14.3 prior to further functionalization.

2.9. Contact Angle and Ellipsometry Measurements

All contact angle and dry thickness measurements of K-coil surfaces were performed by Dr. Benoit Liberelle.[95]

2.10. Functionalization of Silicon Chips/Tips

Silicon wafers were cut into small chips (5 x 5 mm^2), and then cleaned as described in section 2.14.4. The cleaned chips were aminated using the same amination procedure described to functionalize AFM tips. Briefly, the chips/tips were first immersed in acetone then in a solution containing VECTABOND™ reagent (50 µL) in acetone (2.5 mL). The amination was allowed to take place for 10 minutes after which time the chips/tips were removed and immediately rinsed with chloroform. The chips/tips were then functionalized as follows: the first group of chips/tips were incubated in a chloroform solution containing Biotin-PEG3400-NHS (1 mg/mL) and triethylamine (0.5% vol.%) for 1 hour. Afterwards, the chips/tips were rinsed with chloroform (3 x 10 minutes) in order to remove any unbound polymer and were then dried. The second group of chips/tips were incubated in a chloroform solution containing PDP-PEG3500-NHS (1 mg/mL) and TEA (0.5% vol. %) for 1 hour. Afterwards the chips/tips were rinsed with chloroform (3 x 10 minutes) and then with Buffer H (10 minutes). The chips/tips were subsequently incubated in a solution of the same buffer containing biotin-PEG3400-SH (1 mg/mL) for 1 hour. Again the chips/tips were rinsed with Buffer H (3 x 10 minutes) and dried. After functionalization with biotin, both groups of chips/tips were rinsed with PBS, followed by PBT (10 minutes each). The chips/tips were then covered with a drop of PBT solution containing ExtrAvidin®-peroxidase (EAP; 10 µg/mL). For tip functionalization, the EAP solution was placed exclusively at the cantilever-end of the substrate. After a period of 15 minutes, the chips/tips were rinsed with PBT (3 x 10 minutes). As a control for non-specific binding, a third group of chips/tips were directly incubated in the EAP solution without prior functionalization with the PEG spacer.

Another group of control chips/tips was prepared by immersing the functionalized chips in EAP solution pre-blocked with *d*-biotin (80 μg/mL in PBT).

The functionalization efficiency was then tested through a quantitative UV assay where a cuvette was filled with the assay mixture (3 mL of 0.8 mg/mL *o*-phenylenediamine•2HCl (OPD) in Buffer L, to which 30 μL of 3% H_2O_2 was added with mixing). All functionalized chips/tips were immersed into the assay mixture and the absorbance at 490 nm was recorded every minute until no changes were observed.

2.11. AFM Imaging

AFM imaging (Tapping mode) was performed in air, using silicon nitride NP-20 tips. A fresh AFM tip was used for each new surface/sample scanned. Image flattening was the only processing used in AFM images.

2.12. Force Measurements (SMFS)

Single molecule force experiments were carried out using an Asylum Research MFP-1D (USA) operating with IgorPro version 8 software or a Digital Instruments' AFM equipped with the PicoForce control module. Silicon nitride triangular Microlever MLCT-AUNM tips from Vecoo (USA) with nomical spring constants of 0.01 – 0.03 N/m were used. The effective spring constant of the cantilever used (C cantilever) was determined at the beginning of each experiment using the thermal noise method from the integral of the resonance peak in the power spectral density plot.[86] In each experiment, several thousand force curves were collected and saved for subsequent analyses. The

cantilever tip was positioned at different areas on the surface, and at least 50 curves were collected at each point.

2.12.1. SMFS of ds-DNA

All measurements were performed at room temperature in Buffer K. Upon manual approach of the probe to the sample surface, force curves were collected with a 0.5 – 1.5 nN relative trigger, 1 s surface dwell time and a probe velocity of 200 nm/s.

2.12.2. SMFS of Biotin/Streptavidin

The first set of SMFS measurements for the biotin/steptavidin system was performed using the Digital Instruments' AFM equipped with the PicoForce control module. In these experiments, the vertical velocity was set to 200 nm/s, the z-range was set to 100 nm, the maximum deflection force was set to 50 pN, and the delay time to 2 s. The remaining measurements were performed using the Asylum Research MFP-1D (USA), applying the same experimental settings. All biotin/streptavidin force measurements were carried out in 10% PBS.

2.12.3. SMFS of E/K Coiled-Coil

All measurements were performed at room temperature in PBS. Upon manual approach of the probe to the sample surface, force curves were collected with a 200 pN relative trigger, 1 s surface dwell time and probe velocities of 400, 800, 1200 and 1600 nm/s.

2.12.4. SMFS of ConA/Mannose

All measurements were performed at room temperature in Buffer M. Upon manual approach of the probe to the sample surface, force curves were collected with a 200 pN relative trigger, 1 s surface dwell time and a probe velocity of 400 nm/s.

2.13. Data Analysis

Data analysis was performed using *Hooke* software[99], IGOR Pro version 5.0.4.8 software and Microsoft Excel 2007. Force curves exhibiting typical tether stretching events were identified. The individual rupture events were fit with a simplified extended freely jointed chain model (e-FJC$_{PEG}$), as described below to extract the tether Kuhn length and the maximum rupture distance.

The e-FJC model describing PEG stretching in aqueous solutions is given by Equation 6:

$$x(F) = N\left(\frac{L_{planar}}{e^{+\Delta G/k_BT}+1} + \frac{L_{helical}}{e^{-\Delta G/k_BT}+1}\right)\left[\coth\left(\frac{Fl_K}{k_BT}\right) - \frac{k_BT}{Fl_k}\right] + N\frac{F}{K_s} \qquad \text{Equation 6.}$$

From the slope of the curve at the high-force region, the segmental elasticity K_s was measured to be equal to *ca.* 150 N/m. Taking into account the number of segments in the PEG chains used in the experiments, calculated according to Table 3

Table 3) and the relatively low rupture forces obtained (*ca.* 100 pN), the last term in Equation 6 adds no more than *ca.* 0.05 nm to the overall extension at maximum applied load and was therefore removed in the data analyses. In this case, considering the maximum rupture distance ($L_{c,\max}$) to be the number of total segments (N) multiplied by the length of the extended polymer (L_{planar}), a simplified version of the e-FJC$_{PEG}$ equation can be written as:[101]

$$x(F) = L_{c,\max}\left(\frac{1}{e^{+\Delta G(F)/k_BT}+1} + \frac{L_{helical}}{L_{planar}}\frac{1}{e^{-\Delta G(F)/k_BT}+1}\right)\left[\coth\left(\frac{Fl_K}{k_BT} - \frac{k_BT}{Fl_K}\right)\right] \quad \text{Equation 10.}$$

This model was applied to fit the force curves with two free parameters: the maximum rupture distance $L_{c,\max}$ (*i.e.* maximum polymer length) and the Kuhn length. The Kuhn length was set as the free parameter to obtain the best fit to the data near the rupture force. The force curves with tether Kuhn lengths and maximum rupture distances in agreement with literature values (L_K = 7Å and $L_{c,\max}$ estimated according to Table 3) were selected for subsequent analyses. The rupture forces as well as distances were binned into histograms prepared using OriginPro version 8 software. A Gaussian fit was applied to each histogram in order to determine the most probable events. The quality of the fit was defined by the standard deviation. This value was used to represent error bars in force *versus* applied loading rate curves. The dependency of force on loading rate was used to calculate the kinetic binding parameters according to Equation 8:

$$f^* = \frac{k_BT}{x_\beta}\ln\left(\frac{x_\beta}{k_{of}k_BT}\right) + \frac{k_BT}{x_\beta}\ln r_l$$

Table 3. Estimated maximum rupture distances for PEG

Polymer	M_W (Da)	Polydispersity	M_n (Da)	Number of monomers	Contour length* (nm)
Biotin-PEG5000-NHS	5147	1.03	5301	120	40
Biotin-PEG3400-SH	3400	N/A	N/A	77	26
NHS-PEG3500-PDP	3555	1.03	3662	80	27

* The maximum rupture distance (*i.e.* length of PEG chain in its full extended state) is estimated using the monomer unit length of 3.36 Å and average weight of 44 g/mol. The effect of polydispersity on the average molecular weight (and therefore number of monomers) was also taken into account according to: polydispersity = M_w/M_n and number of monomers = $M_n/M_{monomer}$.

2.14. Cleaning Procedure

Piranha solution was prepared by carefully adding 3 parts concentrated sulfuric acid to 1 part 30% hydrogen peroxide, by volume. The RCA cleaning solution was prepared by carefully adding 5 parts of Milli-Q water to 1 part 30% ammonium hydroxide and 1 part 30% hydrogen peroxide, by volume. Extreme care was taken in preparing and using these solutions as they are very reactive.

2.14.1. Glassware Cleaning Procedure

All glassware (including microscope slides) was first rinsed with acetone and then sonicated for 30 min in 2% Hellmanex solution at 50 °C. The glassware was rinsed with Milli-Q water (5 x), and was subsequently incubated for 30 minutes in the RCA cleaning solution at 50 °C. The glassware was then rinsed again with Milli-Q water (5 x) and dried in an oven prior to immediate use. In the case of glass slides, they were sometimes stored in Milli-Q water for no longer than 5 days prior to use.

2.14.2. AFM Tip Cleaning Procedure

Prior to their functionalization, AFM tips were cleaned in the UV-ozone oven for 45 minutes in order to remove any organic and other oxidizable surface contaminants. The exact time for this cleaning process depends on the power of the instruments used.

2.14.3. Gold-coated Surface Cleaning Procedure

Gold-coated surfaces were incubated in the RCA cleaning solution at 80 °C for 5 minutes. The surfaces were then rinsed with Milli-Q water (5 x) and dried under a stream of nitrogen.

2.14.4. Silicon Chip Cleaning Procedure

Silicon chips were first immersed in a 1:1 mixture of concentrated HCl in MeOH for 30 minutes. The chips were then rinsed with Milli-Q water (5 x) and dried. Afterwards, the chips were immersed in concentrated H_2SO_4 for 30 minutes before rinsing once again with Milli-Q water (5 x) and dried under a stream of nitrogen. The chips were either used immediately or stored in Milli-Q water for no longer than 1 hour.

Chapter 3. Single Molecule Force Spectroscopy of DNA

The mechanical properties of DNA have always attracted the interest of both biologists as well as physicists because the intramolecular forces that control the DNA structure are fundamental to life processes. Experiments where single molecules of double-stranded DNA (dsDNA) or single-stranded DNA (ssDNA) are stretched, and the resulting forces measured, have yielded new information regarding the physical, chemical and biological properties of this essential biomolecule.[102]

The structure of the right-handed DNA double helix, revealed by Watson and Crick in 1953, is arguably the most classical model for intramolecular interactions controlling structure (Figure 21). Hydrogen bonding between the complementary base pairs of the two DNA strands in combination with favourable hydrophobic effects create a stable structure over a wide range of environmental conditions. At the same time, electrostatic repulsion between the negatively-charged phosphate-sugar backbone determines the width and twist of the double-helix. Steric hindrance between the sugar residues favour a twisted stacking, where particular sequences and conditions can result in either A- or Z-DNA conformations instead of the most common B-form (Figure 21).[103]

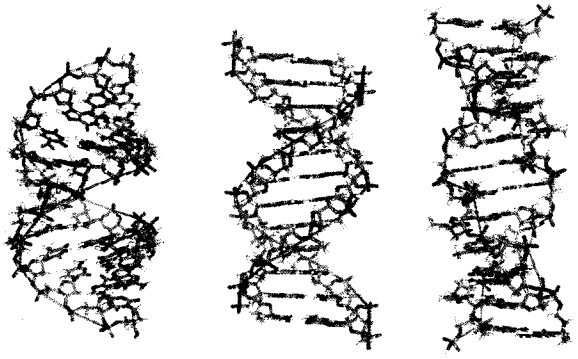

Figure 21. Structures of A, B and Z DNA conformations (from left to right)

Watson and Crick's seminal discovery significantly changed the view of cellular processes including DNA replication and cell division, and ever since, it became clear that a deep understanding of its biological interactions is essential for understanding its functions. Despite its pseudo-random sequence of four different nucleo-bases, DNA is remarkably stable and uniform, acting as an optimal genetic storage carrier. Yet, it is capable of being processed by enzymes (such as topoisomerases, polymerases, helicases, translocases, *etc.*) through tension and torsion, suggesting the relationship of its mechanical integrity to its function. DNA is therefore an ideal candidate for force-based techniques for probing its structural properties and interactions. Single molecule force studies of DNA started about 15 years ago using several techniques including: AFM[104,105], magnetic tweezers,[8] and optical tweezers.[84] In all these experiments, one end of the DNA molecule is fixed and the other end is extended under force (Figure 22).

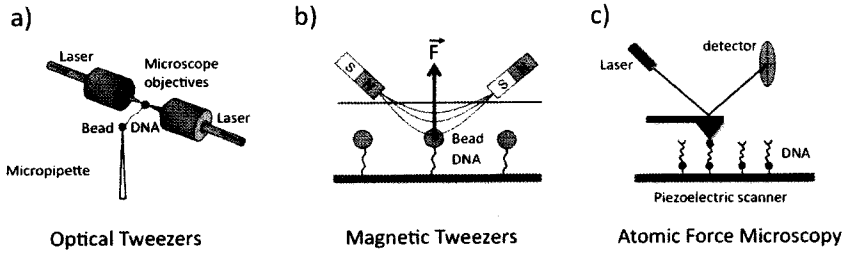

Figure 22. Single molecule force measurements of DNA stretching using (a) optical tweezers, (b) magnetic tweezers, and (c) AFM[102]

This wide range of experiments started in 1992, where the force-extension of dsDNA was addressed using magnetic beads and a salt concentration dependence of its persistence length was demonstrated.[8] A few years later, the Bustamante group used dual beam optical tweezers to access higher forces and complemented their earlier work by revealing a structural transition that takes place in dsDNA at forces higher than 60 pN where the natural B-DNA form overstretches about 1.7 times its contour length.[84] Since the two DNA strands only separate at forces higher than 100 pN, this transition was not attributed to dissociation but rather conversion to another conformation (S-DNA) where the dsDNA overstretches and unwinds; the base pairs unstack but remain hydrogen bonded.[106] More studies showed that a less cooperative conformational transition was observed at 110 pN when the dsDNA is attached to beads and not free to rotate.[107] Figure 23 shows the force-induced melting profile for dsDNA when torsionally constrained or relaxed. While trying to unravel the mystery of DNA overstretching, three more forms, in addition to S-DNA, were encountered: a Pauling-like form (P-DNA), a left-handed helical form (Z-DNA) and a supercoiled sc-P form. It is no coincidence that these unusual conformations may have significant biological relevance. It is indeed speculated that S-DNA may be biologically important, since it would allow easier access to the basepairs for transcription purposes.[107]

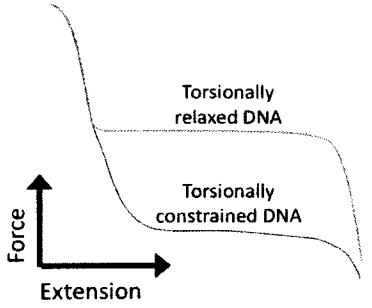

Figure 23. Schematic diagram of DNA force-induced melting transitions: (blue curve) when the DNA is attached by both strands and is therefore torsionally constrained (unable to rotate), and (red curve) when it is torsionally relaxed (able to rotate)[108]

The application of new theoretical models and molecular dynamics simulations has revealed new insights about the molecular details of the overstretching B to S transition.[109,110] Furthermore, the significance of the twist within the double helix structure has been investigated, both theoretically as well as experimentally.[111,112] For example, experiments on unzipping single lambda DNA demonstrated a relation between the unzipping forces and the average basepair content (GC and AT) of the unzipped portion of the molecule.[113] Unzipping synthetic poly(GC) and poly(AT) fragments showed sequence-dependent base pairing forces, where dsDNA fragments with GC content show the overstretching transition about 40 pN higher than those with AT content, an observation consistent with the melting temperature difference measured for these fragments.[104]

In the present study, the principles of SMFS were applied to study the mechanical properties of overstretching dsDNA. The DNA system was chosen as it is very-well studied and easy to prepare. In order to study the DNA overstretching transitions, which only occur at the single molecule level, very low concentrations (100 μg/mL) of lambda-digest dsDNA were allowed to adsorb on a gold surface, without the need for any special

functionalization steps. An individual dsDNA strand was then adsorbed to the AFM tip by applying a force of *ca.* 1 nN and a delay time of 1s. During the retraction cycle of the SMFS measurement, the dsDNA strand is stretched between the tip and the surface and from the deflection of the AFM cantilever, the forces involved in the stretching process can be determined. In fact, this same simple approach has been previously shown to be applicable to study the stability of DNA as a function of temperature, ionic strength and sequence. [104,105] An example of the force curves obtained in experiments where lambda-digest DNA is stretched between the AFM tip and a gold substrate is shown in Figure 24.

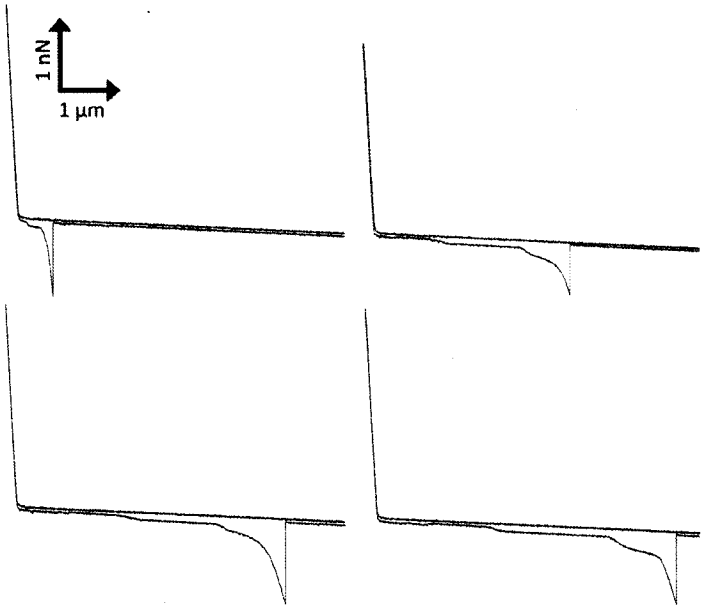

Figure 24. Representative force curves of single molecule force spectroscopy measurements of lambda-DNA (approach is shown in red and retract in blue). Note the different rupture lengths which highlight the distribution in tethering length of the DNA strands between the tip and the surface

The previously-described dsDNA transition was indeed detected when the force reached a threshold in the range of *ca.* 50 – 100 pN. The observed constant-force plateau represents the B to S overstretching transition, which is followed by a more drastic increase in force represented by the rupture peak where the two DNA stands finally

separate or desorb. The force distribution for the overstretching transition, calculated from the plateau height for more than 150 force curves, is shown in Figure 25. Most of the overstretching transition forces appear to be centered about 62 pN. The variable plateau lengths can be attributed to: (*i*) the length distribution of the lambda-DNA used, and (*ii*) the different attachment points of the lambda-DNA on the tip and the surface. In all cases, the detected events occur at a distance far from the surface, supporting the fact that they represent single DNA molecules bridging the AFM tip and the substrate surface, rather than non-specific adhesion.

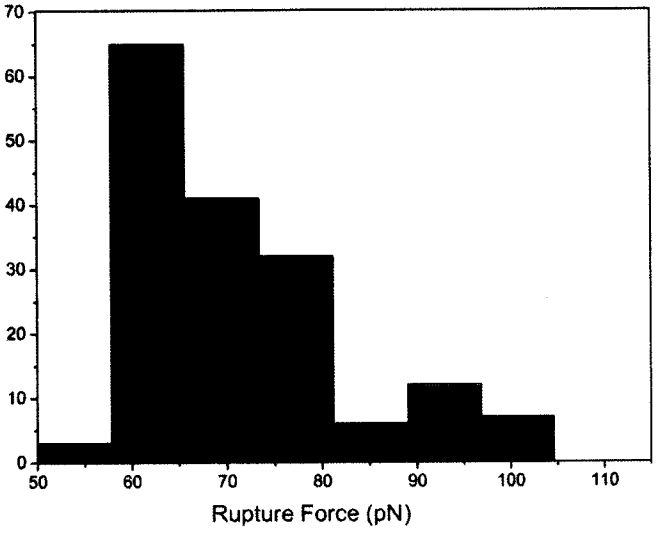

Figure 25. Force distribution histogram for SMFS of lambda-DNA

It is important to note that there are several scenarios that can be envisaged under these circumstances. For example, the dsDNA molecule can attach to the substrate through one strand only and attach to the AFM tip at the complementary strand (*i.e.* the molecule is attached between the AFM tip and the substrate with either both of its 3' ends or both of its 5' ends). In this case, the connection will be lost once the double helix melts and two strands separate from one another. However, if the molecule attaches through only one of

its strands, then melting may or may not lead to detachment from between the AFM tip and the substrate depending on the possibility of single strand disengagement. Finally, if the dsDNA attaches through both of its strands, and after melting the single strands do not detach, then the complete conversion to ssDNA is not possible.[105]

The experiments presented here did not aim to analyze the mechanisms by which DNA undergoes conformational transitions under force, but rather to demonstrate our use of AFM for measuring events at the single molecule level. The fact that the DNA system is very well-studied and experimentally straightforward allowed us a gentle introduction into the field of SMFS, including basic data analysis procedures.

Chapter 4. Single Molecule Force Spectroscopy of Biotin/Streptavidin

All living systems employ both strong as well as weak chemical interactions in order to carry out their functions. Strong covalent bonds are involved in mostly static associations, where enzymes and a source of energy are required for their formation and destruction. In contrast, weak non-covalent interactions (*i.e.* hydrogen bonds, van der Waals interactions, ion-dipole forces, *etc.*) are transitory and more adequate for associations that require rapid formation and dissociation. Although one individual weak bond might not be sufficient, in terms of strength as well as lifetime, for most biological processes, a collection of these cooperative interactions allow the formation of stable, highly specific intra- and intermolecular associations within, for example, proteins and nucleic acids and enzymes with their substrates. Such molecular recognition interactions underlie the spatial architecture and dynamic properties within these biological systems. [3, 4,114] Many biophysical studies have been applied to address biomolecular interactions and, as discussed in Chapter 1, single molecule force-based measurements have allowed the exploration of the biophysical properties governing the interactions within and between biological molecules.

The interaction of biotin with avidin, as well as streptavidin, has been the focus of a large number of force measurement studies, including SMFS.[6,115-120] Chicken avidin and bacterial streptavidin are homotetrameric proteins, having one binding site within each subunit for biotin (vitamin H) (Figure 26). Multiple non-covalent bonds are involved in

the binding of biotin to these proteins, including van de Waals interactions with aromatic side chains as well as multiple hydrogen bonding.[121,122,123]

Figure 26. Schematic representation of avidin, streptavidin and biotin: (a) Chemical structure of biotin, (b) Avidin bound to biotin, and (c) streptavidin bound to biotin. Structures prepared using Pymol[124]

The basis for choosing the biotin/(strept)avidin system as a model for studying receptor-ligand interactions originates from its unique structural and functional features: (*i*) high binding affinity as well as specificity (dissociation constant of 10^{-13} – 10^{-15} M),[125] (*ii*) symmetric features of the (strept)avidin homotetramer enabling its orientation-specific immobilization where biotin binding sites on one side of the tetrameter can be used for immobilization leaving the binding sites on the other side available for investigation, [122,126,127] (*iii*) the extreme stability of the streptavidin tertiary structure,[12] and (*iv*) the presence of a reactive carboxyl group in biotin gives a handle for a variety of immobilization chemistries.[12]

Investigating biomolecular interactions in the biotin/(strept)avidin system using SMFS has been performed by several groups. [3,62,117,119,120,128-133] The first reported SMFS study of the biotin/avidin interaction yielded unbinding forces of *ca.* 160 pN.[117] More SMFS experiments on this system described an energy landscape where there are many nearly isoenergetic minima in the complex dissociation resulting in a variety of possible

unbinding paths and unbinding force values (Table 4).[134] Comparison with experiments performed on mutant forms of the proteins or synthetic derivatives of biotin was used to elucidate the characteristics of this biomolecular interaction.[3,119] Recent measurements where the loading rate was varied 8 orders of magnitude revealed a detailed picture of unbinding forces ranging from 5 pN to 200 pN.[135] The unbinding force of biotin/avidin was found to be *ca.* 20 pN higher than that of biotin/streptavidin, when the operating loading rate was less than 1700 pN/s.[136] A variety of experimental protocols that were used to address the biotin/(strept)avidin interaction are summarized in Table 4.

Table 4. Experimental protocols for measuring the unbinding force between biotin and (strept)avidin[12]

Molecular partners	Experimental protocol	Control experiments	Unbinding force (pN)
Biotin/avidin Biotin/streptavidin[137]	Biotinylated BSA adsorbed on tip, with subsequent avidin or streptavidin adsorption/biotinylated surface	Addition of biotin derivatives	*ca.* 160 – 260
biotin or derivatives/avidin[117]	Biotin derivatives immobilized on surface/biotinylated BSA adsorbed on tip and incubated with avidin	Addition of free biotin or avidin	*ca.* 160
Biotin/streptavidin[138]	Biotinylated BSA adsorbed on glass beads (glued to cantilevers) and mica surface/surface further incubated with streptavidin	Biotinylated BSA surface (without streptavidin) or streptavidin surface pre-blocked with biotin	*ca.* 340
Biotin/streptavidin site-directed mutants[119]	Biotinylated BSA adsorbed on tip and mica surface/surface further incubated with wild-type or mutant streptavidin	Addition of free biotin	100 – 450 (for the different mutants)
Biotin/antibiotin antibody (Ab)[3]	Biotinylated BSA covalently bound to tip *via* linker/Ab covalently bound to surface *via* linker (also reverse configuration)	Non-biotinylated BSA on tip. addition of biotin and streptavidin , use of non-specific Ab on surface	*ca.* 110
Biotin/streptavidin[33]	Biotin covalently bound to nanotube tips/streptavidin linked to surface by biotin groups	Use of unmodified nanotube tips or addition of free biotin	*ca.* 200
Biotin/avidin or streptavidin[134]	Biotin covalently attached *via* linkers to glass beads and surfaces/avidin was further adsorbed to both, such that free biotin groups were still available for binding	Use of linkers that do not bind biotin or addition of free biotin	5 – 250 (depending on loading rate from 0.05 – 60000 pN/s)

In the present study, the biotin/streptavidin system was chosen as a model study in order to apply the principles of SMFS in addressing a biomolecular interaction and to test the efficacy of the AFM tip functionalization strategy used herein. The strong and well-studied binding between biotin and streptavidin, as well as the simplicity of sample preparation with commercially available components were the main reasons behind this choice. The experimental protocol used in this study involved using biotin-functionalized tips and a surface on which streptavidin is adsorbed (Figure 27). Immobilization of streptavidin on mica surfaces was achieved by simply incubating streptavidin at very low concentration (0.1 mg/mL) for short periods of time (*ca.* 15 minutes), in order to minimize surface coverage, followed by extensive washing in order to remove unbound streptavidin. For AFM tip functionalization, heterbifunctional PEG spacers containing NHS at one end, which forms stable amide linkages with aminated AFM tips, were used. The other extremity of the PEG spacers either contained biotin (NHS-PEG-biotin) (Figure 27) or the 3-(2-pyridyldithio)propionyl group (PDP), which was subsequently linked to another bifunctional PEG spacer (SH-PEG-Biotin) through a disulfide linkage to the thiol group (Figure 29). The latter procedure was carried out in order to test the compatibility of the PDP group for functionalization as well as to optimize the experimental conditions required for its attachment. In addition, comparisons between the force results obtained in the different experimental protocols allow testing the reliability of the technique. In either case, the functionalization chemistry carried out specifically attempts to limit the number of active ligands (*i.e.* biotin) on the AFM tip by using an excess of mono-functionalized PEG spacer. Although the tip is coated with PEG, only

those carrying biotin will yield specific and meaningful binding events in the force curves.

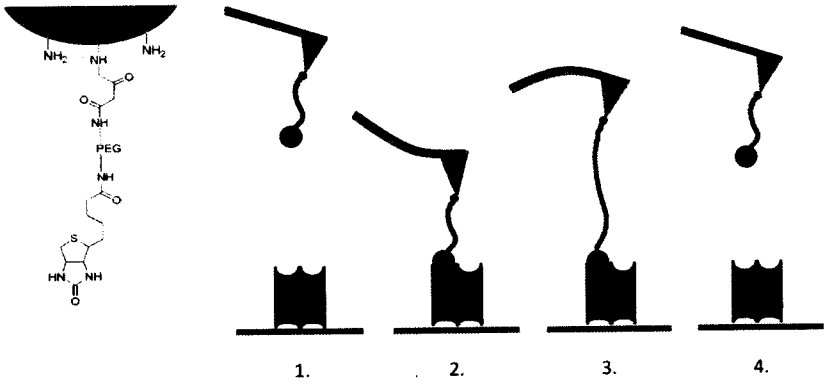

Figure 27. Schematic representation of experimental set up carried out for SMFS of biotin/streptavidin using NHS-PEG-Biotin tether

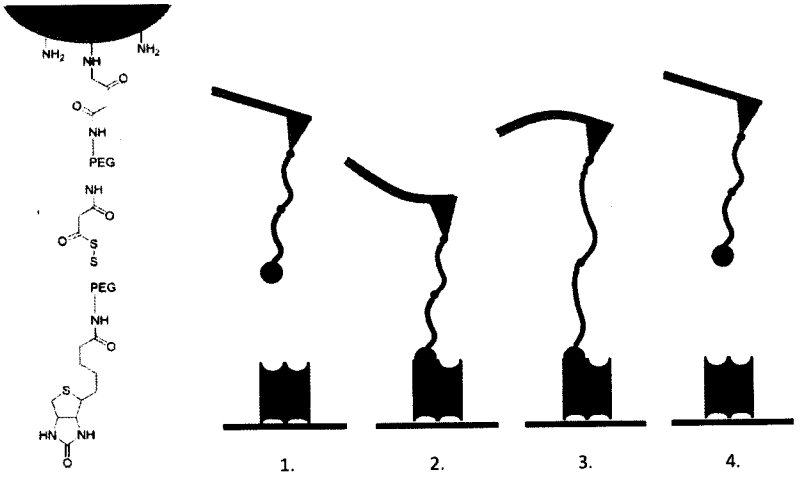

Figure 28. Schematic representation of experimental set up carried out for SMFS of biotin/streptavidin using NHS-PEG-PDP and SH-PEG-Biotin tethers

Interaction forces between single biotin-streptavidin pairs were then measured by SMFS using biotin-functionalized tips and streptavidin-bound mica surfaces. In each force-distance measurement, the biotin-tip was approached to the streptavidin surface and

subsequently retracted. During the approach-retract cycle, the cantilever's deflection, x, which can be directly converted into force, f, using Hooke's law ($f = kx$), was continuously measured and plotted as a function of tip-surface separation. The tip first approaches the surface, the cantilever deflection remains constant, due to the absence of forces acting upon it, until it comes into contact with the surface. Further extension into the surface, coupled with a 1-second delay time, allow the interactions between biotin (on the tip) and streptavidin (on the surface) to be established. Subsequent tip retraction allows the cantilever to relax, however with further retraction it starts to bend towards the surface under the influence of attractive forces (*i.e.* between biotin and streptavidin), which increase with increasing distance until rupture when biotin finally detaches from streptavidin and the cantilever returns to its original position.

The shape of the non-linear rupture peak is determined by the elastic properties of the tethering PEG polymer, whereas the height of the rupture peak is governed by the strength of the biotin-streptavidin interaction at a particular loading rate. When the biotin on the tip does not form an interaction with the streptavidin on the surface, a recognition event (*i.e.* the rupture peak) is absent and both curves (approach and retract) look the same. This is often the case, since the probability of observing single molecule events is very low. However, once events are observed, both the shape and the height of the peak must be taken into account when evaluating the force data. One way to confirm that the observed rupture peaks indeed represent biotin/streptavidin dissociation is to block the interaction with free biotin in the buffer medium. The result of this will be the disappearance of most, if not all, of the specific recognition events and only occasional non-specific adhesion events might be observed. Another control experiment involves the

use of mono-functionalized PEG that do not contain the biotin moiety. Again, this experiment demonstrates the specificity of biotin-streptavidin binding and reinforces the reliability of the force results.

Four representative force curves obtained when NHS-PEG-biotin was used in AFM tip functionalization are shown in Figure 29. The rupture events occur far from the surface, which confirms that they represent specific binding interactions rather than non-specific adhesion interactions which would typically appear close to the surface. This highlights the importance of using molecular spacers in order to distinguish specific recognition events. The distance at which the rupture occurs (*i.e.* rupture distance) corresponds to the length of stretched PEG under the applied force. Therefore the use of a polymer spacer improves the fidelity of the force measurement by uncoupling the non-specific interactions from specific interactions using distance (*i.e.* polymer length). The force curves shown in Figure 29 are normalized to the main rupture peak, and the consistency of their shape highlights that they represent the rupture of the same interaction, in this case the rupture of biotin from streptavidin.

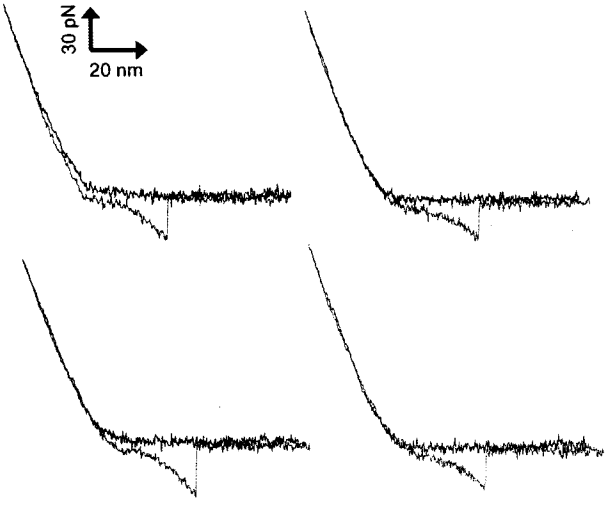

Figure 29. Representative force curves of single molecule force spectroscopy measurements of biotin/streptavidin (approach is shown in red and retract in blue; Set 1)

In the experiment described above, *ca.* 1000 force curves were collected. Featureless curves (*ca.* 70%) were then filtered out and the remaining curves (*ca.* 300) that contained one, or sometimes multiple recognition events, were used for subsequent analysis. As described in Chapter 1, the FJC model was used to fit the rupture peaks in the selected curves (Figure 30, c) and only 10% of the total collected data remained after this second screening process, and were used for determining the unbinding force between biotin and streptavidin. These were the curves where the Kuhn length was between 0.3 and 1.1 nm, and the maximum rupture distance was less than 50 nm. The average Kuhn length of PEG was determined to be 0.75 ± 0.09 nm, which is in agreement to the reported value of 0.7 nm.[28]

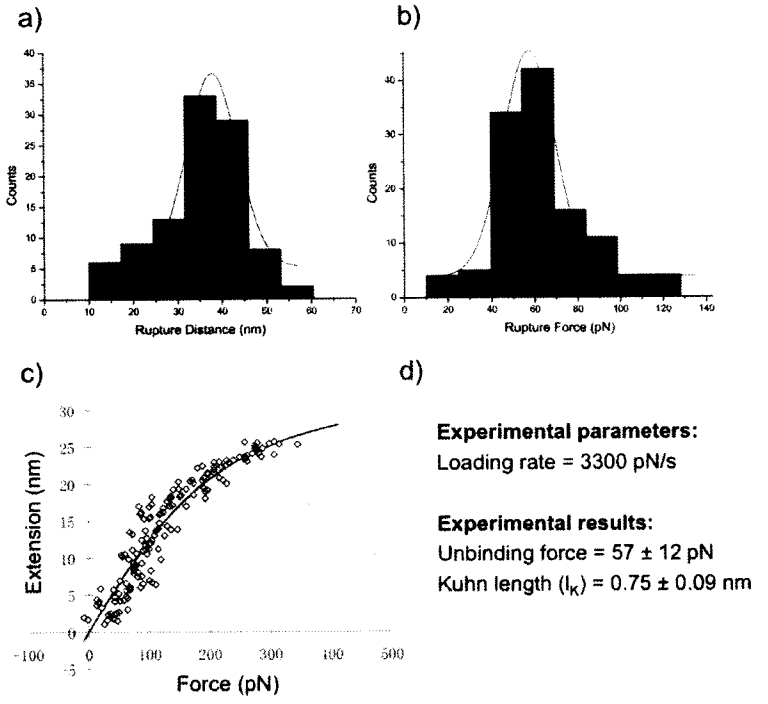

Figure 30. Analysis of biotin/streptavidin SMFS (Set 1): (a) Force distribution histogram, (b) rupture distance histogram, (c) example of fit curve, and (d) experimental details and results

The distribution histogram of the rupture distance, where the applied loading rate was 3300 pN/s, is shown in Figure 30, a. The most probable rupture distance was found to be 38 ± 6 nm by applying a Gaussian fit. The variability in rupture distance can be attributed to: (*i*) the polydispersity of the PEG polymers and more importantly, (*ii*) the different attachment locations of the PEG spacers on the AFM tip. Despite this variability, the measured most probable rupture distance is indeed found to be consistent with the PEG contour length of *ca.* 40 nm. Therefore, the rupture length at which the unbinding force appears provides a means to further discriminate single-molecule rupture events. In other words, events appearing at rupture distances that are much more than the contour length of the PEG used, are not included in constructing the unbinding force histogram.

The same filtered curves were used for calculating the most probable unbinding force. The histogram of the unbinding forces between biotin and streptavidin, measured at a loading rate of 3300 pN/s, is shown in Figure 30, b. The distribution was analyzed using a Gaussian fit to obtain the most probable unbinding force, in this case determined to be 57 ± 12 pN. Variations in the measured rupture force can be attributed to: (*i*) non-optimal binding between biotin and streptavidin, which results in lower forces, and (*ii*) multiple interactions occurring between biotin and streptavidin, which may or may not rupture simultaneously and do not necessarily scale additively, which results in higher forces.[5] There is often a misconception that only one molecule is attached to the AFM tip, however in reality this is definitely not the case. Because of this, a single detected event might actually represent simultaneous rupture of more than one interaction.[101]

Examples of the force curves obtained when NHS-PEG-PED followed by SH-PEG-biotin were used in tandem for AFM tip functionalization are shown in Figure 31. Once again, the rupture events occur far from the surface, which confirms that they represent specific binding events rather than non-specific interactions. In some of the force curves, non-specific adhesion peaks were detected, however these only appear close to the surface. In one experiment, *ca.* 5000 force curves were collected and filtered as described earlier. After fitting using the e-FJC$_{PEG}$ model, only 120 curves (*ca.* 2.5%) remained for subsequent quantitative analysis (Figure 32, c). In these curves the average Kuhn length of PEG was 0.60 ± 0.09 nm which is in agreement to the reported value of 0.7 nm.[28]

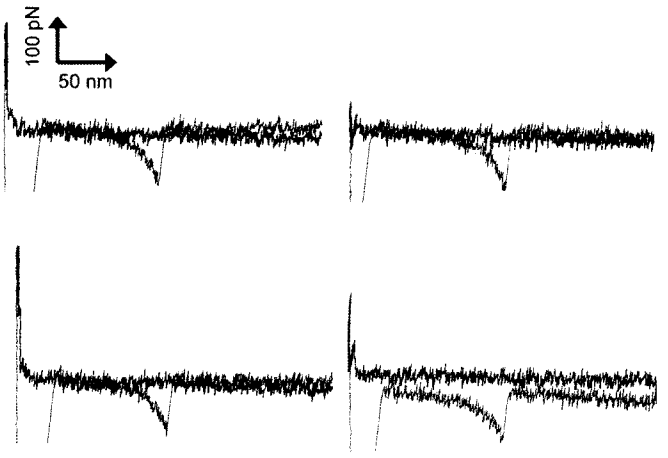

Figure 31. Representative force curves of single molecule force spectroscopy measurements of biotin/streptavidin (approach is shown in red and retract in blue; Set 2)

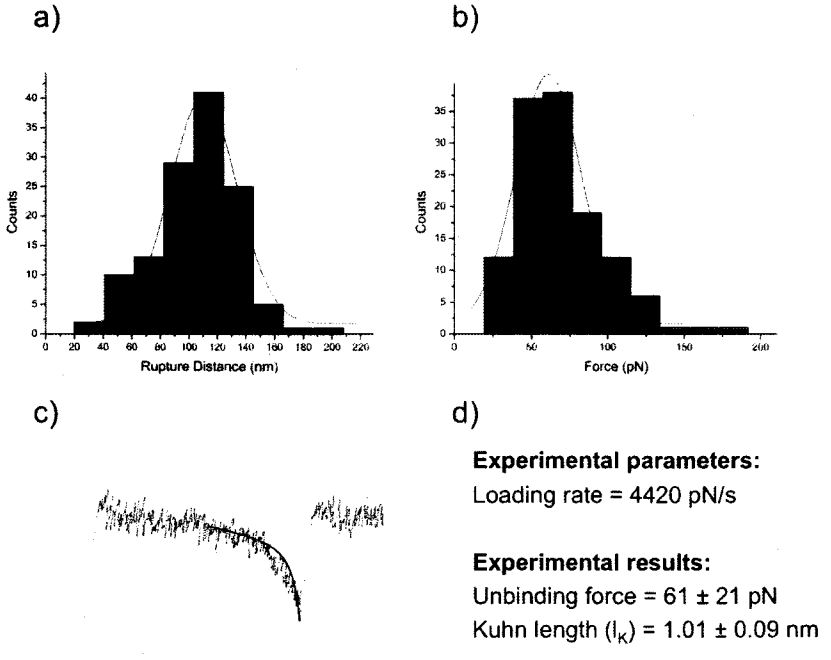

Figure 32. Analysis of biotin/streptavidin SMFS (Set 2): (a) Force distribution histogram, (b) rupture distance histogram, (c) example of fit curve, and (d) experimental details and results

The distribution histogram of the rupture distance of these force curves, where the applied loading rate was 4420 pN/s, is shown Figure 32, a. The most probable rupture distance was found to be 110 ± 23 nm by applying a Gaussian fit. The measured most probable rupture distance was found to be consistent with the combined contour length of both PEGs used (*ca.* 53 nm). Once again, the measured rupture length aided in the discrimination of events that correspond to the interaction between biotin and streptavidin. The histogram constructed from this set of data, measured at a loading rate of 4420 pN/s, is shown in Figure 32, b. The distribution was analyzed using a Gaussian fit to give a most probable unbinding force of 61 ± 21 pN. Variations in the measured rupture force can be expected as discussed above.

The most probable unbinding force for the rupture of the biotin/streptavidin interaction measured with the two different experimental protocols is the same within experimental error. The fact that the obtained results in both experiments are the same confirms the credibility of the technique and verifies the applicability of the PDP group in AFM tip functionalization. The success of this NHS-PEG-PDP spacer confirms its application in tethering a variety of thiol-containing biomolecules to the AFM tip or the surface.[73]

Chapter 5. Single Molecule Force Spectroscopy of Concanavalin A/Mannose

Protein-carbohydrate interactions are of great interest as they play a crucial role in a variety of molecular recognition events involved in biological processes, ranging from cell-cell recognition in viral/bacterial infections, signal transduction, glycoprotein transport, inflammation, organogenesis, and fertilization.[139,140] In addition, these interactions have also been shown to be directly involved in the growth and metastasis of malignant cancer cells.[141,142] Interestingly, the interactions between single carbohydrate ligands with proteins are typically quite weak, and therefore difficult to study.[143,144] However, nature has found a solution for the weak affinity problem by creating multiple concurrent interactions between the carbohydrate sequences that are clustered on cell surfaces, with their protein receptors that have multiple binding sites, resulting in remarkably high binding affinities.[145] In efforts to unravel their highly-significant biological role and to develop new strategies to fight diseases, addressing the mechanisms involved in protein-carbohydrate recognition is essential and widely studied.[36] Measuring protein-carbohydrate interactions at the single molecule level using force spectroscopy is of particular interest for a number of reasons: (*i*) the interactions between these molecules often undergo mechanical stress leading to conformational changes that highly influence their binding properties, particularly amenable to force-based techniques,[146,147] (*ii*) ensemble techniques measure thousands, if not millions of interactions at the same time, and report single averaged values, within which important

aspects of the interactions are often obscured. SMFS offers a solution to overcome this challenge and provides a means to address carbohydrate-protein interactions at their most fundamental level.[147]

In this study, the interaction force between concanavalin A (ConA) and mannose is investigated. ConA belongs to a family of proteins, known as lectins, which recognize and specifically bind different types of carbohydrate sequences. Examples of the sugar moieties recognized by lectins include monosaccharides (*e.g.* mannose, glucose, galactose, *N*-acetyl-glucosamine, fucose) and disaccharides (*e.g.* lactose, cellobiose).[140] Due to their high binding affinity to specific sugar moieties, lectins have been employed in various types of bioassays for studying carbohydrate recognition processes in mitogenic assays, characterization of malignant cells, and purification of glycoproteins, glycolipids and proteoglycans.[148-150]

ConA is a lectin that specifically binds α-mannosyl groups found in sugars, glycoproteins and glycolipids. Extracted from the jack bean *Canavalia ensiformis*, ConA is the first commercially-available lectin that is widely used in biological as well as biochemical applications to characterize and purify sugar-containing entities. Besides being a lymphocyte mitogen, and a stimulant of several metalloproteinases, Con A is thought to be involved in mediating the interactions between α-mannosyl oligosaccharides on HIV viruses and human T lymphocyte cells.[151]

The crystallographic structure of this well-characterized carbohydrate-binding protein is shown in Figure 33. With 237 amino acids and two metal binding sites (Ca^{2+} and Mn^{2+}), ConA forms mainly two anti-parallel β-sheets, one made up of seven strands and the

other of six. The seven-stranded pleated sheet contributes extensively to interactions among the monomer subunits to form dimers as well as tetramers. In each subunit there is a binding site for the sugar adjacent to the metal atoms.[152] Similar to other sugar-binding proteins, ConA binds the saccharide with hydrogen bonds to almost all of its hydroxyl groups.[153] Nitrogen atoms from the amino acids asparagine, leucine, tyrosine, arginine and aspartic acid are involved in binding the saccharide. Aromatic residues, specifically tyrosine, also contribute to the binding through van der Waals interactions.[154] Although not directly involved in the binding, the metal ions, specifically Ca^{2+}, facilitate the binding by organizing the amino acid residues into their required positions in the sugar-binding site, causing ConA to stiffen around the metal ions upon binding.[155,156]

Figure 33. Structure of ConA tetramer bound to mannose. Structure prepared using Pymol[124]

Force spectroscopy studies investigating the interaction between ConA and mannose have been previously reported. [36,48,157,49] Earlier studies reported varying rupture forces: one study measured forces between 75 and 200 pN[157] and another measured a rupture force of 96 ± 55 pN for the single ConA/mannose interaction when the applied loading rate was 4000 pN/s.[49] The variability of these results can be attributed to: (*i*) different loading rates, and (*ii*) the polyvalent nature of the ConA/mannose interaction. In a more

recent study, it was confirmed that the rupture force for multiple carbohydrate interactions with ConA are larger than the rupture for a single interaction and do not necessarily scale additively. By analyzing the tether's stiffness, which is influenced by the multiplicity of the interaction, rupture forces of 46, 68, 85 pN at a loading rate of 10000 pN/s, were attributed to the monovalent, divalent, and trivalent interactions of ConA with mannose, respectively.[36]

In this study, the interaction between ConA and its ligand mannose was addressed using SMFS. For this purpose, ConA was attached to the AFM tip and mannose was immobilized on a surface. After establishing contact between the two functionalized surfaces, the force required to break the contact yields the ConA/mannose interaction strength. Similar to previous work, the use of a homobifuncitonal PEG spacer, specifically NHS-PEG-NHS, allowed the immobilization of ConA and the spatial differentiation of non-specific interactions. The NHS moiety binds ConA by forming amide linkages to its terminal amino groups or surface-exposed lysine residues (Figure 34). As described earlier, the chosen functionalization chemistry limits the number of active proteins (*i.e.* ConA) attached to the AFM tip by using excess of the monofunctionalized PEG, specifically CH_3O-PEG-NHS. In addition, the possibility of homobifunctional NHS-PEG-NHS looping and binding twice to the AFM tips can help passivate much of the tip surface thereby effectively reducing the number of NHS groups available for binding ConA. Also, in order to avoid measuring multiple ConA/mannose interactions, experiments were carried out at pH values lower than 7 (*i.e.* DMG buffer pH 6), since ConA exists as a dimer at this pH.[158] Upon their preparation, the ConA-functionalized AFM tips were extensively rinsed with phosphate buffer at pH 8 and then

at pH 5, in order to remove excess unbound tetrameric ConA.[48] In some of the earlier studies, force experiments were performed in the presence of ConA in the buffer medium assuming that the excess proteins will effectively block most of the interactions. Although this certainly reduces the number of interaction events detected, it does not necessarily guarantee detecting single ConA/mannose rupture events.

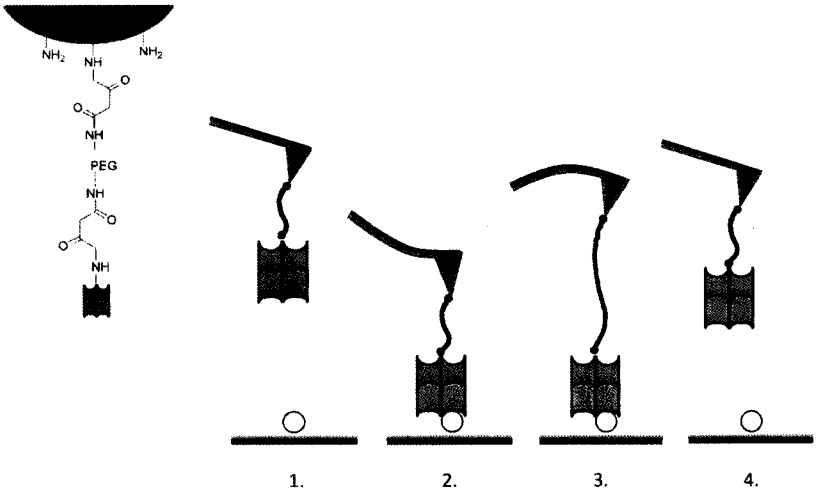

Figure 34. Schematic representation of experimental set up carried out for SMFS of ConA/mannose using NHS-PEG-NHS tether

Recently, a considerable number of different functionalization chemistries have been described for attaching both naturally-occurring as well as chemically-synthesized carbohydrate entities to hard substrates (*e.g.* glass, mica or gold).[159-161] Examples include: (*i*) non-covalent attachment of biotinylated carbohydrates to streptavidin-functionalized dextran matrices,[162] (*ii*) covalent attachment of amino-modified carbohydrates to commercial carboxylated surfaces using conventional EDC/NHS chemistry,[163] (*iii*) covalent attachment of thiolated-carbohydrates to gold-coated surfaces using alkanethiol self-assembled monolayers (SAMs),[164,165] and (*iv*) covalent attachment of thiolated-carbohydrates to gold-coated surfaces using bifunctionalized PEG spacers.[36,48]

A new and versatile strategy, involving the photochemistry of arylazides, was applied in order to immobilize carbohydrates on surfaces.[166] The present study employs this newly described photochemistry for the attachment of modified-mannose to gold-coated surfaces, which has not been used previously for SMFS studies. The method was originally developed to generate ultra-thin polymer films on silicon or gold-coated surfaces for applications including sensors or devices operating under fluidic conditions.[167] The covalent attachment is based on the photochemistry of perflurophenylazides (PFPAs) (Figure 35). When PFPAs are exposed to UV irradiation, their azide functionality gets converted into a nitrene. This highly reactive perflurophenyl nitrene can then insert into any neighbouring C–H or N–H bond.[168]

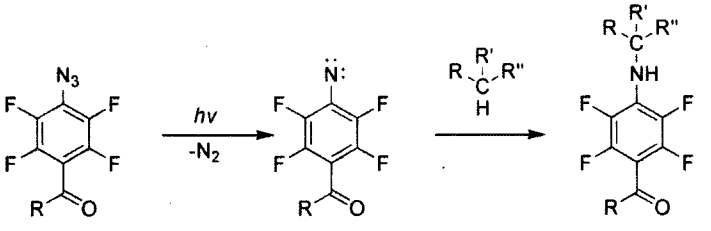

Figure 35. Photochemistry of PFPA

For example a PFPA-modified carbohydrate can be attached to virtually any organic surface with a simple photochemical protocol. The only caveat being that the molecule of interest cannot be sensitive to the wavelength of UV irradiation used. The PFPA photochemical method has indeed been popular for surface modification and introducing functional groups into fullerenes, proteins, polymers as well as carbohydrates.[94,166, 167,169-173] The synthesis of a series of functionalized PFPAs for the development of PEG-modified carbohydrate microarrays has been described by Zhichao *et al.*. The carbohydrate surfaces were then used to study their interactions with different lectins,

including ConA, using the quartz crystal microbalance (QCM) technique.[94,166,172] Following their approach, mannose immobilization on gold-coated glass surfaces was achieved using the same PFPA reagents (Figure 36). The method involves three steps: (*i*) a SAM of PFPA is formed on the gold-coated surface by incubation with disulfide-PFPA, (*ii*) a thin PEG layer is covalently attached to the surface using the PFPA photochemistry, and (*iii*) PFPA-derivatized mannose is attached to this surface *via* UV irradiation.

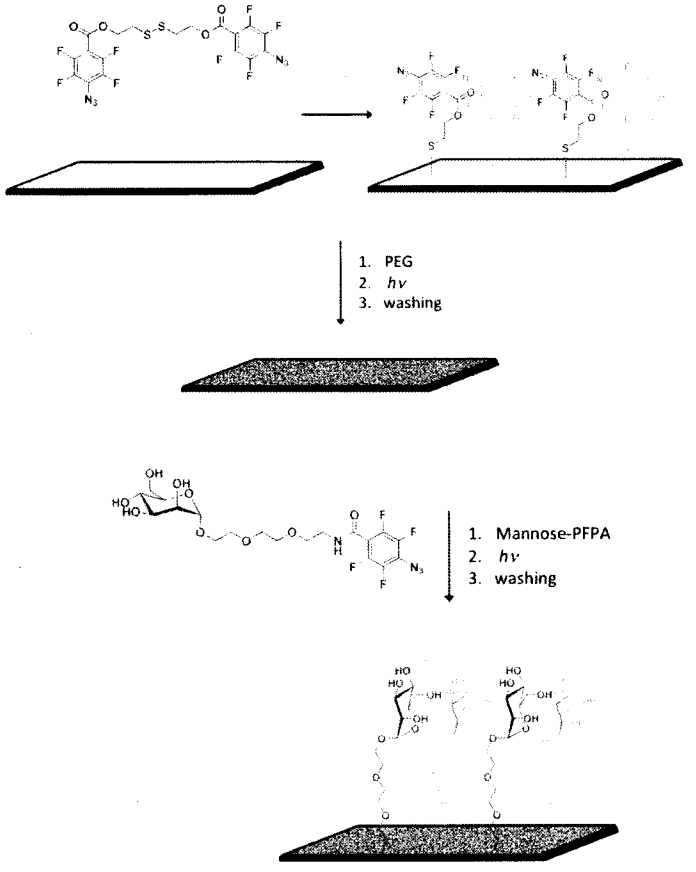

Figure 36. Experimental protocol for mannose immobilization on surfaces using PFPA chemistry

Due to the high-reactivity of PFPAs under UV light exposure, the surface modification chemistry becomes rather simple and quick with only one key requirement, *i.e.* synthesizing the functionalized-PFPAs. The synthetic routes for PFPA-disulfide and

PFPA-mannose which were used in preparing mannose-functionalized surfaces are described in Figure 37 and Figure 38.

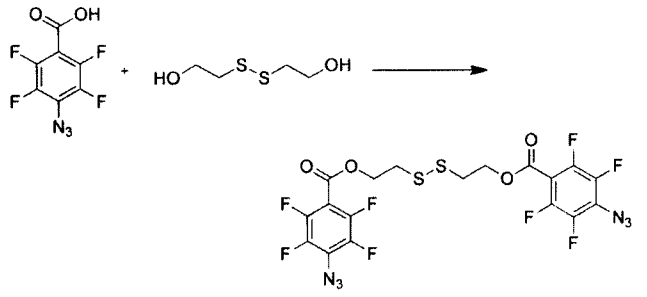

Figure 37. Synthesis of PFPA-disulfide used in mannose surface immobilization

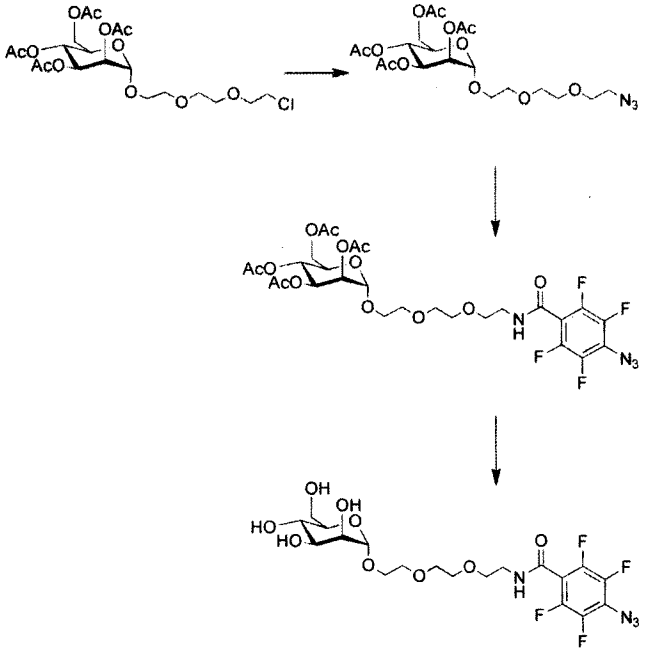

Figure 38. Synthesis of PFPA-mannose used in mannose surface immobilization

SMFS experiments were carried out to measure the interaction strength between the ConA-functionalized AFM tips and the mannose-derivatized surface. The same

experimental approach described for the biotin/streptavidin system (Chapter 4) was used (Figure 34). Examples of the collected force curves are given in Figure 39.

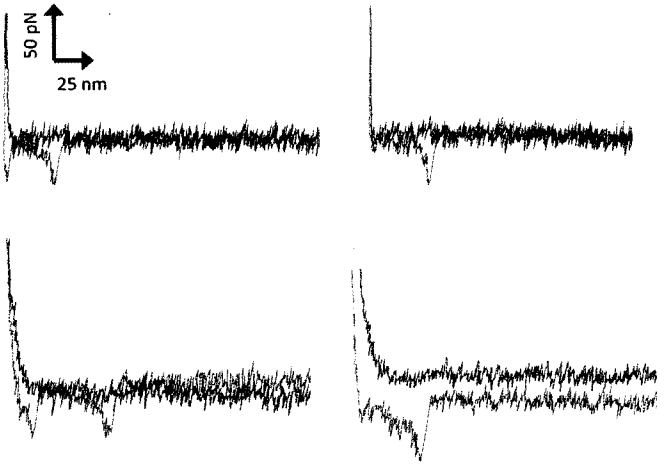

Figure 39. Representative force curves of single molecule force spectroscopy measurements of ConA/mannose (approach is shown in red and retract in blue; Set 1)

A subset of selected force curves, showing rupture events, were fit with the e-FJC$_{PEG}$ model in order to determine if the events were due to breaking the interaction between PEG-attached partners. The analysis process was performed on two different sets of data, using two different AFM tips and two different mannose-surfaces, in order to confirm the reliability of the technique. In the first set of experiments (Figure 40), *ca.* 5000 force curves were collected and only *ca.* 300 curves (*ca.* 6%) were accepted for fitting analysis resulting in a final count of 240 force curves (*ca.* 5%) to be used in calculating the most probable rupture force between ConA and mannose. The average Kuhn length of PEG was 0.56 ± 0.09 nm , which is in agreement to the reported value of 0.7 nm.[28]

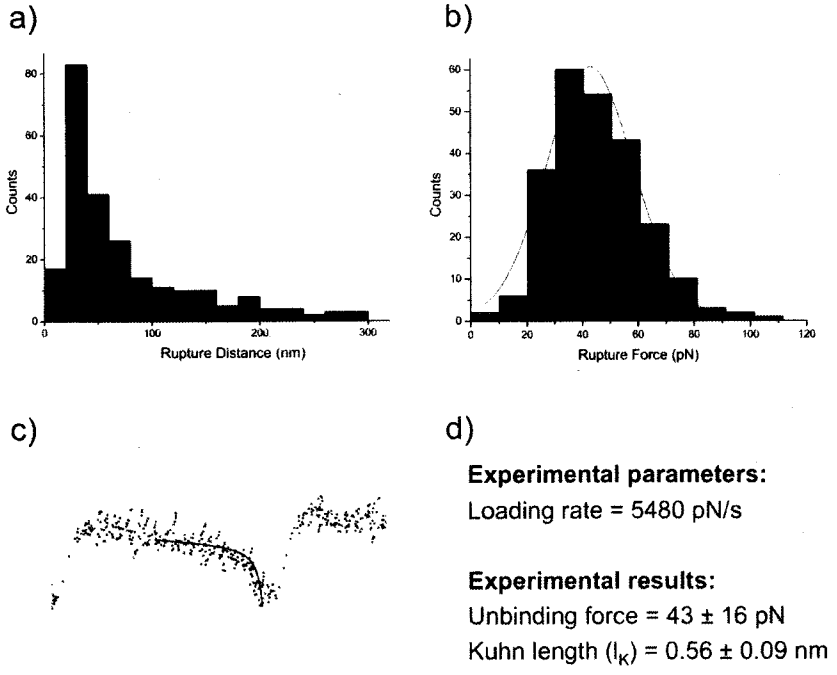

Figure 40. Analysis of ConA/mannose SMFS (Set 1): (a) Force distribution histogram, (b) rupture distance histogram, (c) example of fit curve, and (d) experimental details and results

Long PEG spacers (20000 MW; *ca.* 470 nm) were used in functionalizing the surface with mannose, in addition to the PEG spacer (*ca.* 27 nm) used in attaching ConA to the AFM tip. Considering that the photo-activated PFPA molecules can insert into any C–H bond, varying tether distances are expected throughout the entire surface, with a maximum of *ca.* 500 nm (*i.e.* the combined lengths of both PEG polymers used). This variation manifests itself in the rupture distance histogram as a random distribution. In this case, the rupture distance was not used as a discriminating factor in filtering the force curves. The curves were filtered based only on the Kuhn length value calculated from the e-FJC$_{PEG}$ fit. The distribution of unbinding forces of accepted curves were analyzed using a Gaussian fit resulting in a most probable unbinding force of 43 ± 16 pN, when the

measurement was performed with a loading rate of 5480 pN/s. As discussed previously, variations in the measured rupture force can be due to improper or multiple interactions.

The same experimental parameters were applied in acquiring the second set of data (Figure 41 and Figure 42). Similarly, *ca.* 5% of the collected force curves remained after fitting. The average Kuhn length of PEG was 0.87 ± 0.05 nm , which is in agreement to the reported value of 0.7 nm.[28] The rupture distance distribution obtained in this experiment displays similar results to the first set of data. The rupture force distribution in this case yielded a most probable unbinding force of 57 ± 20 pN, when the measurement was performed with a loading rate of 6960 pN/s. This result is also comparable to that obtained from the first set of experiments within experimental error, and also taking into consideration the change in loading rate due to the use of a different AFM tip/cantilever. In both cases, the results are in agreement with the previously reported rupture force for the ConA/mannose interaction.

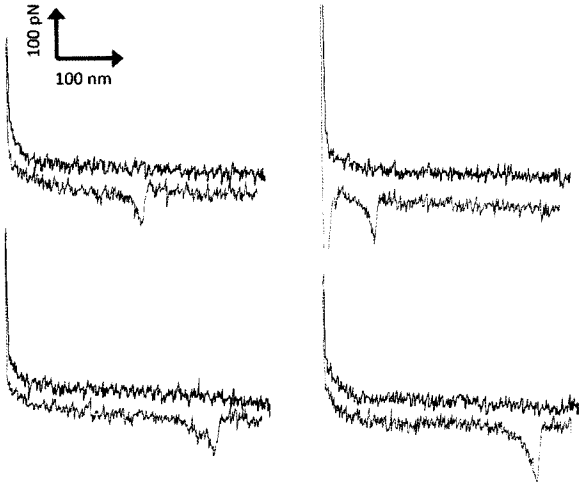

Figure 41. Representative force curves of single molecule force spectroscopy measurements of ConA/mannose (approach is shown in red and retract in blue; Set 2)

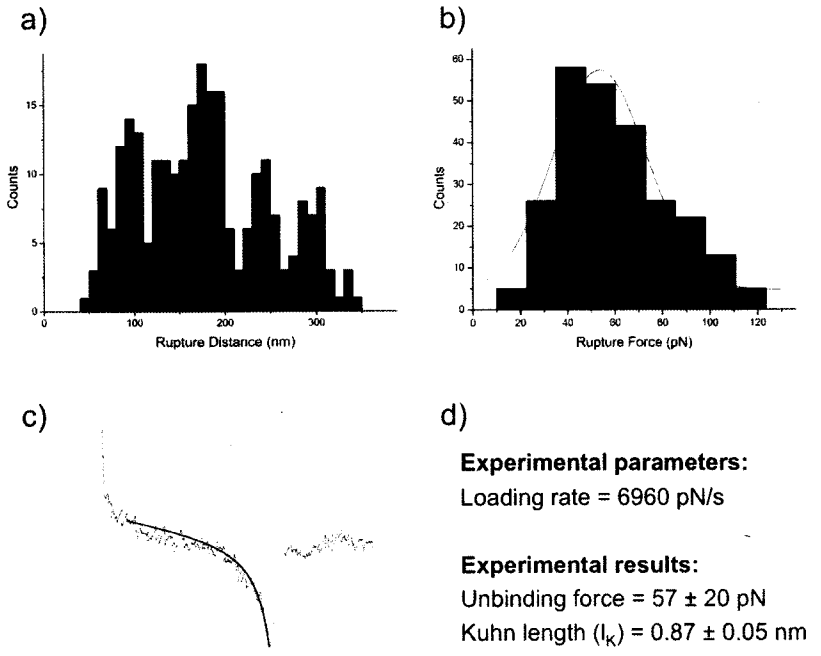

Figure 42. Analysis of ConA/mannose SMFS (Set 2): (a) Force distribution histogram, (b) rupture distance histogram, (c) example of fit curve, and (d) experimental details and results

This new carbohydrate immobilization technique, based on the use of photo-reactive PFPAs proved to be applicable and useful for force experiments. This method is especially attractive for SMFS applications because it allows the attachment of sugar molecules to the surface through long polymer spacers. Furthermore, the versatility of PFPA derivatives makes them useful for attaching a wide variety of biomolecules and polymers to surfaces. In addition, surface patterning may also be achieved by functionalizing different areas with different biomolecules, which would be interesting to study using force mapping, which is a combination of SMFS and AFM imaging.[174]

Chapter 6. Single Molecule Force Spectroscopy of the E/K Coiled-Coil

6.1. Studying the E/K coiled-coil Interaction using SMFS

Coiled-coil interactions are structural association motifs ubiquitous in a variety of important proteins (including fibrous proteins,[175] intermediate filaments,[176] as well as DNA binding proteins[177]), where two (and up to seven[178]) identical or different α-helices wrap around each other in a parallel or antiparallel fashion adopting some sort of 'super coil' as exemplified in Figure 43.

Figure 43. Structure of tropomyosin: a well-known example of dimeric coiled-coil. Structure prepared using Pymol[124]

In addition to their significance in understanding supramolecular organizations among proteins and designing new tertiary structures such as hydrogels,[179] coiled-coils are advantageous to many capture techniques and biosensor applications in therapeutic, diagnostic as well as purification systems.[95,97,180,181] The structural features required for

the formation and specific binding in coiled-coils are discussed below in light of a relatively new designed synthetic dimerization motif, known as the E/K coiled-coil.

The existence of coiled-coils was first predicted in 1953, by Crick when analyzing the X-ray diffraction pattern of α-keratin.[182] He proposed that, similar to a two-stranded rope, the coiled-coil consists of two α-helices folded around each other with, most probably, hydrophobic interactions primarily driving their self-assembly. In his classical analysis, Crick speculated that at the interface between the two α-helices, non-polar side chains of one strand stack in-between those of the opposite strand in a *'knobs-into-holes'* fashion resulting in super-coiled α-helical ribbons. It was nearly 20 years later that the amino acid sequence of the first coiled-coil in tropomyosin was identified, to reveal the existence of a seven-residue repeating motif $(a\text{-}b\text{-}c\text{-}d\text{-}e\text{-}f\text{-}g)_n$ where positions *a* and *d* were found to be usually hydrophobic amino acid residues, such as leucine, isoleucine, valine and alanine.[183] Indeed, this repeat motif was later shown to be continuous throughout the entire polypeptide chain of tropomyosin. More studies, starting with the infamous leucine zipper sequence, where there is a continuous presence of leucine residues at position *d*, confirmed Crick's speculations and verified the hydrophobic core to be necessary for the formation and stability of a coiled-coil dimer.[184] In addition, it was found that there is a particular preference for certain combinations of hydrophobic residues in the coiled-coil core. For example, β-branched non-polar amino acid residues, such as isoleucine and valine were found to contribute more to the core stability when present at position *a* compared to *d*. This is mainly due to the fact that the two positions are not exactly the same in terms of their relative orientation to the coiled-coil axis: side chains at position *a* point away from the coils interface whereas those at position *d* point towards it. This

explains how certain side chains, in either position, might stabilize or destabilize the close packing of the core.[185] Similarly, the presence of large hydrophobic groups, such as aromatic amino acids can disrupt the close packing within the hydrophobic core and destabilize the coiled-coil.[186]

Beyond the role of core hydrophobic residues as the main driving force for their assembly, coiled-coils also employ intra- as well as inter-strand electrostatic interactions in order to tune their overall stability. Polar and charged amino acid residues, which are frequently found in positions *e* and *g*, are involved in the electrostatic interactions which highly contribute to the conformational selectivity of coiled-coils.[187,188] Interestingly, polar amino acid residues may contribute to the overall hydrophobicity of the core by interacting hydrophobically, with the non-polar residues at the coiled-coil interface, through their side chain methylene groups and thereby shielding the hydrophobic core from unfavourable solvent exposure.[189] More importantly, inter-chain salt bridges between oppositely charged amino acid residues can highly stabilize the coiled-coil binding. It must be noted, however, that the contribution of such electrostatic interactions is highly dependent on the coils local environment and are especially effective when the surroundings have lower dielectric constant (*e.g.* near the hydrophobic interface).[189] In addition, the preference of attractive over repulsive interactions can play an important role in controlling the binding specificity in coiled-coils, *i.e.* the extent of homodimer *vs* heterodimer formation in model *de novo* designs.[187] Although polar and charged residues can destabilize close packing if present in the *a* or *d* positions, they can highly stabilize the overall coiled-coil structure when present at the *e* and *g* positions. It can be concluded

that both, hydrophobicity and side chain packing in the hydrophobic core, as well as electrostatic interactions are interdependent and contribute to the stability of coiled-coils.

A synthetic heterodimeric coiled-coil, known as the E/K coiled-coil, was designed based on the following structural features: (*i*) choosing amino acids that complement the formation of helical structures, (*ii*) placing complementary non-polar amino acids at positions *a* and *d* for the formation of a stable hydrophobic core, (*iii*) placing oppositely charged amino acids at positions *e* and *g* to favor the formation of heterodimeric coiled-coils, (*iv*) adding charged amino acids at position *f* to increase the solubility and balance the net charge of each coil, and (*v*) realizing the most appropriate chain length for the desired applications.[184,190] The synthetic design of the E/K coiled-coil (Figure 44) was chosen to satisfy all the previously-mentioned requirements for a stable heterodimer, at neutral pH, that can be used as a capture technique in a variety of applications.

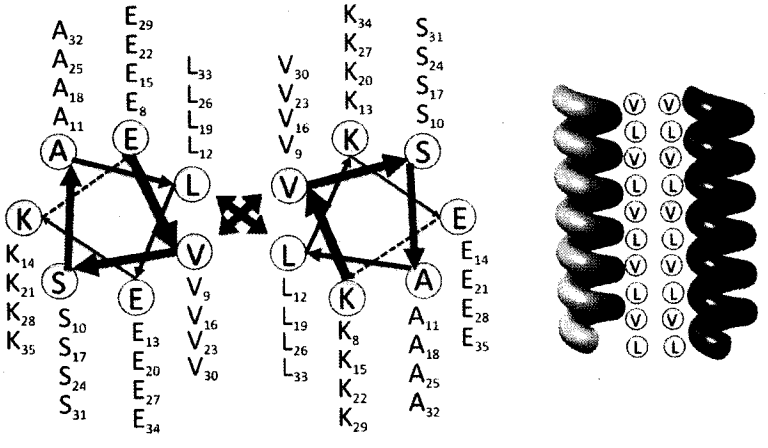

Figure 44. Helical wheel diagram for the E/K coiled-coil: the E-coil is shown in red and the K-coil is shown in red

In this design, the non-polar amino acids, valine (V) and leucine (L) (positions *a* and *d*, respectively) were chosen to form the hydrophibic core of the E/K coiled-coil since: (*i*)

they are frequently found in natural as well as synthetic coiled-coil cores, especially dimers,[190] and (*ii*) their combination is expected to form a weaker hydrophobic core, compared to that formed from all-leucine or even isoleucine and leucine, which is particularly desirable in this situation. If the interactions of the hydrophobic core are too strong, oligomerization and homodimerization can compete with heterodimerzation, especially when the contribution of electrostatic interactions is negatively influenced by the surrounding environment.[191,192]

Charged amino acids, specifically glutamate (E) or lysine (K) were chosen for both positions *e* and *g* in the E-coil and the K-coil, respectively. These residues were selected as they are commonly observed in these positions in natural coiled-coil structures.[193] Inter-chain salt bridges between ionized glutamate and lysine residues (*i.e.* position *e* of the E-coil with position *g* of the K-coil at neutral pH) significantly add to the stability of the coiled-coil structure.[194] In addition, interactions between methylene groups in their side chains with the partially exposed hydrophobic interface contribute to the core stability, by shielding water molecules as explained earlier.[187] However, their most important feature is their ability to encourage the formation of heterodimers over homodimers by favouring attractive interactions between oppositely-charged residues in the different coils.[194]

The effect of chain length on the overall E/K coiled-coil stability was also taken into account when designing the peptides. In fact, varying lengths of both E and K peptides (three to five heptads) were synthesized and their kinetic as well as thermodynamic interaction constants were determined using surface plasmon resonance (SPR).[96] In

addition to SPR, the association and dissociation behaviour of the 5-heptad E/K coiled-coil system has been addressed using a variety of physical characterization techniques.[96,195,196] The estimated dissociation constants for this coiled-coil all indicate the remarkably high affinity between the two coils, exemplified with a fast association and slow dissociation (*i.e.* low equilibrium dissociation constant; Table 5).

Table 5. Summary of equilibrium dissociation and rate constants in the E/K coiled-coil system

Method	K_d (x 10^{-6} M)
Gdn•HCl denaturation[1]	3.53 ± 0.44
Dilution study[2]	2.45 ± 0.71
BIAcore™ biosensor[3]	0.50 ± 0.13

[1] Equilbrium dissociation constant, K, estimated from Gdn•HCl denaturation data using the relationship $\Delta G = -RT \ln K$, where ΔG is the free energy of unfolding, R is the gas constant, and T is the temperature in Kelvin.

[2] Equilibrium dissociation constant estimated from protein dilution experiments as monitored by CD spectroscopy.

[3] Dissociation constant, K, calculated from a BIAcore™ biosensor study using the relationship $K_d = k_{off} / k_{on}$ where k_{on} and k_{off} are the individual on and off rate constants.

In all studies, the interaction in the 5-heptad E/K coiled-coil system was found to follow a simple association mechanism where the unfolded individual coils (*i.e.* random coils) join together forming a fully-folded dimer (*i.e.* coiled-coil heterodimer) with no apparent intermediates. The fact that the individual coils exist as random coils when present on their own confirm the requirement of hydrophobic (from *a* and *d* residues) as well as electrostatic (from *e* and *g* residues) interactions for their proper folding into α-helices that heterodimerize.[184]

The strong binding between the E and K coils and the overall stability of their heterodimeric system encouraged their utility as a capture or immobilization technique for biosensor applications as well as purification systems.[184] In either case, one of the peptides is co-expressed with a biomolecule of interest and the other is immobilized on the sensorchip/column surface. Due to their highly specific binding, the coiled-functionalized surface recognizes its partner and captures it. The formation of stable and strong E/K coiled-coil interactions effectively retains the biomolecular asembly on the surface. In fact the use and applicability of E/K heterodimeric coiled-coils for such purposes have been proven by a number of research groups.[95,181]

In the present study, the interaction strength between the E and K coils was addressed using SMFS. In this approach, one of the coils is attached to the AFM tip and the other to a surface (Figure 44). Force-distance curves are developed when the coil-functionalized AFM tip is approached to the complementary coil-functionalized surface. In this manner the coils are allowed to fold and self assemble into the coiled-coil structure. Subsequently retracting the tip will cause the two coils to break apart. As explained previously, changes in the cantilever's deflection during the force measurement can be directly converted into force using Hooke's law, and the stability of the E/K coiled-coil system can be expressed in terms of unbinding force values. More interestingly, performing the force measurement at varying probe velocities (*i.e.* dynamic force spectroscopy) allows measuring the dissociation rate constant k_{off} (according to Equation 8) and exploring the force-induced energy landscape in this system at the single molecule level. The use of single molecule techniques such as SMFS will contribute significantly to the previous ensemble studies that have been employed to investigate the E/K coiled-coil heterodimer.

Although the E/K coiled-coil system has not been previously studied using SMFS, the technique has been applied to study the unfolding of other synthetic as well as natural coiled-coils. The high complexity of protein unfolding was a key motivation for the Rief group to study the mechanical unfolding of coiled-coils as a relatively simple yet physiologically relevant model system.[197-201] In one of their AFM-based force studies, the unfolding process of a leucine zipper sequence was investigated (Figure 45). In this experimental approach, the coiled-coil sequence was co-expressed with an actin cross-linker protein, whose force-induced unfolding has been well-characterized.[202] The rationale behind using actin was 2-fold: (*i*) it provided a means for immobilizing the coiled-coil between the AFM tip and the surface, and (*ii*) it provided a characteristic internal reference on the force-distance curves to identify events corresponding to the coiled-coil unfolding. Moreover, the insertion of a disulfide linkage at the proper site in the coiled-coil sequence allowed the force-induced unzipping to occur in one direction only.

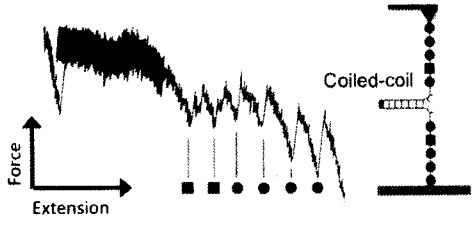

Figure 45. Example of SMFS of coiled-coils: leucine zipper conjugated to actin[197]

A specific unzipping pattern for the leucine coiled-coil was observed with unbinding forces of *ca.* 9 to 15 pN. An equilibrium model previously used to describe force-induced DNA unzipping was applied to the coiled-coil system in order to calculate the energy

required for unfolding.[113] It is important to highlight that such partially unzipped conformations accessed by the SMFS approach are very likely masked when applying conventional ensemble techniques.[203]

Another experimental approach used to study the force-induced dissociation of the same leucine zipper using SMFS was carried out by Dietz *et al.*, where the coiled-coil sequence was co-expressed with the Ig27 domain of titin acting as an internal reference protein.[198] As presented in Figure 46, the titin domain is expressed with one coil at each of its ends. The homodimeric coiled-coil interaction leads to the formation of a linear coiled-coil-linked poly(protein) chain, whose force-induced unfolding has been previously studied and is well-characterized.[26,204-206,128]

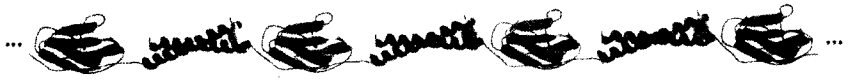

Figure 46. Example of SMFS of coiled-coils: poly(protein) chain consisting of leucine zipper coiled-coils conjugated to titin[198]

In addition to the saw tooth pattern well-known for titin unfolding, overstretching as well as unzipping events were observed at forces lower than 30 pN, which was expected for the mechanically-induced dissociation of the studied coiled-coil.[197,201] From the previously-reported free folding energy for the coiled-coil dissociation, and the measured increase in length (due to either overstretching or unzipping) the work involved in each force-induced event can be calculated. In addition, fitting the force-distance data to a simple two-state equilibrium model allowed calculation of the number of coiled-coils included within the (poly)peptide chain construct.

Another example of SMFS studies on the mechanical properties of coiled-coils is the force-induced stretching of myosin, the essential protein for muscle assembly and contraction.[207] Single molecules of myosin coiled-coils were passively adsorbed on gold-coated surfaces and subsequently stretched by approaching the AFM tip to the surface, picking up a myosin molecule (at random points of the coiled-coil) and then retracting the tip thus stretching the attached coiled-coils. The resulting force curves displayed coiled-coil stretching events, recognized by a rise (R), a plateau (P), as well as an additional exponential phase (E) caused by stretching the hinges present within the myosin coiled-coil rods. The coiled-coil detaches, after stretching, at forces around 200 pN (Figure 47).

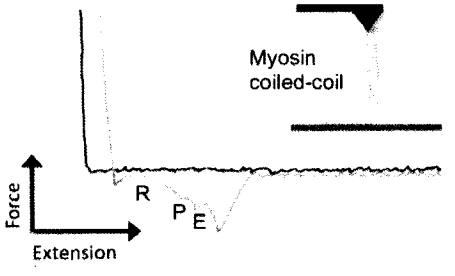

Figure 47. Example of SMFS of coiled-coils: myosin[207]

Since the R and P phases are not usually observed in the force-induced stretching of non-coiled-coil proteins, they are thought to be caused by specific conformational changes that take place within the coiled-coil structure during stretching. The E phase, on the other hand, is a typical protein unfolding event that can be fit using the WLC model, typically used in describing polypeptide chain stretching force peaks. This analysis allows measuring the persistence length of the polypeptide chain, as well as its contour length.[207]

The experimental protocol adopted in this study for investigating the E/K coiled-coil interaction includes: (*i*) immobilizing a cysteine-terminated E-coil on the AFM tip surface using NHS-PEG-PDP, and (*ii*) immobilizing a cysteine-terminated K-coil on the surface using the commercially-available linker LC-SPDP (Figure 49). Unlike the previously described experimental protocols, the approach followed in this study does not involve fusing the coiled-coil with another reference protein. During the force experiment, all observed unbinding events correspond to the coiled-coil force-induced dissociation. In addition, unlike the myosin force experiment, it involves the attachment of the coiled-coil between the tip and the surface using specific functionalization chemistry, thus increasing the probability of detecting single molecule events.

AFM tip functionalization chemistry, similar to that described for the biotin/streptavidin system, involved aminating the surface in order to attach the NHS-PEG-PDP spacer by a stable amide linkage to the NHS group (Figure 48). The PDP group at the other end of the PEG spacer was used to attach the cysteine-terminated E-coil by disulfide bond formation. The PEG spacer is used to: (*i*) avoid detecting non-specific interactions by increasing the distance between the AFM tip and the surface, and (*ii*) help distinguish the coiled-coil dissociation events using the PEG stretching signature. The surface functionalization chemistry is quite similar to that followed for the AFM tip, except that: (*i*) the silicon surfaces were aminated using APTES, and (*ii*) the commercial LC-SPDP linker does not have a PEG chain.

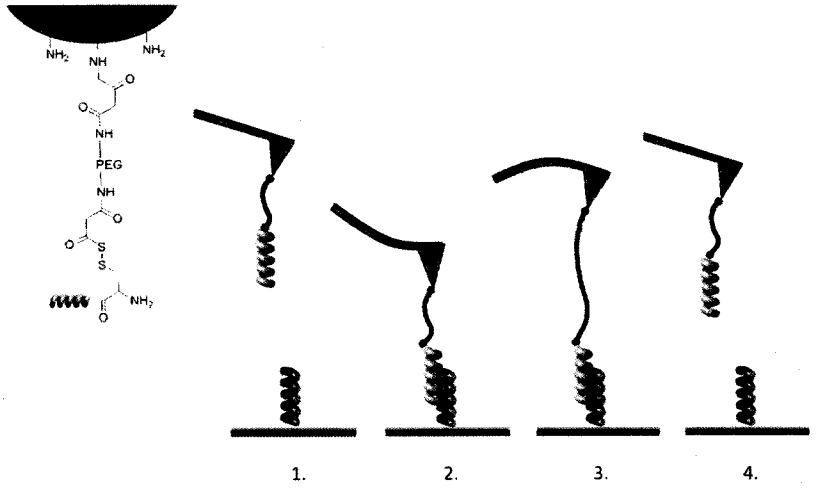

Figure 48. Schematic representation of experimental set up carried out for SMFS of E/K coiled-coils using NHS-PEG-PDP tether

The presence of a cysteine residue at the C-terminus of each peptide allowed their covalent attachment to either the tip or the surface by the formation of a strong disulfide bond, with the required anti-parallel orientation. Both cysteine-terminated peptides were prepared by solid phase synthesis. The K-coil functionalized surfaces were prepared by Dr. B. Liberelle in the De Crescenzo laboratory, as described in Figure 49.[95]

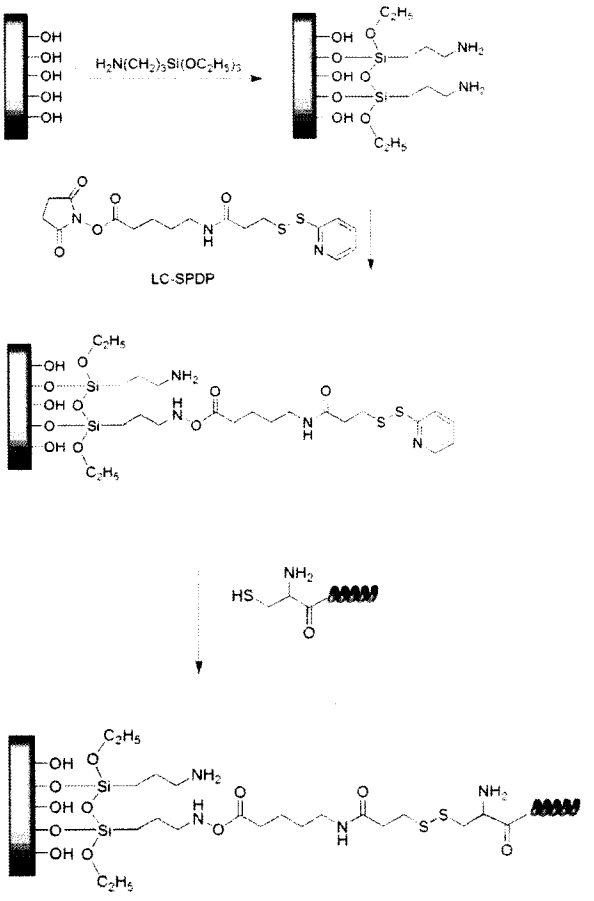

Figure 49. Immobilization of K-coil on silicon surfaces

The prepared surfaces were characterized by contact angle as well as ellipsometry measurements, and at each functionalization step showed variations in both the hydrophobicity as well as thickness thus confirming changes at the surface. However, such techniques do not give information about the surface functional groups, but rather their properties. AFM surface imaging allowed examining the surface coverage as well as its homogeneity. An example of a K-coil functionalized surface examined by different characterization methods is given in Figure 50. K-coil layers were successfully immobilized on the silicon surface, as indicated by the change in ellipsometric and water contact angle measurements. Although the changes are subtle, the key finding here is that

the surfaces are uniform and homogenous, which is exemplified in the AFM topography images.

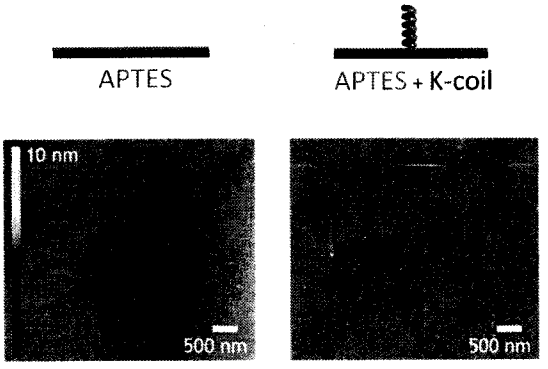

Sample	Roughness (nm)	Dry thickness (nm)	Contact angle (water)
APTES	0.2	0.8	52°
APTES + K-coil	0.3	2.2	66°

Figure 50. Characterization of K-coil surfaces using AFM, water-contact angle as well as ellipsometric measurements

The adequacy of the designed force experiment and its applicability to study the E/K-coiled coil interaction was evaluated using SPR. (For a detailed description, refer to Section 4.1 in Appendix I). In this assay, cysteine-terminated K-coil peptides were covalently immobilized on aminated CM4 sensor chips using either LC-SPDP or PDP-PEG-NHS, in order to examine both surface, as well as AFM tip functionalization strategies. The ability of immobilized K-coil to capture an E-coil conjugated protein, epidermal growth factor (EGF), *via* the E/K coiled-coil interaction was then examined by observing the change in signal on the sensogram. The SPR experiments confirmed the efficiency and stability of the functionalization chemistry and also demonstrated the stability of E-coiled EGF/K-coil complexes. In addition, the reversibility of the coils'

binding was exemplified by using guanidinium hydrochloride which promotes the dissociation of the coiled-coil complex without affecting the surface chemistry or the coils ability to re-fold and associate. This was further verified by the fact that additional E-coiled EGF was captured by the surface K-coils resulting in a similar change in signal to the that originally observed. The observed SPR signal changes for K-coil surfaces prepared using LC-SPDP or NHS-PEG-PDP were found to be analogous, confirming the reliability of the results as well as the technique.[95] In addition, mock surfaces on which cysteine residues, rather than cysteine-K-coil peptides, were attached but did not yield any detectable changes on the sensogram when subjected to the same conditions, confirming the specificity of the measured binding signals. The SPR results clearly validated the efficiency of the functionalization chemistry developed to immobilize the coil peptides and confirmed the suitability of the design for studying their binding interactions. The results also demonstrated the stability and specificity of E/K coiled-coil interactions and their usefulness as a capture technique for other biomolecular systems.

SMFS experiments using E-coil functionalized AFM tips and K-coil functionalized surfaces were carried out in order to investigate the strength of the E/K coiled-coil interaction. The resulting force curves display rupture events, similar to those observed for unbinding ligand-receptor complexes (*e.g.* biotin/streptavidin and ConA/mannose) (Figure 51). The peaks occur at a distance far from the surface, which confirms that they represent specific binding interactions and once again highlight the importance of the PEG spacer. Occasionally some non-specific adhesion interactions were detected but were still easy to distinguish as they only appear close to the surface.

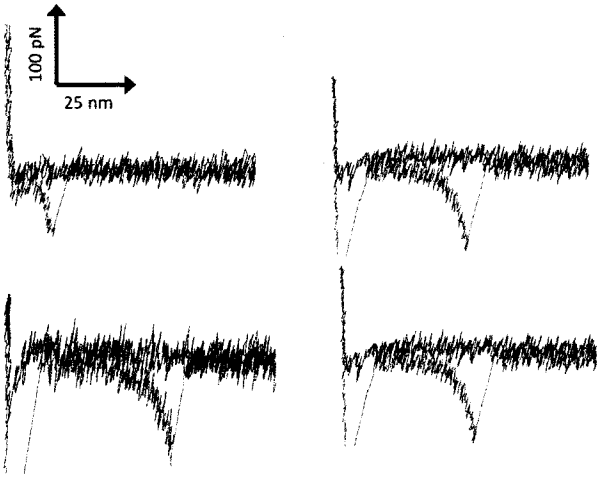

Figure 51. Representative force curves of single molecule force spectroscopy measurements of E/K coiled-coil (approach is shown in red and retract in blue; Set 1)

In one experiment, *ca.* 5000 force curves were collected, from which *ca.* 90% were featureless. The remaining *ca.* 500 curves contained one or sometimes multiple unbinding events and were therefore used for subsequent analysis. As described in earlier chapters, the shape of the peaks is governed by the elastic properties of the PEG tether and fitting the selected curves with the e-FJC$_{PEG}$ model allowed eliminating events that are not caused by PEG-linked bimolecules. Fitting parameters, Kuhn length and maximum rupture distance, were used to evaluate the filtered curves yielding *ca.* 1% of all collected data to be used in calculating the most probable unbinding force in the E/K coiled-coil system. The average PEG Kuhn length was determined to be 0.51 ± 0.20 nm, which is in agreement to the reported value of 0.7 nm.[28]

The distribution histograms for both the rupture distance, as well as the rupture force calculated from the 41 force curves, when the experiment was carried out at an applied loading rate of 7240 pN/s, are shown in Figure 52. The most probable rupture distance was found to be 22 ± 10 nm by applying a Gaussian fit. A wide distribution of rupture

distances was observed resulting in a large standard deviation value, however this does not affect the credibility of the results in any way. As mentioned earlier the different rupture distance values can be caused by the polydispersity of the PEG polymers and more importantly by the different attachment locations of the PEG spacers on the AFM tip. The measured most probable rupture distance was, however, found to be consistent with the PEG contour length of *ca.* 27 nm. When the force distribution was analyzed with a Gaussian fit, the most probable unbinding force was found to be 46 ± 7 pN. Although there might be a contribution of multiple interactions, this unbinding force value suggests a stronger binding in the E/K coiled-coil system, compared with other coiled-coil systems studied with SMFS. In order to confirm the obtained results, another set of SMFS measurements were analyzed in the same manner. From a total of *ca.* 5000 collected force curves, only *ca.* 2% remained after fitting analysis. The average PEG Kuhn length was found to be 0.92 ± 0.11nm, which is in agreement to the reported value of 0.7 nm.[28]

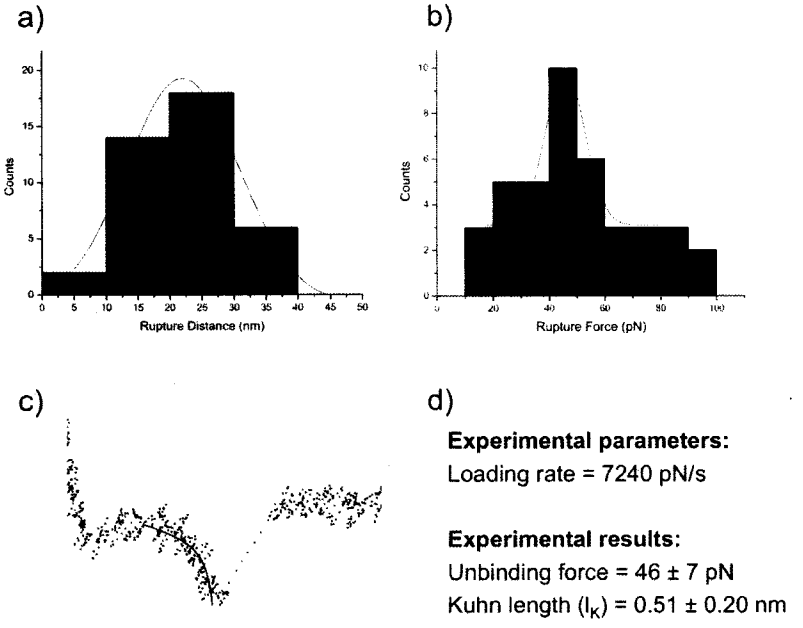

Figure 52. Analysis of E/K coiled-coil SMFS (Set 1): (a) Force distribution histogram, (b) rupture distance histogram, (c) example of fit curve, and (d) experimental details and results

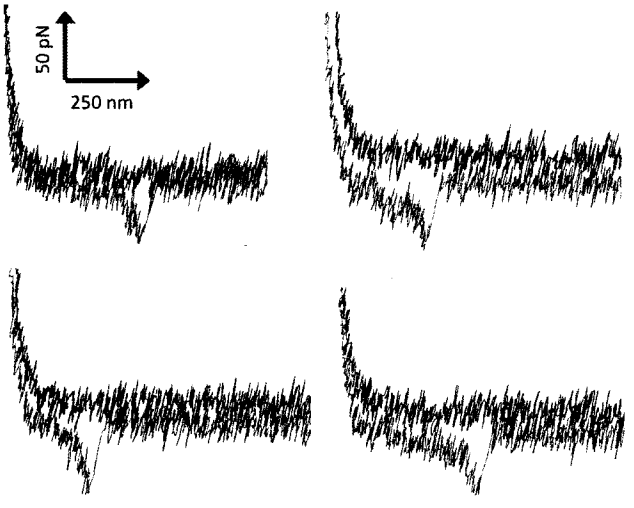

Figure 53. Representative force curves of single molecule force spectroscopy measurements of E/K coiled-coil (approach is shown in red and retract in blue; Set 2)

The distribution histograms for both the rupture distance, as well as the rupture force calculated from the 100 force curves, when the experiment was carried out at a loading rate of 6920 pN/s, are shown in Figure 54. The most probable rupture distance was found to be 18 ± 4 nm by applying a Gaussian fit, which is consistent with the PEG contour length of 27 nm. When the force distribution was analyzed using a Gaussian fit, the most probable unbinding force was found to be 36 ± 12 pN. This value is more in line with reported unbinding forces for other coiled-coil systems described above.[198,207] Possible reasons for the force variation between the two sets of measurements for the E/K coiled-coil are: (*i*) the different loading rate at which the two experiments were performed, and (*ii*) the difference in the total number of events used in constructing the histograms. This later point suggests that the second set of data should be more reliable.

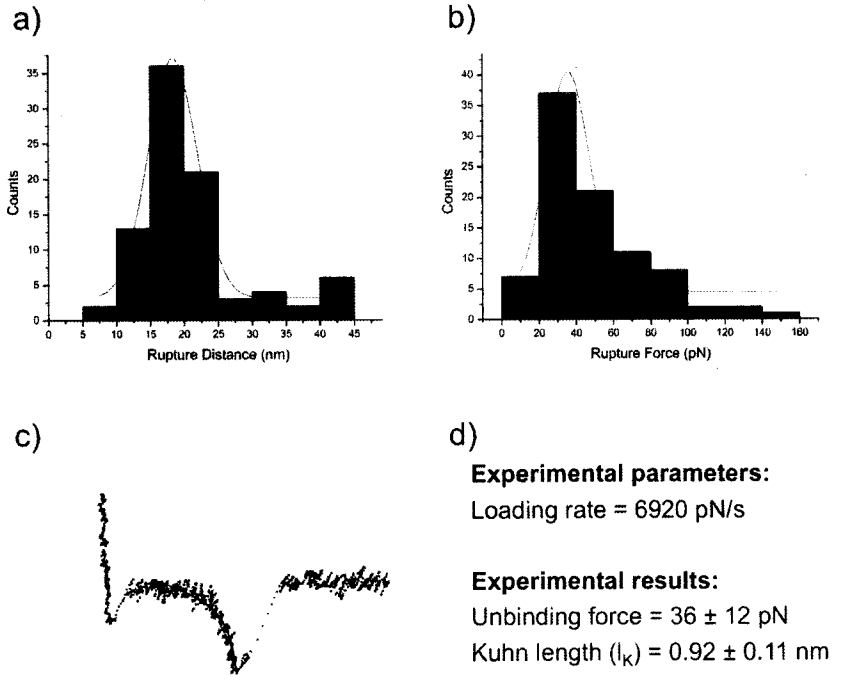

Figure 54. Analysis of E/K coiled-coil SMFS (Set 2): (a) Force distribution histogram, (b) rupture distance histogram, (c) example of fit curve, and (d) experimental details and results

In order to validate the force measurements, control AFM tips were prepared by using only a mono-functionalized PEG spacer (CH_3O-PEG-NHS), which cannot bind the E-coil. Similarly, control surfaces were prepared following the same procedure used for surface functionalization, except for the last step where cysteine, rather than cysteine-terminated K-coil, was attached. Under the same experimental condition, SMFS experiments performed using control tips and/or control surfaces showed force curves without repeatable specific rupture events, except for non-specific adhesion peaks detected at the surface.

Dynamic force spectroscopy of the E/K coiled-coil interaction was obtained by varying the force loading rate. This was achieved by changing the probe velocity while performing the force measurement, without changing any other experimental parameters. The histograms of the unbinding forces for the E/K coiled-coil interaction measured at different loading rates are shown in Figure 55. Analyzing the distributions using a Gaussian fit allowed the determination of the most probable unbinding forces. These values were plotted as a function of loading rate and the resulting relationship is shown in Figure 56. As explained in Chapter 1, the measured unbinding forces are not only a fundamental property of the interacting partners, but also depend of the loading rate that is applied to the system. At sufficiently low loading rates, the system is being pulled apart slowly and therefore there is enough time for thermal fluctuations to help the system overcome the transition state energy barrier resulting in smaller unbinding forces. [52,208]

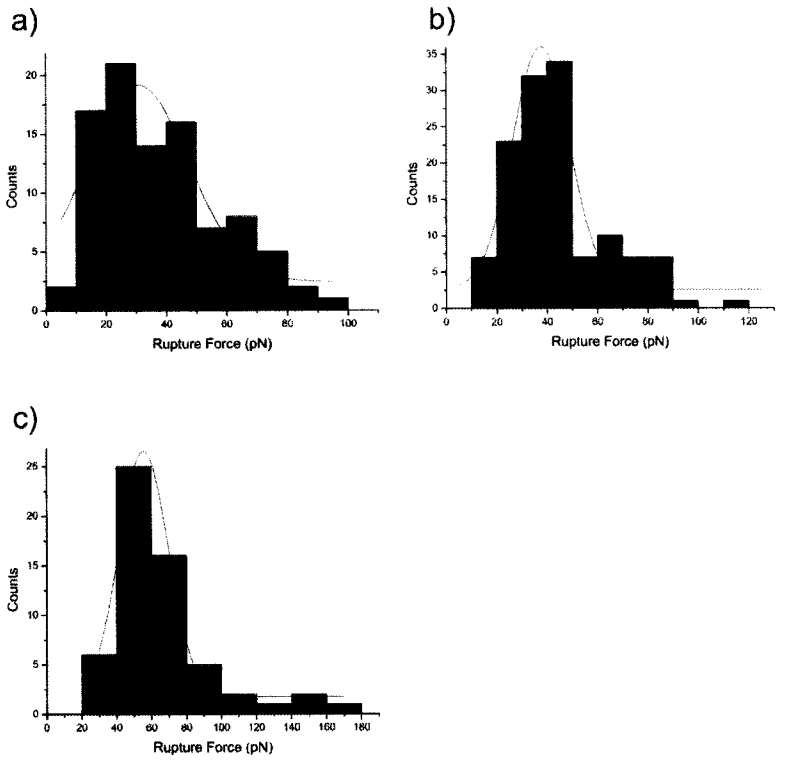

Figure 55. Force distribution histograms for SMFS of E/K coiled-coil at probe velocities of (a) 200 nm/s, (b) 400 nm/s, and (c) 800 nm/s

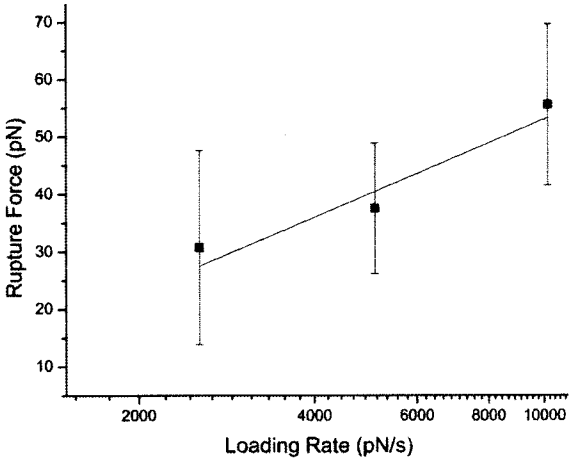

Figure 56. Dynamic force spectroscopy of E/K coiled-coil

The dissociation rate constant k_{off} estimated from the intercept of the vertical axis (*i.e.* when $\ln(r_f) = 0$) was found to be 15.8 s^{-1}. Other dynamic force spectroscopy studies reported a wide range of k_{off} values ranging from 10^{-6} to 150 s^{-1}. In comparison, the k_{off} value measured for the E/K coiled-coil is therefore considered to represent a strong interaction. Although this value should not be directly compared to binding parameters determined using conventional techniques, it is clearly related. It is important to keep in mind that this relationship is characteristic only for a single-energy barrier in the thermally activated regime, which has been confirmed for the E/K coiled-coil system.

Assessing the strength of E/K coiled-coil binding allows extending the range of their application as a capture technique for SMFS measurements. As mentioned earlier, studies have shown the usefulness of the E/K coiled-coil as a research tool to detect and purify as well as analyze other biomolecular systems, by a versatile number of techniques. Similarly, the E/K coiled-coil interaction can serve to immobilize biomolecules between the AFM tip and a surface in order to study them by SMFS. In fact, in this work the E-coil has been genetically conjugated to a number of protein entities (*e.g.* the epidermal growth factor, EGF and the calpain small subunit, 21k) in order to use the E/K coiled-coil interaction to attach them to surfaces for SMFS measurements.

6.2. Applications of the E/K coiled-coil in Single Molecule Force Spectroscopy

6.2.1. Epidermal Growth Factor and Receptor

Epidermal growth factor (EGF) plays a number important roles, and it performs its biological function by binding to its cellular receptor, EGFr, which initiates a complex cascades of intracellular events including the phospohorylation of other proteins resulting in a broad spectrum of phenotypic responses such as the regulation of cellular growth as well as their proliferation and differentiation.[209] The structure of EGF bound to its cellular receptor EGFr is shown in Figure 57.[210]

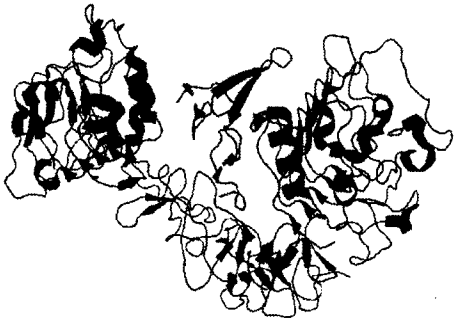

Figure 57. Structure of EGF (red) bound to its receptor EGFr (blue). Structure prepared using Pymol[124]

EGF is a small protein (6045 Daltons) containing 53 amino acids, which is found in many human tissues including the salivary glands. Once released, EGF is recruited by its receptor (EGFr), which is present in the cell membrane, causing EGFr dimerization with other receptors. The receptor is composed of two globular extracellular domains that bind EGF and two cysteine-rich intracellular domains.[210] A number of aggressive types of cancer have been found to have overactive signaling through the EGF system, therefore an understanding of the mechanism underlying the EGF interaction with its cellular

receptor is of critical importance. In particular, addressing the mechanical properties of this binding at the single molecule level might be quite relevant to its function, since many cellular recognition processes are initiated under stress or shear force.[22]

In order to study the EGF system using SMFS, both the protein as well as its receptor must be immobilized between the AFM tip and the surface. The E/K coiled-coil system may be used as a capture technique for such measurements (Figure 58).

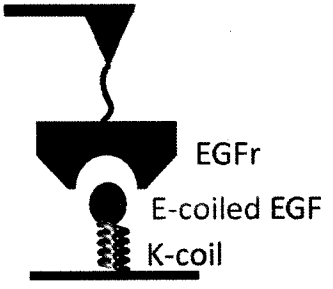

Figure 58. Experimental design for SMFS of EGF/EGFr using E/K coiled-coil as tether

As mentioned earlier, the ability of K-coil immobilized peptides to capture the E-coiled EGF conjugate has been previously examined by means of SPR.[95-97] Following a similar approach, E-coiled EGF can be immobilized on K-coil-functionalized surfaces for SMFS studies. In this design, a biotinylated EGFr can be immobilized on biotinylated AFM tips using the biotin/streptavidin interaction. The EGFr could also be attached using homo-bifunctional PEG spacers containing NHS groups, similar to the previously described ConA AFM tip functionalization.

6.2.2. Calpain Ca^{2+}-Binding Domain

The caplain calcium binding domain (21k) is another protein that has been conjugated to the E-coil in order to be immobilized between the AFM tip and a surface for SMFS

measurements. Calpains are a family of calcium-dependent cytosolic cysteine proteases that have been identified in organisms ranging from mammals to bacteria.[211] In response to calcium signalling, these enzymes catalyze the proteolysis of numerous substrates linked to processes including cell motility, apoptosis, cell differentiation and cell-cycle regulation.[212] Abnormal changes in calpain activity, caused by defects in calcium homeostasis or mutations in calpain genes are linked to a number of pathologies, including cancer, Type II diabetes, muscular dystrophy, Alzheimer's disease, as well as other neurological disorders. [211,213] The two best-characterized members of the family are calpains 1 and 2 (also known as μ- and m-, respectively). They are heterodimers of a large catalytic subunit (80 kDa) and a small regulatory subunit (28 kDa).[214] A schematic representation of the human m-calpain is shown in Figure 59.[215]

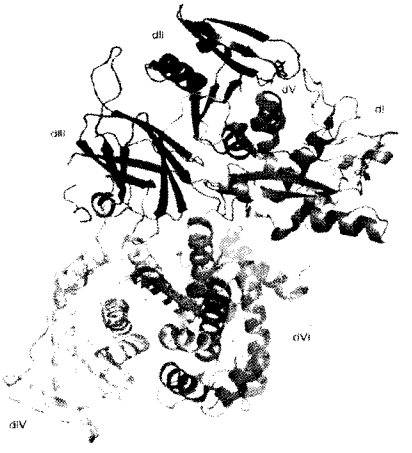

Figure 59. Structure of m-caplain (domains dI – dVI, the calcium-binding domain is coloured in orange) Structure prepared using Pymol[124]

As an initial step in understanding the function, regulation and activation of calpains by calcium, the C-terminal portion of the 21 kDa rat calpain small subunit (domain VI) has been cloned, expressed, purified and crystallized.[216] Gel permeation chromatography, sedimentation equilibrium centrifugation as well as laser light-scattering experiments

have shown 21k to exist as a dimer with a predicted molecular weight of 42 kDa. Figure 60 shows the calpain small subunit homodimer (21k) bound to calcium.

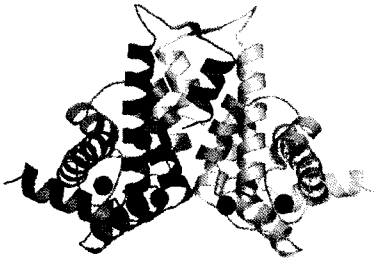

Figure 60. Structure of 21k homodimer bound to calcium. Structures prepared using Pymol[124]

Just as the fifth EF-hand of domain VI in the small subunit is the association site to domain IV in the large subunit, it is also believed that the fifth EF-hand of domain VI is the site of its dimerization in the homodimer.[217] In order to address the dimerization interactions in the 21k homodimer at the single molecule level by means of SMFS, they must be immobilized between the AFM tip and a surface. Co-expression with either the E or the K-coil is an attractive immobilization technique that was attempted in this study. The specific experimental design for this study requires the conjugation of 21k with the E-coil in order to use the E/K coiled-coil interaction to capture the 21k dimer between the tip and a surface (Figure 60). In efforts to achieve this goal, a straight forward procedure of plasmid construction, bacterial transformation followed by PCR amplification was used to design the 21k dimer protein with the E-coil attached to its N-terminus. Upon purification of the expressed conjugate by column chromatography, it was characterized by conventional gel electrophoresis in order to assess its purity and molecular weight. In addition, analytical ultracentriguation (AUC) sedimentation velocity experiments were carried out to confirm that the E-coiled 21k exists in the dimeric form, as designed. In order to capture the E-coiled 21k, K-coil will be immobilized on both the AFM tip and

the surface, following the same strategy as described previously (Figure 61). The molecular spacer NHS-PEG-PDP provides an ideal tool for attaching a cysteine-terminated K-coil, in this case at the C-terminus, to allow the required coiled-coil anti-parallel heterodimerization. SMFS measurements will provide information on the binding stability within the 21k system as well as the applicability of the E/K coiled-coil system as an immobilization technique in this domain.

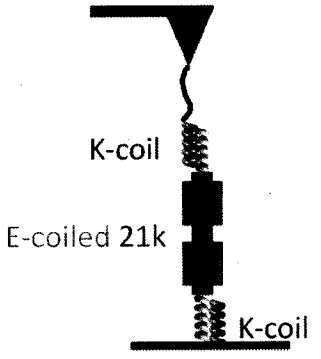

Figure 61. Experimental design for SMFS of 21k homodimer using E/K coiled-coil as tether

The specific binding affinity, unique specificity, high stability, as well as appropriate size make the E/K coiled-coil system an ideal candidate as an immobilization tool for many techniques, including SMFS. The results described in this study suggest strong binding within the E/K coiled-coil system, compared with other natural coiled-coils. In order to use the E/K coiled-coil system as an SMFS technique, their binding must be stronger than that of the biopartners being investigated. If necessary, the design of other more applicable *de novo* coiled-coils can be initiated to widen the scope of the coiled-coil as a capture tool for SMFS.

Chapter 7. Conclusions and Future Directions

The main goal of this thesis was to apply single molecule force spectroscopy (SMFS) to address, detect and measure biomolecular interactions. Carrying out force measurements at the single molecule level is indeed relevant for many biological systems. Many biomolecular interactions, including pathogen-host infections, antibody-antigen recognition, as well as cellular adhesion, are initiated under shear stress or an applied force. The molecular binding in these, and many other biological systems, has commonly been investigated using ensemble techniques where the interacting biomolecules are free in solution, or directly fixed to a solid substrate. However, under physiological conditions, many of these biomolecules are tethered, to cellular membranes for example, and their interactions occur under non-equilibrium conditions and within limited interaction volumes. In such cases, the biomolecules may undergo restricted motion, which could affect their recognition capability and their kinetic response. Although conventional ensemble techniques have yielded valuable insight into molecular recognition interactions, it is often more relevant to address these interactions using force-based techniques at the single molecule level, which offers the advantage of eliminating spatial and temporal averaging that can obscure significant binding details, including transient phenomena, rare events, population heterogeneity and crowding effects.

Studying biomolecular interactions using the AFM-based force technique, has indeed revealed new insight into the chemistry, biology, and physics of biological systems. In

this study, the potential of force spectroscopy is realized by investigating various types of biomolecular interactions in different systems, namely the DNA double helix, biotin/streptavidin, concanavalin A/mannose and the two coils in a synthetic E/K coiled-coil. Using the AFM to conduct force measurements at the single molecule level in these systems required their immobilization between the AFM tip and a surface, which was achieved by: (*i*) generating amino groups on the silicon nitride tip surface, (*ii*) attaching a heterobifunctional PEG spacer *via* an amide linkage to its NHS end, and (*iii*) covalently linking biomolecules to its other end. Molecular spacers effectively aid in distinguishing the interactions of interest from the wide range of non-specific interactions between the tip and the sample, which occur when the tip and the sample surface are in close proximity. The rupture of such non-specific adhesion is large (nN range) and could easily mask the rupture force of single biomolecular interactions (typically in the pN range). SMFS measurements carried out in this study confirmed the efficacy of PEG as the spacing tether. In all resulting data, the rupture events were detected at a distance further out from the surface facilitating their analysis. It is important to highlight that all the force curves represented for the different biomolecular systems under investigation were quite similar, and often identical, which is of no coincidence since they all represent the forced-induced stretching of the PEG spacer prior to the bio-partners rupture. The fact that the shape of the resulting force curve is governed by the elastic properties of the polymer tether greatly facilitates their analysis. The use of fitting mathematical models, that describe the non-linear elastic behaviour of tether chains under applied force help discriminate rupture events that correspond to tethered biomolecules, thereby further eliminating any events that do not represent the interaction of interest. The fitting process

is necessary and very advantageous for analyzing force curves in tethered systems, as exemplified in the force data presented herein. In all cases, thousands of force curves were collected within the SMFS experiments and only a small fraction (often as low as 1%) were used in the final quantitative analyses. In fact the experimental conditions in all cases aimed towards lowering the number of interacting molecules immobilized between the tip and the AFM surface in order to increase the probability of detecting single, rather than multiple, interactions. Therefore, the low frequency of rupture events that correctly correspond to the molecular interaction of interest is expected and indeed desirable.

Applying the above mentioned principles allowed for measuring specific interaction forces within the different biomolecular systems at the single molecule level. SMFS of dsDNA displayed the previously-reported conformational transitions that takes place upon stretching and unwinding the double helix. SMFS of biotin/streptavidin yielded unbinding forces that are consistent with the literature thereby confirming the credibility of our results as well as the fidelity of this technique. SMFS of concanavalin A/mannose was also consistent with previous studies and further reinforced the applied methodology. Dynamic force spectroscopy, where the energy landscape of a complex is explored by measuring unbinding forces at different loading rates may also allow measuring kinetic parameters for the concanavalin A/mannose interaction. In addition, the use of new immobilization techniques, namely the versatile PFPA photochemistry allows extending this force study to a large library of lectin-carbohydrate interactions, and possibly to other biomolecular systems. A future experiment involves microcontact printing where patterned surfaces can be developed using various PFPA-derivatized carbohydrates. Force mapping, which combines AFM imaging with force measurements can then be

used to investigate these patterned multi-carbohydrate surfaces. SMFS of the E/K coiled-coil revealed their strong binding, as previously observed using various techniques. However, it must be noted that the experimental protocol developed for tethering the E/K coiled-coil involved immobilizing each individual coil on either the AFM tip or the surface. Unlike the binding partners in each of the abovementioned biomolecular systems, the E and K coils must properly fold and wrap around each other, which might be demanding at the level of this experimental design. Although the details of the interaction, in this specific design, are not fully established, dynamic force spectroscopy allowed measuring an apparent kinetic unbinding rate constant for the E/K coiled-coil system. The obtained value was again in agreement with a strong binding interaction and therefore encourages the use of this system as a capture technique for other biological systems in SMFS studies. SMFS measurements can provide information regarding the binding strength in this system as well as stability under different environmental conditions. For example, the E/K coiled-coil binding affinity is expected to change as a function of pH due to its effects on the ionic charges essential for the E/K coiled-coil heterodimer formation. Following the experimental approach of dynamic force spectroscopy, one can perform a series of SMFS measurements while varying the buffer pH. This should yield information regarding the importance of ionic interactions and the extent of their contribution to the overall stability of the coiled-coil structures. SMFS of the different biomolecular systems were not only successful and informative, but also promising for a variety of future applications. Advances in the field SMFS will open avenues for exploring biomolecular interactions at the single molecule level, complementing ensemble methods currently used.

References

(1) Bizzari, A. R.; Cannistraro, S. *Chem. Soc. Rev.* **2010**, DOI: 1039/b811426a
(2) *Single-molecule techniques - A laboratory manual*; Slevin, P. R.; Ha, T., Eds.; Cold Spring Harbor: New York, 2008.
(3) Dammer, U.; Hegner, M.; Anselmetti, D.; Wagner, P.; Dreier, M.; Huber, W.; Guentherodt, H. J. *Biophys. J.* **1996**, *70*, 2437-2441.
(4) Bongrand, P. *Rep. Prog. Phys.* **1999**, *62*, 921-968.
(5) Cappella, B.; Dietler, G. *Surf. Sci. Rep.* **1999**, *34*, 1-104.
(6) Israelachvili, J. N. *Academic Press, New York* **1992.**
(7) Evans, E.; Berk, D.; Leung, A.; Mohandas, N. *Biophys. J.* **1991**, *59*, 849-60.
(8) Smith, S. B.; Finzi, L.; Bustamante, C. *Science* **1992**, *258*, 1122-6.
(9) Pierres, A.; Benoliel, A.-M.; Bongrand, P. *J. Immunol. Methods* **1996**, *196*, 105-120.
(10) Ashkin, A. *Proc. Natl. Acad. Sci. U. S. A.* **1997**, *94*, 4853-4860.
(11) Ashkin, A.; Dziedzic, J. M.; Yamane, T. *Nature* **1987**, *330*, 769-71.
(12) Zlatanova, J.; Lindsay, S. M.; Leuba, S. H. *Prog. Biophys. Mol. Biol.* **2000**, *74*, 37-61.
(13) Muller, D. J. *Biochemistry* **2008**, *47*, 7986-7998.
(14) Conroy, R. In *Handbook of molecular force spectroscopy*; Noy, A., Ed.; Springer Science: New York, 2008, p 23-96.
(15) Neuman, K. C.; Nagy, A. *Nat Methods* **2008**, *5*, 491-505.
(16) De Jager, M.; van Noort, J. In *Encylcopedia of Life Sciences*; John Wiley & Sons: New York, 2007, p 1-10.
(17) Butt, H.-J.; Cappella, B.; Kappl, M. *Surf. Sci. Rep.* **2005**, *59*, 1-152.
(18) Binnig, G., Quate, C.F., Rohrer, C. *Phys. Rev. Lett.* **1986**, *56*, 930-933.
(19) *Veevo probes*, https://www.veecoprobes.com/c-15-probes.aspx, December 1, 2009.
(20) Allison, D. P.; Hinterdorfer, P. *Curr. Opin. Biotechnol.* **2002**, *13*, 47-51.
(21) Hinterdorfer, P. *Nat Methods* **2007**, *3*, 347-355.
(22) Ashby, P. D. In *Handbook of Molecular Spectroscopy*; Noy, A., Ed.; Springer Science: New York, 2008, p 273-285.
(23) *Handbook of molecular spectroscopy*; Noy, A., Ed.; Springer Science: New York, 2008.
(24) Weeks, B. L.; Vaughn, M. W.; DeYoreo, J. J. *Langmuir* **2005**, *21*, 8096-8098.
(25) Strunz, T.; Oroszlan, K.; Schafer, R.; Guntherodt, H.-J. *Proc. Natl. Acad. Sci. U. S. A.* **1999**, *96*, 11277-11282.
(26) Rief, M.; Gautel, M.; Gaub, H. E. *Adv. Exp. Med. Biol.* **2000**, *481*, 129-141.
(27) Marszalek, P. E.; Li, H. B.; Fernandez, J. M. *Nat. Biotechnol.* **2001**, *19*, 258-262.
(28) Oesterhelt, F.; Rief, M.; Gaub, H. E. *New J. Phys.* **1999**, *1*, 6.1-6.11.
(29) Kienberger, F.; Kada, G.; Gruber, H. J.; Pastushenko, V. P.; Riener, C.; Trieb, M.; Knaus, H.-G.; Schindler, H.; Hinterdorfer, P. *Single Mol.* **2000**, *1*, 59-65.
(30) Kienberger, F.; Kada, G.; Mueller, H.; Hinterdorfer, P. *J. Mol. Biol.* **2005**, *347*, 597–606.

(31) Venzenov, D. V.; Noy, A.; Lieber, C. M. In *Handbook of molecular force spectroscopy*; Noy, A., Ed.; Springer Science: New York, 2008, p 123-143.
(32) Frisbie, C. D.; Rozsnyai, L. F.; Noy, A.; Wrighton, M. S.; Lieber, C. M. *Science* **1994**, *265*, 2071-4.
(33) Wong, S. S.; Joselevich, E.; Woolley, A. T.; Cheung, C. L.; Lieber, C. M. *Nature* **1998**, *394*, 52-55.
(34) Ebner, A.; Hinterdorfer, P.; Gruber, H. J. *Ultramicroscopy* **2007**, *107*, 922-927.
(35) Hinterdorfer, P.; Baumgartner, W.; Gruber, H. J.; Schilcher, K.; Schindler, H. *Proc. Natl. Acad. Sci. U. S. A.* **1996**, *93*, 3477-81.
(36) Ratto, T. V.; Rudd, R. E.; Langry, K. C.; Balhorn, R. L.; McElfresh, M. W. *Langmuir* **2006**, *22*, 1749-1757.
(37) Fritz, J.; Katopodis, A. G.; Kolbinger, F.; Anselmetti, D. *Proc. Natl. Acad. Sci. U. S. A.* **1998**, *95*, 12283-12288.
(38) Dettmann, W.; Grandbois, M.; Andre, S.; Benoit, M.; Wehle, A. K.; Kaltner, H.; Gabius, H.-J.; Gaub, H. E. *Arch. Biochem. Biophys.* **2000**, *383*, 157-170.
(39) Noy, A.; Vezenov, D. V.; Kayyem, J. F.; Meade, T. J.; Lieber, C. M. *Chem. Biol.* **1997**, *4*, 519-527.
(40) Zou, S.; Schoenherr, H.; Vancso, G. J. *J. Am. Chem. Soc.* **2005**, *127*, 11230-11231.
(41) Tormoen, G. W.; Drelich, J. *PMSE Prepr.* **2004**, *90*, 614.
(42) Ebner, A.; Wildling, L.; Zhu, R.; Rankl, C.; Haselgrubler, T.; Hinterdorfer, P.; Gruber Hermann, J. *Top. Curr. Chem.* **2008**, *128*, 29-76.
(43) Lo, Y.-S.; Huefner, N. D.; Chan, W. S.; Dryden, P.; Hagenhoff, B.; Beebe, T. P., Jr. *Langmuir* **1999**, *15*, 6522-6526.
(44) Ossenkamp, G. C.; Kemmitt, T.; Johnston, J. H. *Langmuir* **2002**, *18*, 5749-5754.
(45) Trau, M.; Murray, B. S.; Grant, K.; Grieser, F. *J. Colloid Interface Sci.* **1992**, *148*, 182-9.
(46) Blanchette, C. D.; Loui, A.; Ratto, T. V. In *Handbook of molecular force spectroscopy*; Noy, A., Ed.; Springer Science: New York, 2008, p 185-204.
(47) Vezenov, D. V.; Zhuk, A. V.; Whitesides, G. M.; Lieber, C. M. *J. Am. Chem. Soc.* **2002**, *124*, 10578-10588.
(48) Ratto, T. V.; Langry, K. C.; Rudd, R. E.; Balhorn, R. L.; Allen, M. J.; McElfresh, M. W. *Biophys. J.* **2004**, *86*, 2430-2437.
(49) Touhami, A.; Hoffmann, B.; Vasella, A.; Denis, F. A.; Dufrene, Y. F. *Langmuir* **2003**, *19*, 1745-1751.
(50) Brant, J. A.; Johnson, K. M.; Childress, A. E. *Colloids and Surfaces, A Physicochemical and Engineering Aspects* **2006**, *280*, 45-57.
(51) Kienberger, F.; Rankl, C.; Pastushenko, V.; Zhu, R.; Blaas, D.; Hinterdorfer, P. *Structure* **2005**, *13*, 1247-1253.
(52) Friedsam, C.; Del Campo Becares, A.; Jonas, U.; Gaub Hermann, E.; Seitz, M. *ChemPhysChem* **2004**, *5*, 388-93.
(53) Hinterdorfer, P.; Dufrene Yves, F. *Nat Methods* **2006**, *3*, 347-55.
(54) Langry, K. C.; Ratto, T. V.; Rudd, R. E.; McElfresh, M. W. *Langmuir* **2005**, *21*, 12064-12067.
(55) Conti, M.; Bustanji, Y.; Falini, G.; Ferruti, P.; Stefoni, S.; Samori, B. *ChemPhysChem* **2001**, *2*, 610-613.

(56) Hinterdorfer, P.; Kienberger, F.; Raab, A.; Gruber, H. J.; Baumgartner, W.; Kada, G.; Riener, C.; Wielert-Badt, S.; Borken, C.; Schindler, H. *Single Mol.* **2000**, *1*, 99-103.
(57) Hukkanen, E. J.; Wieland, J. A.; Gewirth, A.; Leckband, D. E.; Braatz, R. D. *Biophys. J.* **2005**, *89*, 3434-3445.
(58) Wieland, J. A.; Gewirth, A. A.; Leckband, D. E. *J. Biol. Chem.* **2005**, *280*, 41037-41046.
(59) Hinterdorfer, P. *Methods Cell Biol.* **2002**, *68*, 115-139.
(60) Hinterdorfer, P.; Schilcher, K.; Baumgartner, W.; Gruber, H. J.; Schindler, H. *Nanobiology* **1998**, *4*, 177-188.
(61) Riener, C. K.; Kienberger, F.; Hahn, C. D.; Buchinger, G. M.; Egwim, I. O. C.; Haselgrubler, T.; Ebner, A.; Romanin, C.; Klampfl, C.; Lackner, B.; Prinz, H.; Blaas, D.; Hinterdorfer, P.; Gruber, H. J. *Anal. Chim. Acta* **2003**, *497*, 101-114.
(62) Ebner, A.; Kienberger, F.; Kada, G.; Stroh, C. M.; Geretschlaeger, M.; Kamruzzahan, A. S. M.; Wildling, L.; Johnson, W. T.; Ashcroft, B.; Nelson, J.; Lindsay, S. M.; Gruber, H. J.; Hinterdorfer, P. *ChemPhysChem* **2005**, *6*, 897-900.
(63) Ros, R.; Schwesinger, F.; Anselmetti, D.; Kubon, M.; Schafer, R.; Pluckthun, A.; Tiefenauer, L. *Proc. Natl. Acad. Sci. U. S. A.* **1998**, *95*, 7402-7405.
(64) Schwesinger, F.; Ros, R.; Strunz, T.; Anselmetti, D.; Guntherodt, H.-J.; Honegger, A.; Jermutus, L.; Tiefenauer, L.; Pluckthun, A. *Proc. Natl. Acad. Sci. U. S. A.* **2000**, *97*, 9972-9977.
(65) Tournier, E. J. M.; Wallach, J.; Blond, P. *Anal. Chim. Acta* **1998**, *361*, 33-44.
(66) Walsh, M. K.; Wang, X.; Weimer, B. C. *J. Biochem. Biophys. Methods* **2001**, *47*, 221-231.
(67) Cross, B.; Ronzon, F.; Roux, B.; Rieu, J.-P. *Langmuir* **2005**, *21*, 5149-5153.
(68) Desmeules, P.; Grandbois, M.; Bondarenko, V. A.; Yamazaki, A.; Salesse, C. *Biophys. J.* **2002**, *82*, 3343-3350.
(69) Nevo, R.; Stroh, C.; Kienberger, F.; Kaftan, D.; Brumfeld, V.; Elbaum, M.; Reich, Z.; Hinterdorfer, P. *Nat. Struct. Biol.* **2003**, *10*, 553-557.
(70) Klein Dionne, C.; Stroh Cordula, M.; Jensenius, H.; van Es, M.; Kamruzzahan, A. S.; Stamouli, A.; Gruber Hermann, J.; Oosterkamp Tjerk, H.; Hinterdorfer, P. *ChemPhysChem* **2003**, *4*, 1367-71.
(71) Herman, S.; Loccufier, J.; Schacht, E. *Macromol. Chem. Phys.* **1994**, *195*, 203-9.
(72) Goodson, R. J.; Katre, N. V. *Bio/Technology* **1990**, *8*, 343-6.
(73) Kamruzzahan, A. S. M.; Ebner, A.; Wildling, L.; Kienberger, F.; Riener, C. K.; Hahn, C. D.; Pollheimer, P. D.; Winklehner, P.; Hoelzl, M.; Lackner, B.; Schoerkl, D. M.; Hinterdorfer, P.; Gruber, H. J. *Bioconjugate Chem.* **2006**, *17*, 1473-1481.
(74) Kienberger, F.; Ebner, A.; Gruber Hermann, J.; Hinterdorfer, P. *Acc. Chem. Res.* **2006**, *39*, 29-36.
(75) Haselgrubler, T.; Amerstorfer, A.; Schindler, H.; Gruber, H. J. *Bioconjugate Chem.* **1995**, *6*, 242-8.
(76) Carlsson, J.; Drevin, H.; Axen, R. *Biochem. J.* **1978**, *173*, 723-37.
(77) Bustamante, C.; Macosko, J. C.; Wuite, G. J. L. *Nat. Rev. Mol. Cell Biol.* **2000**, *1*, 130-136.

(78) *Olympus*, http://probe.olympus-global.com/en/en/outlineprodctE.html, December 1, 2009.
(79) Rabbi, M.; Marszalek, P. E. In *Single Molecule Techniques - A Laboratory Manual*; Selvin, P. R., Ha, T., Eds.; Cold Spring Harbor: New York, 2008, p 371-394.
(80) Ohler, B. *Practical Advice on the Determination of Cantilever Spring Constants*, Veeco Instruments Inc.
(81) Flory, P. J. *Principles of polymer chemistry*; Cornell University Press: New York, 1953.
(82) Flory, P. J. *Statistical mechanics of chain molecules*; Hanser Publishers: New York, 1989.
(83) Bustamante, C.; Marko, J. F.; Siggia, E. D.; Smith, S. *Science* **1994**, *265*, 1599-600.
(84) Smith, S. B.; Cui, Y.; Bustamante, C. *Science* **1996**, *271*, 795-9.
(85) Scott, D. *Biometrika* **1979**, *66*, 605-610.
(86) Williams, P. In *Handbook of molecular force spectroscopy*; Noy, A., Ed.; Springer Science: New York, 2008, p 143-161.
(87) Evans, E.; Ritchie, K. *Biophys. J.* **1997**, *72*, 1541-1555.
(88) Hummer, G.; Szabo, A. *Biophys. J.* **2003**, *85*, 5-15.
(89) Hummer, G.; Szabo, A. *Acc. Chem. Res.* **2005**, *38*, 504-513.
(90) Bell, G. I. *Science* **1978**, *200*, 618-27.
(91) Janshoff, A.; Neitzert, M.; Oberdorfer, Y.; Fuchs, H. *Angew. Chem., Int. Ed.* **2000**, *39*, 3212-3237.
(92) Evans, E. *Biophys. Chem.* **1999**, *82*, 83-97.
(93) Overney, R. M.; Takano, H.; Fujihira, M.; Paulus, W.; Ringsdorf, H. *Phys. Rev. Lett.* **1994**, *72*, 3546-9.
(94) Pei, Z. Ph.D. Carbohydrate synthesis and study of carbohydrate-lectin interactions using QCM biosensors and microarray technologies KTH, 2006, 106.
(95) Boucher, C.; Liberelle, B.; Jolicoeur, M.; Durocher, Y.; De Crescenzo, G. *Bioconjugate Chem.* **2009**, *20*, 1569-1577.
(96) De Crescenzo, G.; Litowski Jennifer, R.; Hodges Robert, S.; O'Connor-McCourt Maureen, D. *Biochemistry* **2003**, *42*, 1754-63.
(97) Boucher, C.; St-Laurent, G.; Loignon, M.; Jolicoeur, M.; De Crescenzo, G.; Durocher, Y. *Tissue Eng., Part A* **2008**, *14*, 2069-2077.
(98) Hanna, R. A.; Garcia-Diaz, B. E.; Davies, P. L. *FEBS Letters* **2007**, *581*, 2894-2898.
(99) Sandal, M.; Benedetti, F.; Brucale, M.; Gomez-Casado, A.; Samori, B. *Bioinformatics* **2009**, *25*, 1428-1430.
(100) Liberelle, B.; Banquy, X.; Giasson, S. *Langmuir* **2008**, *24*, 3280-3288.
(101) Gu, C.; Kirkpatrick, A.; Ray, C.; Guo, S.; Akhremitchev, B. B. *J. Phys. Chem. C* **2008**, *112*, 5085-5092.
(102) Williams, M. C.; Rouzina, I. *Curr. Opin. Struct. Biol.* **2002**, *12*, 330-336.
(103) Richmond, T. J.; Davey, C. A. *Nature* **2003**, *423*, 145-150.
(104) Rief, M.; Clausen-Schaumann, H.; Gaub, H. E. *Nat. Struct. Biol.* **1999**, *6*, 346-349.

(105) Clausen-Schaumann, H.; Rief, M.; Tolksdorf, C.; Gaub, H. E. *Biophys. J.* **2000**, *78*, 1997-2007.
(106) Cluzel, P.; Lebrun, A.; Heller, C.; Lavery, R.; Viovy, J.-L.; Chatenay, D.; Caron, F. *Science* **1996**, *271*, 792-4.
(107) Leger, J. F.; Romano, G.; Sarkar, A.; Robert, J.; Bourdieu, L.; Chatenay, D.; Marko, J. F. *Phys. Rev. Lett.* **1999**, *83*, 1066-1069.
(108) Williams, M. C.; Rouzina, I.; McCauley, M. *PNAS* **2009**, *106*, 18047-18048.
(109) Ahsan, A.; Rudnick, J.; Bruinsma, R. *Biophys. J.* **1998**, *74*, 132-137.
(110) Kosikov, K. M.; Gorin, A. A.; Zhurkin, V. B.; Olson, W. K. *J. Mol. Biol.* **1999**, *289*, 1301-1326.
(111) Allemand, J. F.; Bensimon, D.; Lavery, R.; Croquette, V. *Proc. Natl. Acad. Sci. U. S. A.* **1998**, *95*, 14152-14157.
(112) Strick, T. R.; Allemand, J. F.; Bensimon, D.; Croquette, V. *Biophys. J.* **1998**, *74*, 2016-2028.
(113) Bockelmann, U.; Essevaz-Roulet, B.; Heslot, F. *Phys. Rev. Lett.* **1997**, *79*, 4489-4492.
(114) Fersht, A. R.; Shi, J. P.; Knill-Jones, J.; Lowe, D. M.; Wilkinson, A. J.; Blow, D. M.; Brick, P.; Carter, P.; Waye, M. M.; Winter, G. *Nature* **1985**, *314*, 235-8.
(115) Helm, C. A.; Knoll, W.; Israelachvili, J. N. *Proc. Natl. Acad. Sci. U. S. A.* **1991**, *88*, 8169-73.
(116) Moy, V. T.; Florin, E.-L.; Gaub, H. E. *Colloid Surface A* **1994**, *93*, 343-8.
(117) Florin, E. L.; Moy, V. T.; Gaub, H. E. *Science* **1994**, *264*, 415-17.
(118) Pierce, M.; Stuart, J.; Pungor, A.; Dryden, P.; Hlady, V. *Langmuir* **1994**, *10*, 3217-21.
(119) Chilkoti, A.; Boland, T.; Ratner, B. D.; Stayton, P. S. *Biophys. J.* **1995**, *69*, 2125-30.
(120) Allen, S.; Davies, J.; Dawkes, A. C.; Davies, M. C.; Edwards, J. C.; Parker, M. C.; Roberts, C. J.; Sefton, J.; Tendler, S. J. B.; Williams, P. M. *FEBS Letters* **1996**, *390*, 161-164.
(121) Freitag, S.; Le Trong, I.; Klumb, L.; Stayton, P. S.; Stenkamp, R. E. *Protein Sci.* **1997**, *6*, 1157-1166.
(122) Livnah, O.; Bayer, E. A.; Wilchek, M.; Sussman, J. L. *Proc. Natl. Acad. Sci. U. S. A.* **1993**, *90*, 5076-80.
(123) Grubmuller, H.; Heymann, B.; Tavan, P. *Science* **1996**, *271*, 997-9.
(124) *PyMol*, http://www.pymol.org., December 1, 2009.
(125) Green, N. M. *Adv. Protein Chem.* **1975**, *29*, 85-133.
(126) Weber, P. C.; Ohlendorf, D. H.; Wendoloski, J. J.; Salemme, F. R. *Science* **1989**, *243*, 85-8.
(127) Hendrickson, W. A.; Paehler, A.; Smith, J. L.; Satow, Y.; Merritt, E. A.; Phizackerley, R. P. *Proc. Natl. Acad. Sci. U. S. A.* **1989**, *86*, 2190-4.
(128) Marszalek, P. E.; Lu, H.; Li, H.; Carrion-Vazquez, M.; Oberhauser, A. F.; Schulten, K.; Fernandez, J. M. *Nature* **1999**, *402*, 100-103.
(129) Wong, J.; Chilkoti, A.; Moy, V. T. *Biomol. Eng.* **1999**, *16*, 45-55.
(130) Yuan, C.; Chen, A.; Kolb, P.; Moy, V. T. *Biochemistry* **2000**, *39*, 10219-10223.
(131) Lo, Y.-S., 2001.
(132) Zhang, X.; Moy, V. T. *Biophys. Chem.* **2003**, *104*, 271-278.

(133) Ebner, A.; Wildling, L.; Kamruzzahan, A. S. M.; Rankl, C.; Wruss, J.; Hahn, C. D.; Hoelzl, M.; Zhu, R.; Kienberger, F.; Blaas, D.; Hinterdorfer, P.; Gruber, H. J. *Bioconjugate Chem.* **2007**, *18*, 1176-1184.
(134) Merkel, R.; Nassoy, P.; Leung, A.; Ritchie, K.; Evans, E. *Nature* **1999**, *397*, 50-53.
(135) Kienberger, F.; Gruber, H.; Hinterdorfer, P. *Appl. Scanning Probe Methods II* **2006**, 143-164.
(136) Piramowicz, M. d. O.; Czuba, P.; Targosz, M.; Burda, K.; Szymonski, M. *Acta Biochim. Pol.* **2006**, *53*, 93-100.
(137) Moy, V. T.; Florin, E. L.; Gaub, H. E. *Science* **1994**, *266*, 257-259.
(138) Lee, G. U.; Kidwell, D. A.; Colton, R. J. *Langmuir* **1994**, *10*, 354-357.
(139) Varki, A. *Glycobiology* **1993**, *3*, 97-130.
(140) Lis, H.; Sharon, N. *Chem. Rev.* **1998**, *98*, 637-674.
(141) Litynska, A.; Przybylo, M.; Pochec, E.; Hoja-Lukowicz, D.; Ciolczyk, D.; Laidler, P.; Gil, D. *Melanoma Res* **2001**, *11*, 205-12.
(142) Yarema, K. J.; Goon, S.; Bertozzi, C. R. *Nat. Biotechnol.* **2001**, *19*, 553-558.
(143) Kiessling, L. L.; Pohl, N. L. *Chem. Biol.* **1996**, *3*, 71-7.
(144) Lee, Y. C.; Lee, R. T. *Acc. Chem. Res.* **1995**, *28*, 321-7.
(145) Mammen, M.; Chio, S.-K.; Whitesides, G. M. *Angew. Chem., Int. Ed.* **1998**, *37*, 2755-2794.
(146) Marshall, B. T.; Long, M.; Piper, J. W.; Yago, T.; McEver, R. P.; Zhu, C. *Nature* **2003**, *423*, 190-193.
(147) Merkel, R. *Phys. Rep.* **2001**, *346*, 343-385.
(148) Song, E. Y.; Kim, K. A.; Kim, Y. D.; Lee, E. Y.; Lee, H. S.; Kim, H. J.; Ahn, B. M.; Choe, Y. K.; Kim, C. H.; Chung, T. W. *Hepatol. Res.* **2003**, *26*, 311-317.
(149) Popov, M.; Li, J.; Reithmeier, R. A. F. *Anal. Biochem.* **2000**, *279*, 90-95.
(150) Stewart, W. B.; Touloukian, C. E. *Chem Senses* **1996**, *21*, 13-8.
(151) Hayakawa, T.; Kawamura, M.; Okamoto, M.; Baba, M.; Niikawa, T.; Takehara, S.; Serizawa, T.; Akashi, M. *J. Med. Virol.* **1998**, *56*, 327-331.
(152) Edelman, G. M.; Cunningham, B. A.; Reeke, G. N., Jr.; Becker, J. W.; Waxdal, M. J.; Wang, J. L. *Proc. Natl. Acad. Sci. U. S. A.* **1972**, *69*, 2580-4.
(153) Quiocho, F. A. *Annu. Rev. Biochem.* **1986**, *55*, 287-315.
(154) Derewenda, Z.; Yariv, J.; Helliwell, J. R.; Kalb, A. J.; Dodson, E. J.; Papiz, M. Z.; Wan, T.; Campbell, J. *EMBO Journal* **1989**, *8*, 2189-93.
(155) Sturtevant, J. M. *Proc. Natl. Acad. Sci. U. S. A.* **1977**, *74*, 2236-40.
(156) Jacrot, B.; Cusack, S.; Dianoux, A. J.; Engelman, D. M. *Nature* **1982**, *300*, 84-6.
(157) Gad, M.; Itoh, A.; Ikai, A. *Cell Biol. Int.* **1997**, *21*, 697-706.
(158) Kanellopoulos, P. N.; Tucker, P. A.; Pavlou, K.; Agianian, B.; Hamodrakas, S. J. *J. Struct. Biol.* **1996**, *117*, 16-23.
(159) Paulson, J. C.; Blixt, O.; Collins, B. E. *Nat. Chem. Biol.* **2006**, *2*, 238-248.
(160) Seeberger, P. H.; Werz, D. B. *Nature* **2007**, *446*, 1046-1051.
(161) Park, S.; Shin, I. *Angew. Chem., Int. Ed.* **2002**, *41*, 3180-3182.
(162) Shinohara, Y.; Hasegawa, Y.; Kaku, H.; Shibuya, N. *Glycobiology* **1997**, *7*, 1201-1208.
(163) Nahalkova, J.; Svitel, J.; Gemeiner, P.; Danielsson, B.; Pribulova, B.; Petrus, L. *J. Biochem. Biophys. Methods* **2002**, *52*, 11-18.

(164) Love, J. C.; Estroff, L. A.; Kriebel, J. K.; Nuzzo, R. G.; Whitesides, G. M. *Chem. Rev.* **2005**, *105*, 1103-1169.
(165) Poirier, G. E.; Tarlov, M. J.; Rushmeier, H. E. *Langmuir* **1994**, *10*, 3383-6.
(166) Pei, Z.; Yu, H.; Theurer, M.; Walden, A.; Nilsson, P.; Yan, M.; Ramström, O. *ChemBioChem* **2007**, *8*, 166-168.
(167) Yan, M.; Ren, J. *Chem. Mater.* **2004**, *16*, 1627-1632.
(168) *Azides and nitrenes: reactivity and utility* Scriven, E. F. U., Ed.; Academic Press: New York, 1984.
(169) Joester, D.; Klein, E.; Geiger, B.; Addadi, L. *J. Am. Chem. Soc.* **2006**, *128*, 1119-1124.
(170) Yan, M.; Bartlett, M. A. *Nano Lett.* **2002**, *2*, 275-278.
(171) Yan, M. *Chem.--Eur. J.* **2007**, *13*, 4138-4144.
(172) Pei, Z.; Anderson, H.; Aastrup, T.; Ramström, O. *Biosens. Bioelectron.* **2005**, *21*, 60-66.
(173) Bartlett, M. A.; Yan, M. *Adv. Mater.* **2001**, *13*, 1449-1451.
(174) Zou, S.; Sullan, R. *Biophys. J.* **2009**, *96*, 643a-644a.
(175) Titus, M. A. *Curr. Opin. Cell Biol.* **1993**, *5*, 77-81.
(176) Stewart, M. *Curr. Opin. Cell Biol.* **1993**, *5*, 3-11.
(177) Harbury, P. B.; Zhang, T.; Kim, P. S.; Alber, T. *Science* **1993**, *262*, 1401-7.
(178) Liu, J.; Zheng, Q.; Deng, Y.; Cheng, C.-S.; Kallenbach Neville, R.; Lu, M. *Proc. Natl. Acad. Sci. U. S. A.* **2006**, *103*, 15457-62.
(179) Petka, W. A.; Hardin, J. L.; McGrath, K. P.; Wirtz, D.; Tirrell, D. A. *Science* **1998**, *281*, 389-392.
(180) Tripet, B.; Yu, L.; Bautista, D. L.; Wong, W. Y.; Irvin, R. T.; Hodges, R. S. *Protein Eng.* **1996**, *9*, 1029-1042.
(181) Minten, I. J.; Ma, Y.; Hempenius, M. A.; Vancso, G. J.; Nolte, R. J. M.; Cornelissen, J. J. L. M. *Org. Biomol. Chem.* **2009**, *7*, 4685-4688.
(182) Crick, F. H. C. *Acta Crystallogr.* **1953**, *6*, 685-9.
(183) Sodek, J.; Hodges, R. S.; Smillie, L. B.; Jurasek, L. *Proc. Natl. Acad. Sci. U. S. A.* **1972**, *69*, 3800-4.
(184) Chao, H.; Bautista, D. L.; Litowski, J.; Irvin, R. T.; Hodges, R. S. *J. Chromatogr. B* **1998**, *715*, 307-329.
(185) Monera, O. D.; Zhou, N. E.; Kay, C. M.; Hodges, R. S. *J. Biol. Chem.* **1993**, *268*, 19218-27.
(186) Moitra, J.; Szilak, L.; Krylov, D.; Vinson, C. *Biochemistry* **1997**, *36*, 12567-12573.
(187) O'Shea, E. K.; Lumb, K. J.; Kim, P. S. *Curr. Biol.* **1993**, *3*, 658-67.
(188) Monera, O. D.; Kay, C. M.; Hodges, R. S. *Biochemistry* **1994**, *33*, 3862-71.
(189) Talbot, J. A.; Hodges, R. S. *Acc. Chem. Res.* **1982**, *15*, 224-30.
(190) Graddis, T. J.; Myszka, D. G.; Chaiken, I. M. *Biochemistry* **1993**, *32*, 12664-71.
(191) Lovejoy, B.; Choe, S.; Cascio, D.; McRorie, D. K.; DeGrado, W. F.; Eisenberg, D. *Science* **1993**, *259*, 1288-93.
(192) Zhu, B. Y.; Zhou, N. E.; Kay, C. M.; Hodges, R. S. *Protein Sci.* **1993**, *2*, 383-94.
(193) Zhou, N. E.; Kay, C. M.; Hodges, R. S. *Protein Eng.* **1994**, *7*, 1365-72.
(194) Kohn, W. D.; Kay, C. M.; Hodges, R. S. *Protein Sci.* **1995**, *4*, 237-50.

(195) Chao, H.; Houston, M. E., Jr.; Grothe, S.; Kay, C. M.; O'Connor-McCourt, M.; Irvin, R. T.; Hodges, R. S. *Biochemistry* **1996**, *35*, 12175-12185.
(196) Wishart, D. S.; Sykes, B. D.; Richards, F. M. *J. Mol. Biol.* **1991**, *222*, 311-33.
(197) Bornschlogl, T.; Rief, M. *Langmuir* **2008**, *24*, 1338-42.
(198) Dietz, H.; Bornschloegl, T.; Heym, R.; Koenig, F.; Rief, M. *New J. Phys.* **2007**, *9*, 1-8.
(199) Cappello, G.; Pierobon, P.; Symonds, C.; Busoni, L.; Gebhardt, J. C. M.; Rief, M.; Prost, J. *Proc. Natl. Acad. Sci. U. S. A.* **2007**, *104*, 15328-15333.
(200) Gebhardt, J. C. M.; Clemen, A. E. M.; Jaud, J.; Rief, M. *Proc. Natl. Acad. Sci. U. S. A.* **2006**, *103*, 8680-8685.
(201) Bornschlogl, T.; Rief, M. *Phys. Rev. Lett.* **2006**, *96*, 118102.
(202) Schwaiger, I.; Kardinal, A.; Schleicher, M.; Noegel, A. A.; Rief, M. *Nat. Struct. Mol. Biol.* **2004**, *11*, 81-85.
(203) Zitzewitz, J. A.; Bilsel, O.; Luo, J.; Jones, B. E.; Matthews, C. R. *Biochemistry* **1995**, *34*, 12812-19.
(204) Rief, M.; Gautel, M.; Oesterhelt, F.; Fernandez, J. M.; Gaub, H. E. *Science* **1997**, *276*, 1109-12.
(205) Li, H.; Linke, W. A.; Oberhauser, A. F.; Carrion-Vazquez, M.; Kerkvliet, J. G.; Lu, H.; Marszalek, P. E.; Fernandez, J. M. *Nature* **2002**, *418*, 998-1002.
(206) Sarkar, A.; Caamano, S.; Fernandez, J. M. *Biophys. J.* **2007**, *92*, L36-L38.
(207) Root, D. D.; Yadavalli, V. K.; Forbes, J. G.; Wang, K. *Biophys. J.* **2006**, *90*, 2852-2866.
(208) Evans, E. *Annu. Rev. Biophys. Biomol. Struct.* **2001**, *30*, 105-128.
(209) Carpenter, G.; Cohen, S. *J. Biol. Chem.* **1990**, *265*, 7709-12.
(210) Goodsell David, S. *Oncologist* **2003**, *8*, 496-7.
(211) Sorimachi, H.; Suzuki, K. *J. Biochem.* **2001**, *129*, 653-664.
(212) Carafoli, E.; Molinari, M. *Biochem. Biophys. Res. Commun.* **1998**, *249*, 572.
(213) Huang, Y.; Wang, K. K. W. *Trends Mol. Med.* **2001**, *7*, 355-362.
(214) Hosfield, C. M.; Elce, J. S.; Davies, P. L.; Jia, Z. *EMBO Journal* **1999**, *18*, 6880-6889.
(215) Davies, P. L.; Campbell, R. L.; Moldoveanu, T. *Handbook of Metalloproteins* **2004**, *3*, 489-500.
(216) Blanchard, H.; Li, Y.; Cygler, M.; Kay, C. M.; Arthur, J. S. C.; Davies, P. L.; Elce, J. S. *Protein Sci.* **1996**, *5*, 535-7.
(217) Graham-Siegenthaler, K.; Gauthier, S.; Davies, P. L.; Elce, J. S. *J. Biol. Chem.* **1994**, *269*, 30457-60.

Appendix: Experimental Details

1. Tip Functionalization Strategy

In general, standard tip functionalization method followed in this study involves three main steps (Figure A1): (*i*) generating amino groups ($-NH_2$) on the silicon nitride (Si_3N_4) tip, (*ii*) attaching a heterobifunctional PEG spacer, with *N*-hydroxysuccinimate group (NHS) at one end, to the aminated tip with an amide linkage, and (*iii*) covalent linking of a biomolecule to the free end of the PEG spacer. The biomolecules used either contained a thiol (−SH) group and were attached to PEG containing a 3-(2-pyridyldithio)propionyl group (PDP) by disulfide bond formation, or contained an amino ($-NH_2$) group and were attached to PEG containing a second NHS group by amide bond formation. In some cases, the PEG used already contained the biomolecule (*i.e.*, *d*-biotin) thus eliminating the need for Step (*iii*). It is worthwhile mentioning that, in our hands, the success rate in tip functionalization experiments was as low as 30%.

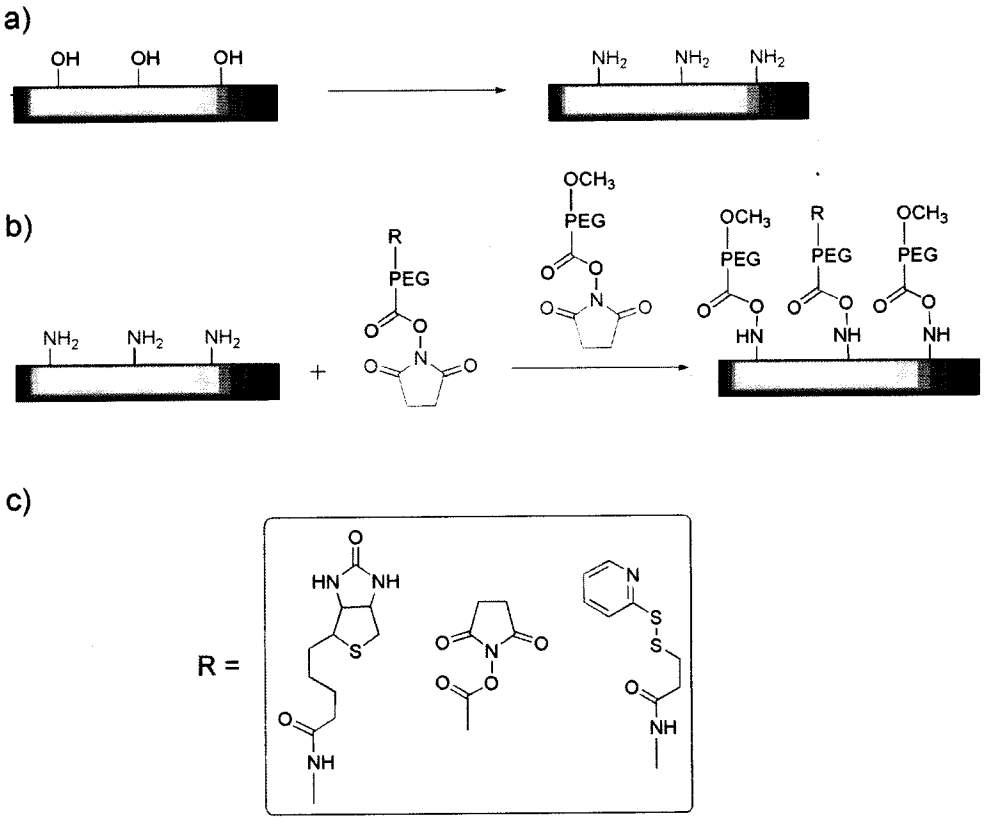

Figure A1. AFM tip functionalization strategy: (a) Surface amination, (b) Attaching PEG spacer to the aminated surface via an amide linkage to its NHS end, and (c) The different functional groups present at the other end of PEG, to which biomolecules can be tethered. A high excess of monofunctionalized PEG is used in order to block most of the tip surface, thereby decreasing the surface coverage.

It's important to mention that before functionalization, AFM tips were exposed to oxygen in the presence of high-intensity ultraviolet (UV) radiation, which efficiently removes contamination *via* ozone oxidation.

With respect to the first step in tip functionalization, amination is achieved by applying VECTABOND™ reagent to clean Si_3N_4 tips. VECTABOND™ is commonly used to fix tissue sections and cell preparations to glass slides and coverslips (*i.e.* silicon-based surfaces), by chemically modifying these materials.[1] Recently, this reagent has been shown to effectively aminate AFM tip surfaces in a very short time period (not more than

10 minutes).[2] The aminated tips were used directly for subsequent functionalization in order to avoid undesirable contamination.

2. Synthesis of PDP-PEG-NHS

Most of the PEG spacers used in the second functionalization step (Figure A1, c) were commercially available with the exception of PDP-PEG-NHS. The synthesis of this versatile heterobifunctional spacer was carried out as outlined in Figure 2. The starting material NH_2-PEG-COOH was first acylated using the crosslinker *o*-succinimidyl 3-(2-pyridyl)-dithiopropionate (SPDP) to give PDP-PEG-COOH, and then the carboxyl group was activated as an NHS ester yielding the final product, PDP-PEG-NHS.[3]

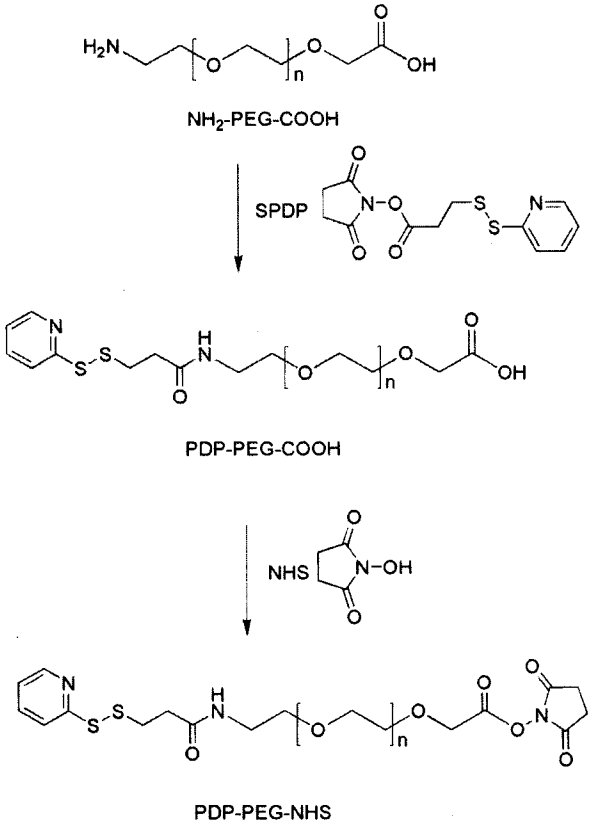

Figure A2. Synthesis of PDP-PEG-NHS

This previously-reported procedure was reproduced successfully, however hydrolyzed SPDP was a by-product. Gel filtration was found to give variable results in purifying the desired product.[3] Instead, a multi-step extraction procedure was developed, as described in Section 2.4 of the experimental chapter, and was shown to effectively remove such impurities in a reproducible manner.[4] In addition, converting the intermediate PDP-PEG-COOH into the NHS ester was achieved using *N,N,N',N'*-tetramethyl-*O*-(*N*-succinimidyl)-uroniumtetrafluroborate (TSTU) instead of the conventional NHS/DCC method.[5] The advantages of this method are the faster reactivity of this reagent and the ease of by-product removal. PDP-PEG-NHS was purified by simply dissolving in chloroform, washing with buffer at neutral pH, applying a drying agent and evaporating the chloroform phase, which is much easier compared to removing the dicyclohexylurea (DCU) by-product.

3. Synthesis of SPDP

O-succinimidyl 3-(2-pyridyl)-dithiopropionate (SPDP) is a heterobifunctional cross-linking reagent containing one NHS ester group and one 2-pyridyldisulfide group (PDS), resembling the spacer NHS-PEG-PDP. The NHS ester reacts with amino groups to give stable amide bonds, while the PDS group reacts with thiols to form disulfide bonds (Figure A3, A4).

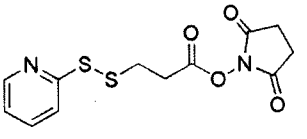

SPDP

Figure A3. Structure of *o*-succinimidyl 3-(2-pyridyl)-dithiopropionate (SPDP)

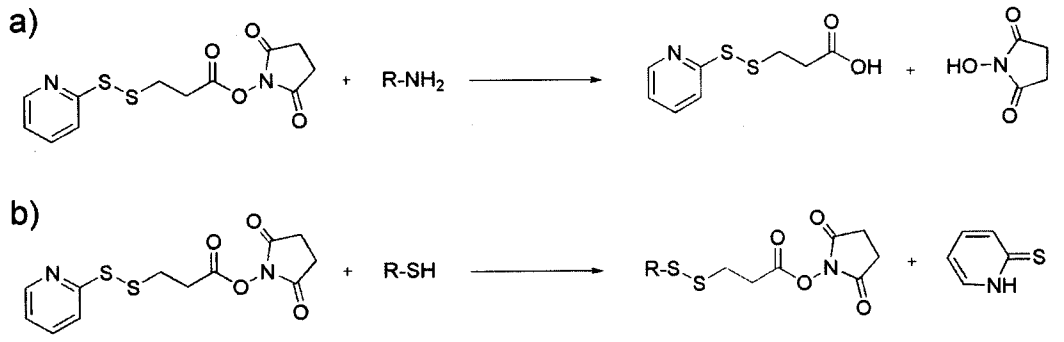

Figure A4. Reactions of SPDP with (a) amino-, and (b) thiol- reactive groups

As mentioned earlier, this reagent was used to introduce the PDS group into NH_2-PEG-COOH by converting the amino end into a PDP moiety. According to the original procedure, reported by Carlsson *et al.*, SPDP is formed by a two-step procedure: (*i*) 2,2'-DTDP is reacted with 3-mercaptopropionic acid to give PDP-OH, (*ii*) NHS with DCC are then added to introduce the NHS ester moiety.[6] 2,2'-DTDP was synthesized by the oxidation of 2-thiopyridone (2-TP) using hydrogen peroxide (H_2O_2) in water (Figure A5).[4] 2,2'-DTDP is insoluble at neutral pH and immediately precipitates upon formation and can be collected by simple gravity filtration. In order to avoid further oxidation of 2,2'-DTDP the reaction mixture was kept at low temperature (*ca.* 10 – 15 °C) and was carried out for a short time period (*ca.* 30 minutes).

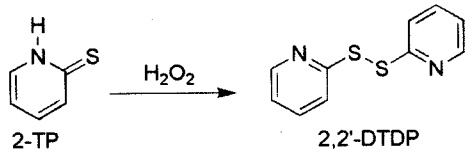

Figure A5. Synthesis of 2,2'-dithiodupyridine (2,2'-DTDP)

2,2'-DTDP was then subjected to disulfide exchange with 3-mercaptopropionic acid to give PDP-OH (Figure A6). The product formed contained a large amount of 3,3'-

dithiopropionic acid (HOOC-CH_2-CH_2-S-S-CH_2-CH_2-COOH), which is formed when PDP-OH further reacts with 3-mercaptopropionic acid, despite the use of excess 2,2'-DTDP.[6]

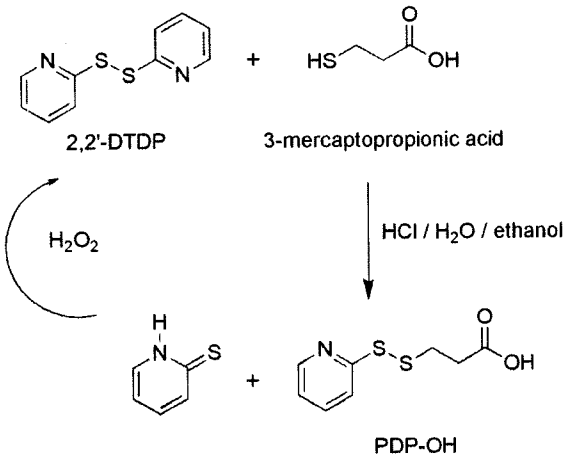

Figure A6. Synthesis of 3-(2-pyridyldithio)-propionic acid (PDP-OH)

Purification of crude PDP-OH by column chromatography, as suggested by Carlsson *et al.*, yields only 40% of pure product. In the procedure followed herein, the slow addition of 3-mercaptopropionic acid along with the use of strong acidic conditions, known to disfavour disulfide exchange reactions, were used in efforts to reduce the side product formation.[4] In addition, the released 2-TP was re-oxidized to 2,2'-DTDP and a multi-step extraction procedure was carried out in order to purify PDP-OH (from 2,2'-DTDP as well as HOOC-CH_2-CH_2-S-S-CH_2-CH_2-COOH).[7] PDP-OH is much more soluble in aqueous solution and therefore it was first extracted from chloroform at neutral pH. Since 2-TP has similar solubility in water and chloroform, its conversion to 2,2'-DTDP, which completely partitions into the chloroform phase, was indeed useful. In order to remove the remaining impurity HOOC-CH_2-CH_2-S-S-CH_2-CH_2-COOH, the pH was lowered to

ca. 2.5, at which point PDP-OH separates into the chloroform phase. Silica chromatography was sufficient to remove any side-products that might have been present in the chloroform phase. After purification, PDP-OH was converted to SPDP (Figure A7) by the addition of NHS and DCC as described in earlier studies,[7] except for using isopropanol rather than 70% ethanol for re-crystallization, which was carried out to reduce the extent of hydrolysis (Figure A8). The obtained white crystals were stable at – 25 °C for more than 3 months.

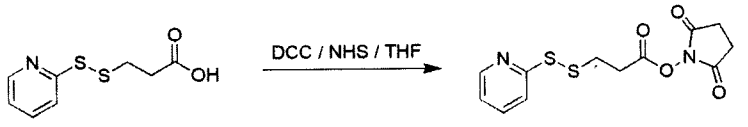

Figure A7. Synthesis of SPDP from PDP-OH

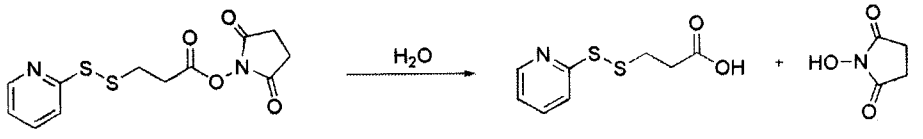

Figure A8. Hydrolysis of SPDP

4. Tip Functionalization Assays

The characterization of AFM tips, after their functionalization (with the PEG spacer followed by the biomolecule of interest) is difficult and limited because of their extremely small size. At the moment, there is no single independent method for determining the number of functional biomolecules on an AFM tip. Therefore in SMFS

studies, multiple control experiments are necessary for high confidence results. These include blocking the measured interactions by adding free ligand in the solution or measuring interactions with non-functionalized tips or samples expected to not have any binding properties.[8]

In this work, SMFS control studies were complemented with parallel macroscopic experiments by means of surface plasmon resonance (SPR) as well as a UV-based assay. The efficiency of the developed tip functionalization technique and the suitability of the synthesized spacer were examined using both techniques as follows.

4.1. SPR Assays

Surface plasmon resonance (SPR) is a technique that enables the quantification of interaction dynamics (including molecular binding and recognition) by detecting changes in refractive index at the surface of a sensorchip. As described in Figure A9, the incident light (typically in the visible or infrared region) impinges at the interface between the gold-coated sensorchip and the biomedium in contact with it, at specific angles corresponding to the excitation of the surface plasmon electromagnetic waves.

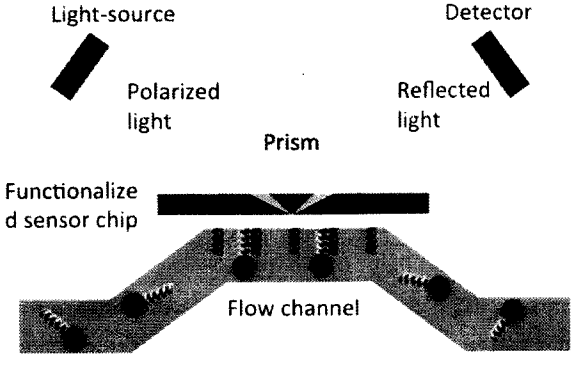

Figure A9. A schematic representation of surface plasmon resonance experiment

SPR penetrates only near the vicinity of the sensor chip surface, and the optical reflectivity in this thin region is highly sensitive to thickness changes. Thickness and mass changes, due to biomolecular binding, alter the refractive index thereby shifting the SPR angle. In a typical SPR experiment, the change in resonant angle is monitored in real time by plotting the resonance signal *versus* time.[9]

The efficiency of synthesized PDP-PEG-NHS and the adequacy of the chemical strategy involved in the AFM tip functionalization procedure (described in the beginning of this appendix) were evaluated by using SPR (Figure A10).

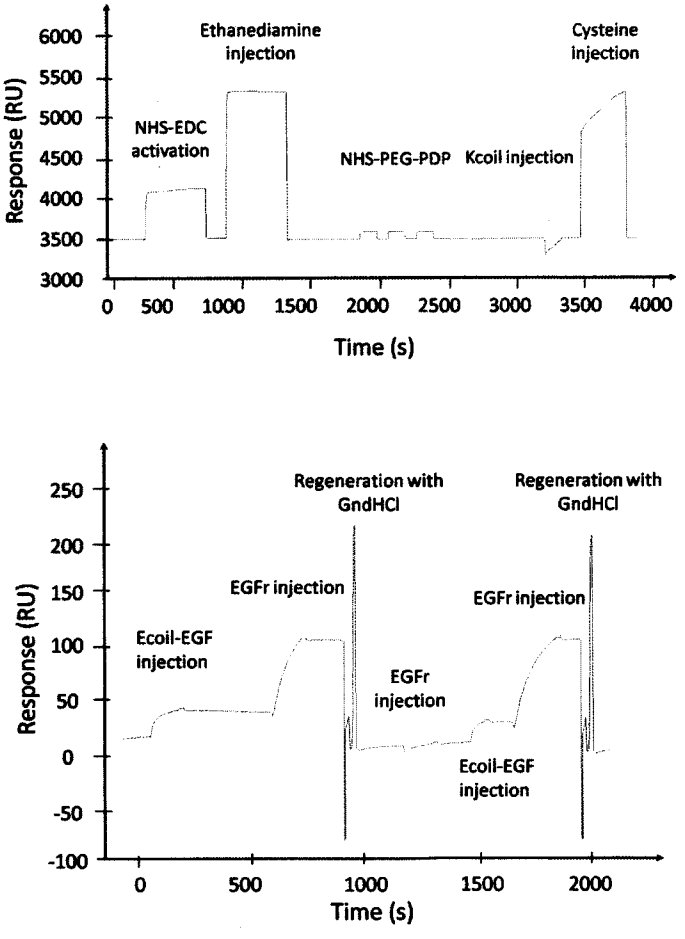

Figure A10. SPR assay sensograms

Carboxymethylated dextran sensorchips (CM4) were first aminated, as described in section 2.5, to mimic the AFM tip surface after treatment with VECTABOND™. Cysteine-terminated K-coil peptides were covalently immobilized on the aminated surface using the synthesized PDP-PEG-NHS spacer. As described earlier, the NHS moiety couples to the surface amino group with a stable amide linkage and the PDP moiety forms a strong disulfide bond with the K-coil cysteine residue. After their oriented coupling, the K-coils present on the sensorchip surfaces were then used to immobilize the E-coil conjugated protein, epidermal growth factor (EGF) *via* the E/K coiled-coil interaction. SPR experiments not only confirmed the efficiency of the functionalization chemistry but also demonstrated the stability of E-coiled EGF/K-coil complexes: (*i*) there was no observed dissociation during the subsequent buffer injection, and (*ii*) a subsequent injection of the EGF receptor (EGFr) caused another signal increase and confirmed binding to the complex. In order to confirm that the observed signal change was due to specific EGFr binding, guanidinium hydrochloride (Gdn•HCl) was injected to promote the dissociation of the E/K coiled-coil complex, and indeed upon subsequent addition of EGFr no binding was observed. At this stage, the E-coiled EGF was injected one more time and only then did the subsequent injection of EGFr result in a signal change due to specific binding. This finding further confirmed that the addition of Gdn•HCl promotes the coiled-coil dissociation without affecting the surface chemistry, the stability of the surface-immobilized K-coils or their subsequent ability to capture E-coiled conjugated proteins. Mock surfaces (where K-coil peptides were not coupled to the surface) were exposed to the same conditions and no changes were observed. In addition, signal changes upon E-coiled EGF and EGFr injections were analogous to those observed when

the K-coil had been coupled using the commercial LC-SPDP spacer.[10] Altogether, the SPR results clearly validate the efficiency of the functionalization chemistry developed to immobilize biomolecules on surfaces and confirm the suitability of synthesized PDP-PEG-NHS for such a purpose.

4.2. Marker Enzyme UV-based Assay

In order to further demonstrate the efficiency of the functionalization procedure used in this work, a UV-based study was carried out on both AFM tips as well as silicon chips functionalized exactly in the same manner as those prepared for SMFS measurements.[4] As detailed in Section 2.10, the tips/chips were first aminated using VECTABOND™ and then reacted with bifunctional PEG spacers: (*i*) NHS-PEG-biotin, or (*ii*) NHS-PEG-PDP followed by SH-PEG-biotin. The tips/chips-bound biotin were then quantified using a commercially-available conjugate of avidin and a marker enzyme (*i.e.* ExtrAvidin®-peroxidase). As described in Figure A11, the amount of ExtrAvidin-peroxidase bound to biotin-functionalized tips/chips was estimated from its enzymatic activity (*i.e.* color production) in a solution containing the substrate *o*-phenylenediamine•2HCl (OPD).

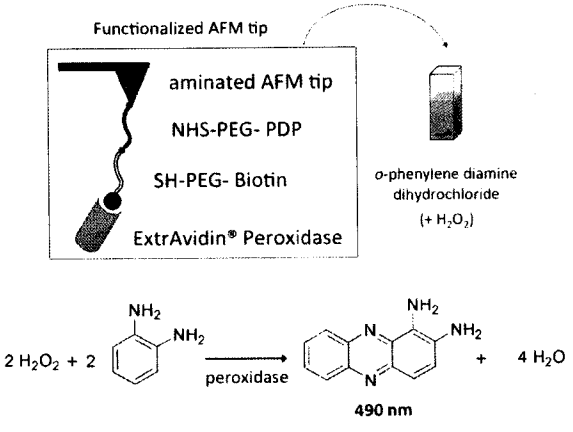

Figure A11. Marker enzyme UV assay

The increase in absorbance at 490 nm (A_{490}) demonstrated the presence of ExtrAvidin®-peroxidase bound to biotin-functionalized tips/chips, which was not observed for control experiments where functionalized tips/chips were incubated in ExtrAvidin®-peroxidase pre-blocked with *d*-biotin or the spacers were not attached (Figure A12). Therefore, the measured A_{490} cannot be attributed to passive adsorption of ExtrAvidin®-peroxidase but rather to specific binding with biotin functionalized on the tips/chips surface.

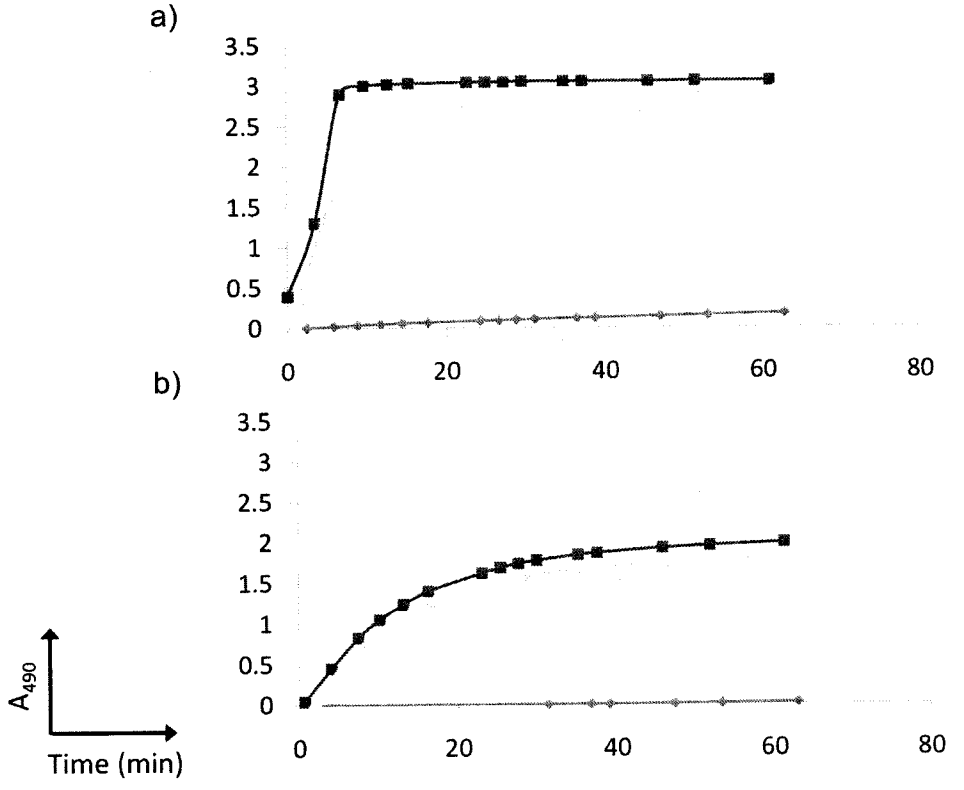

Figure A12. Marker enzyme reaction progress (absorbance *vs* time): (a) Functionalized chips, and (b) Functionalized tips with NHS-PEG-biotin (red), NHS-PEG-PDP followed by SH-PEG-biotin (green) or without any spacer (blue).

It is worthwhile mentioning that after labelling with ExtrAvidin®-peroxidase, the tips/chips were extensively rinsed with buffer (again, similar to the procedure carried out in tip functionalization for SMFS) in order to remove non-specifically bound marker

enzyme. In addition, 0.5% Tween®-20 was added to all buffers to help minimize the extent of non-specific binding.[4]

In conclusion, marker enzyme UV-based assay simulated the functionalization strategy described for AFM tips and examined its efficiency at the macroscopic level. The results proved that the developed functionalization technique to be successful and indeed useful for the specific attachment of biomolecules.

5. Data Analysis Software

Analyzing force curves is an extremely critical process in SMFS studies. As explained previously, hundreds, and more often thousands, of curves are collected in a typical SMFS experiment. Many of the collected curves do not contain useful information: (*i*) the (bio)molecules on the tip did not interact with those on the substrate resulting in no events on the curve, or (*ii*) multiple interactions occurred resulting in complicated or not-clearly defined events. In almost all cases, only a small fraction of the force curves are used in the final quantitative analysis. There is no doubt that manual sorting (*i.e.* opening, viewing, saving or deleting) through thousands of data files in order to choose the useful curves is an extremely tedious and daunting task. Furthermore, this would introduce undesirable personal bias to the process. Therefore, the use of data analysis software is not only an attractive, but a necessary solution.

There are a number of computer-based programs specifically designed to analyze SMFS data. An example of which is the free online-available software *Hooke*, developed by Sandal *et al.*.[11] The *Hooke* program automatically scans through large sets of force curve files, filters the ones that have events, with user-defined parameters and then allows

fitting those events (*i.e.* peaks) to a mathematical model of choice. In this study the *Hooke* program was used for data analysis with the incorporation of major improvements performed by Dr. Rolf Schmidt at Concordia University. Mainly, the command line interface (CLI) operating system of *Hooke* was changed into a graphical user interface (GUI), which helped simplify the work significantly. For example, in order to perform a function, one has to only click an icon rather than type out a text command in a separate window, which allows easier access to functions as well as simplifies multitasking. In addition, an export function was added in order to allow exporting the results into OriginPro software for further analysis (*i.e.* constructing histograms). Figure A13 describes the process by which *Hooke* operates on a typical SMFS set of data.

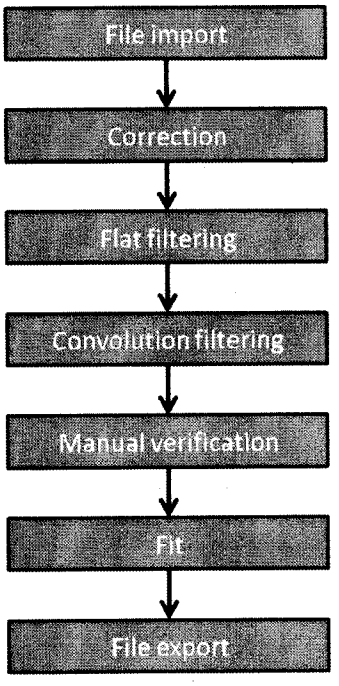

Figure A13. Description of the *Hooke* analysis procedure

It's worthwhile mentioning that although it might be unpleasant to manually filter through force curve files, in some cases it does become necessary and indeed more

effective to screen through the data and evaluate them visually to appreciate the nuances of the curves. However, the software algorithm is still helpful by, for example, lowering the number of curves to screen from thousands to most likely hundreds. In addition, the operation of *Hooke* was tested by comparing data sets that were filtered manually with those carried out using the software. It was concluded that the *Hooke* software renders the data analysis process much simpler and productive, especially the improved version.

(1) *Vector labs*, http://www.vectorlabs.com/catalog.aspx?prodID=16, December 1, 2009.

(2) Horinek, D.; Serr, A.; Geisler, M.; Pirzer, T.; Slotta, U.; Lud, S. Q.; Garrido, J. A.; Scheibel, T.; Hugel, T.; Netz, R. R. *Proc. Natl. Acad. Sci. U. S. A.* **2008**, *105*, 2842-2847.

(3) Riener, C. K.; Kienberger, F.; Hahn, C. D.; Buchinger, G. M.; Egwim, I. O. C.; Haselgrubler, T.; Ebner, A.; Romanin, C.; Klampfl, C.; Lackner, B.; Prinz, H.; Blaas, D.; Hinterdorfer, P.; Gruber, H. J. *Anal. Chim. Acta* **2003**, *497*, 101-114.

(4) Kamruzzahan, A. S. M.; Ebner, A.; Wildling, L.; Kienberger, F.; Riener, C. K.; Hahn, C. D.; Pollheimer, P. D.; Winklehner, P.; Hoelzl, M.; Lackner, B.; Schoerkl, D. M.; Hinterdorfer, P.; Gruber, H. J. *Bioconjugate Chem.* **2006**, *17*, 1473-1481.

(5) Bannwarth, W.; Knorr, R. *Tetrahedron Lett.* **1991**, *32*, 1157-60.

(6) Carlsson, J.; Drevin, H.; Axen, R. *Biochem. J.* **1978**, *173*, 723-37.

(7) Shval'e, A. F.; Ofitserov, V. I.; Samukov, V. V. *Zhurnal Obshchei Khimii* **1985**, *55*, 2152.

(8) *Single-molecule techniques - A laboratory manual*; Slevin, P. R.; Ha, T., Eds.; Cold Spring Harbor: New York, 2008.

(9) Smith, E. A.; Corn, R. M. *Appl. Spectrosc.* **2003**, *57*, 320A-332A.

(10) Boucher, C.; Liberelle, B.; Jolicoeur, M.; Durocher, Y.; De Crescenzo, G. *Bioconjugate Chem.* **2009**, *20*, 1569-1577.

(11) Sandal, M.; Benedetti, F.; Brucale, M.; Gomez-Casado, A.; Samori, B. *Bioinformatics* **2009**, *25*, 1428-1430.